IVW - Schriftenreihe Band 50

Institut für Verbundwerkstoffe GmbH - Kaiserslautern

Panagiota Tsotra

Electrically Conductive Epoxy Matrix Composites

Bibliografische Information Der Deutschen Bibliothek

Die Deutsche Bibliothek verzeichnet diese Publikation in der Deutschen Nationalbibliografie; detaillierte bibliografische Daten sind im Internet über <http://dnb.ddb.de> abrufbar.

Bibliographic information published by Die Deutsche Bibliothek

Die Deutsche Bibliothek lists this publication in the Deutsche Nationalbibliografie; detailed bibliographic data is available in the Internet at <http://dnb.ddb.de>.

Herausgeber: Institut für Verbundwerkstoffe GmbH
Prof. Dr.-Ing. Alois K. Schlarb
Erwin-Schrödinger-Straße
TU Kaiserslautern, Gebäude 58
67663 Kaiserslautern
http://www.ivw.uni-kl.de

Verlag: Institut für Verbundwerkstoffe GmbH

Druck: Technische Universität Kaiserslautern
ZBT – Abteilung Foto-Repro-Druck

D 386

Als Manuskript gedruckt. Printed in Germany.

ISSN 1615-021X
ISBN 3-934930-46-8

Electrically Conductive Epoxy Matrix Composites

Vom Fachbereich für Maschinenbau und Verfahrenstechnik
der Technischen Universität Kaiserslautern
zur Verleihung des akademischen Grades

Doktor-Ingenieurin (Dr.-Ing.)

Genehmigte Dissertation

von

Dipl.-Ing. Panagiota Tsotra

aus Patras, Griechenland

Tag der mündlichen Prüfung:	21.Juli 2004
Dekan und Prüfungsvorsitzender:	Prof. Dr.-Ing. R. Renz
1. Berichterstatter:	Prof. Dr.-Ing. Dr.h.c. K. Friedrich
2. Berichterstatter:	Prof. Dr.-Ing. V. Kostopoulos

D 386

ACKNOWLEDGEMENTS

The present work was completed between August 2000 and February 2004 at the Institut für Verbundwerkstoffe GmbH (IVW), at the University of Kaiserslautern.

I would like to express my gratitude to my supervisor, Prof. Dr.-Ing. Dr.h.c. Klaus Friedrich for his scientific support and interest about the progress of my work. I would like to thank Prof. Dr.-Ing. Rainer Renz for accepting the presidency of the examination committee and Prof. Vassilis Kostopoulos for the co-reference of this thesis and moreover for giving me the motivation to begin my PhD work.

I am thankful to the IVW for providing the financial, technical and scientific means, required for the realization of this work. Many thanks also to the students who offered their help during the experimental part of this work. My special thanks to the IVW-staff and especially to my colleges of division II for their friendly attitude and helpful advices.

I wish also to thank the Deutsch Forschungsgemeinschaft (DFG) for the financial support of this work.

I would like to state my special thanks to Prof. Dr.-Ing. Dr.h.c. József Karger-Kocsis for the interesting discussions and his helpful suggestions. Many thanks also to Dr. Jannis Hatziosifidis from Resolution Performance Products for his help and the gratuitous supply of materials, and to MSc.-Ing. Heli Funk from Panipol Ltd. for the useful information and support. I would like to express my appreciation to Dr.-Ing. Jorg Nass, Dr.-Ing. Juha Hartikainnen, and Dr.-Ing. Oleg Gryshchuk for their interest in my work and their always helpful comments.

I would like to give my most special thanks to my sister Eleni and my parents in Greece for their love, understanding and support.

Kaiserslautern, July 2004 Panagiota Tsotra

Table of Contents

Abstract

Materials in general can be divided into insulators, semiconductors and conductors, depending on their degree of electrical conductivity. Polymers are classified as electrically insulating materials, having electrical conductivity values lower than 10^{-12} S/cm. Due to their favourable characteristics, e.g. their good physical characteristics, their low density, which results in weight reduction, etc., polymers are also considered for applications where a certain degree of conductivity is required. The main aim of this study was to develop electrically conductive composite materials based on epoxy (EP) matrix, and to study their thermal, electrical, and mechanical properties. The target values of electrical conductivity were mainly in the range of electrostatic discharge protection (ESD, 10^{-9}-10^{-6} S/cm).

Carbon fibres (CF) were the first type of conductive filler used. It was established that there is a significant influence of the fibre aspect ratio on the electrical properties of the fabricated composite materials. With longer CF the percolation threshold value could be achieved at lower concentrations. Additional to the homogeneous CF/EP composites, graded samples were also developed. By the use of a centrifugation method, the CF created a graded distribution along one dimension of the samples. The effect of the different processing parameters on the resulting graded structures and consequently on their gradients in the electrical and mechanical properties were systematically studied.

An intrinsically conductive polyaniline (PANI) salt was also used for enhancing the electrical properties of the EP. In this case, a much lower percolation threshold was observed compared to that of CF. PANI was found out to have, up to a particular concentration, a minimal influence on the thermal and mechanical properties of the EP system.

Furthermore, the two above-mentioned conductive fillers were jointly added to the EP matrix. Improved electrical and mechanical properties were observed by this incorporation. A synergy effect between the two fillers took place regarding the electrical conductivity of the composites.

The last part of this work was engaged in the application of existing theoretical models for the prediction of the electrical conductivity of the developed polymer

composites. A good correlation between the simulation and the experiments was observed.

Kurzfassung

Allgemein werden Materialien in Bezug auf ihre elektrische Leitfähigkeit in Isolatoren, Halbleiter oder Leiter unterteilt. Polymere gehören mit einer elektrischen Leitfähigkeit niedriger als 10^{-12} S/cm in die Gruppe der Isolatoren. Aufgrund vorteilhafter Eigenschaften der Polymere, wie z.B. ihren guten physikalischen Eigenschaften, ihrer geringen Dichte, welche zur Gewichtsreduktion beiträgt, usw., werden Polymere auch für Anwendungen in Betracht gezogen, bei denen ein gewisser Grad an Leitfähigkeit gefordert wird. Das Hauptziel dieser Studie war, elektrisch leitende Verbundwerkstoffe auf der Basis von Epoxidharz (EP) zu entwickeln und deren elektrische, mechanische und thermische Eigenschaften zu studieren. Die Zielwerte der elektrischen Leitfähigkeit lagen hauptsächlich im Bereich der Vermeidung elektrostatischer Aufladungen (ESD, 10^{-9}-10^{-6} S/cm).

Bei der Herstellung elektrisch leitender Kunststoffen wurden als erstes Kohlenstofffasern (CF) als leitfähige Füllstoffe benutzt. Bei den durchgeführten Experimenten konnte man beobachten, dass das Faserlängenverhältnis einen bedeutenden Einfluss auf die elektrischen Eigenschaften der fabrizierten Verbundwerkstoffe hat. Mit längeren CF wurde die Perkolationsschwelle bereits bei einer niedrigeren Konzentration erreicht. Zusätzlich zu den homogenen CF/EP Verbundwerkstoffen, wurden auch Gradientenwerkstoffe entwickelt. Mit Hilfe einer Zentrifugation konnte eine gradierte Verteilung der CF entlang der Probenlängeachse erreicht werden. Die Effekte der unterschiedlichen Zentrifugationsparameter auf die resultierenden Gradientenwerkstoffe und die daraus resultierenden, gradierten elektrischen und mechanischen Eigenschaften wurden systematisch studiert.

Ein intrinsisch leitendes Polyanilin-Salz (PANI) wurde auch für das Erhöhen der elektrischen Eigenschaften des EP benutzt. In diesem Fall wurde eine viel niedrigere Perkolationsschwelle verglichen mit der von CF beobachtet. Der Einsatz von PANI hat bis zu einer bestimmten Konzentration nur einen minimalen Einfluß auf die thermischen und mechanischen Eigenschaften des EP Systems.

In einem dritte Schritt wurden die zwei oben erwähnten, leitenden Füllstoffe gemeinsam der EP Matrix hinzugefügt. Erhöhte elektrische und mechanische

Eigenschaften wurden in diesem Fall beobachtet, wobei sich ein Synergie-Effekt zwischen den zwei Füllstoffen bezogen auf die elektrische Leitfähigkeit der Verbundwerkstoffe ergab.

Im letzten Teil dieser Arbeit fand die Anwendung von theoretischen Modelle zur Vorhersage der elektrischen Leitfähigkeit der entwickelten Verbundwerkstoffe statt. Dabei konnte eine gute Übereinstimmung mit den experimentellen Ergebnissen festgestellt werden .

List of Abbreviations and Symbols

Abbreviations

AFM	Atomic force microscopy
BF_3	Boron trifluoride
CB	Carbon black
CF	Carbon fibres
CNT	Carbon nanotubes
CSA	Camphor sulfonic acid
CT	Compact tension
DBSA	Dodecylbenzene sulfonic acid
DMTA	Dynamic mechanical thermal analysis
DSC	Differential scanning calorimetry
EB	Emeraldine base
EMI	Electromagnetic interference
EP	Epoxy resin
ES	Emeraldine salt
ESC	Electrostatic charge
ESD	Electrostatic discharge
FCM	Fibre contact model
FGM	Functionally graded material
HCl	Hydrochloric acid
IC	Integrated circuit
ICP	Intrinsically conductive polymer
INP	Interpenetrating
LCF	Long carbon fibres
LLDPE	Linear low density polyethylene
MCF	Medium carbon fibres
NCG	Nickel-coated graphite
NMP	N-methylpyrrolidone
PA	Polyacetylene

PANI	Polyaniline
PP	Polypropylene
PS	Polystyrene
PTSA	*p*-Toluenesulfonate
SCF	Short carbon fibres
SEM	Scanning electron microscopy
TEM	Transmission electron microscopy
TOM	Transmission optical microscopy
TGA	Thermogravimetric analysis
UV-vis	Ultraviolet visible

Symbols

A	[mm^2]	Surface
b	[mm]	Width
c	[1]	Material constant
D	[g/cm^3]	Density
d	[μm]	Fibre diameter
d	[μm]	Distance across the diagonal of the impression
d_c	[μm]	Diameter of the circle contact between two fibres
dx/dt	[m/s]	Radial velocity of fillers
e	[Coulomb]	Charge
E	[GPa]	Young's modulus
E_f	[GPa]	Flexural modulus
E_{total}	[J]	Total absorbed energy
E_{UH}	[GPa]	Estimated modulus by microhardness test
E^*	[MPa]	Complex modulus
F	[mN]	Load
G	[1]	Ratio of centrifugal acceleration to acceleration due to gravity
G_{IC}	[kJ/m^2]	Fracture energy
g	[m/s^2]	Acceleration due to gravity
I	[A]	Current

J	[A/mm^2]	Current density
h	[μm]	Intender penetration depth
HU	[MPa]	Universal microhardness
HV	[MPa]	Vickers microhardness
K_{IC}	[MPa·m$^{1/2}$]	Critical stress intensity factor
k	[1]	Material constant
L	[mm]	Distance between electrodes
l	[μm]	Fibre length
m	[1]	Numbers of contacts between fibres
n	[cm^{-3}]	Carrier concentration
n	[1]	Number density of particles
R	[m]	Radius of the cast tube
R_s	[Ohms]	Surface resistance
r_i	[1]	Position of the contact point i
S	[mN/μm]	Initial unloading stiffness
SE	[dB]	Shielding effectiveness
s	[1]	Dielectric critical exponent
t	[1]	Critical exponent
$tan\delta$	[1]	Mechanical loss factor
$tan\delta_{max}$	[1]	Maximum of mechanical loss factor
T	[°C]	Temperature
T_g	[°C]	Glass transition temperature
U	[V]	Potential difference
V_c	[vol.%]	Percolation threshold
V_f	[vol.%]	Volume fraction
V_p	[vol.%]	Volume fraction of fibres participating in the conductive network
V_t	[vol.%]	Filler packing fraction
W	[%]	Weight fraction
X	[1]	Function of the number of contacts between fibres
α	[1]	Aspect ratio
β	[1]	Parameter of FCM

δ	[$(J/cm^3)^{0.5}$]	Solubility parameter
ΔH	[J/g]	Heat of curing reaction
η	[Pa·s]	Viscosity
η_o	[Pa·s]	Viscosity of the neat matrix
ε^*	[1]	Complex permittivity
ε'	[1]	Dielectric constant or relative permittivity
ε''	[1]	Loss factor
ε_o	[$F \cdot m^{-1}$]	Permittivity of free space
μ	[$cm^2/V \cdot s$]	Mobility of charge carriers
ν	[1]	Poisson's ratio
ρ, ρ_f	[Ohm.cm]	Volume resistivity, filler resistivity
σ	[S/cm]	Electrical conductivity
τ	[s]	Relaxation time for decay of charge
θ	[°]	Out-of-plane orientation angle
ϕ	[°]	In-plane orientation angle
ψ	[μm]	Distance between fibre contact points
ω	[1/s]	Mould rotation rate

1. Introduction

The ability of polymers to act as electrical insulating materials is the basis for their applications in the electrical and electronic areas. There are many cases, however, where electrical conductivity in polymeric materials is needed, such as the dissipation of electrostatic charge from rubber and plastic parts, and the shielding of plastic boxes from effects of electromagnetic waves. Consequently, material engineers have tried since quite a long time to combine the flexibility of polymers with the electrical properties of metals. The advantages relate not only to the ability to produce electrically conductive materials, but also to the ability to modify the electrical characteristics within a broad spectrum.

There are a number of mechanisms by which a polymeric material can be rendered conductive. A conventional method is to cover them with a conductive surface layer. Numerous difficulties are though associated with these structures, such as limited service life of the conductive layer due to peeling, wear, lengthily processing time, and difficulty of developing parts with complicated geometry.

On the other hand, such drawbacks are not found in polymer composites containing specific conductive fillers, such as metallic powder or fibres, carbon black, and carbon fibres. A wide range of electrical conductivity can be achieved in this way, depending mostly on the concentration and type of the conductive fillers. Additionally, the conductive fillers can lead to enhanced mechanical properties of the developed composites. The critical amount of filler, necessary to initiate a continuous conductive network within the polymer matrix, is referred to as the *percolation threshold*.

Recently, a new type of organic polymers capable of conducting electricity has been developed: the intrinsically conductive polymers (ICPs). These polymers become conductive upon partial oxidation or reduction, a process commonly referred to as doping. ICPs usually exhibit poor mechanical properties, and therefore they are mainly used as conductive additives to common insulating polymers. In this way, all polymeric conductive composites can be developed, having mechanical properties close to those of the insulating polymer matrix.

The main question concerning mixtures of conductive and insulating materials, as those described above, is how the conductivity changes with the content of the

conductive filler. It is clear that the conductivity will increase only when a network of the conductive phase is formed within the insulating one. Various models have been proposed in an effort to predict the electrical conductivity of composites based on numerous factors. While all existing models are based on the filler volume fraction, there are other factors that can influence the conductivity of the composite, such as the physical properties of polymer and filler.

In common applications homogeneous conductive polymer composites are mostly requested. For specific environments though materials with different functional properties within their structure have attracted great interest. One approach to this concept is the development of inhomogeneous composites, known as functionally graded materials (FGMs), in which the filler concentration changes continuously along one direction. FGMs are of practical interest because a wide gradation of physical and/or chemical properties can be achieved across a given material, and lower concentrations of fillers are requested compared to isotropic structures. High filler loadings increase costs since filler materials are in general more expensive than the polymeric materials themselves, and since processing can be made more difficult due to a significant increase in the apparent viscosity.

The main aim of this study was the development of electrically conductive polymer composites based on an epoxy matrix. For this reason different conductive fillers were mixed with the nonconductive matrix in order to achieve various degrees of electrical conductivity. For a better overview of the behaviour of these conductive polymer composites, representatives from the categories of conductive fillers (i.e. carbon fibres) and ICPs (i.e. a polyaniline-salt) were utilized, along with a combination of them. Additionally, the concept of FGMs was applied for developing materials with graded electrical conductivity. A centrifugation method was used and graded distributions of the conductive fillers were created within the epoxy matrix. In real applications, a structural part should not only exhibit the desired electrical conductivity but also have acceptable thermal and mechanical properties. For this reason, the effect of the different conductive fillers on these properties was also studied. It was a further aim of this study to apply existing theoretical models and predict the electrical conductivity of the developed polymer composites.

2. State of the Art

2.1 The Need for Conductive Polymers

Electronic industry has experienced a remarkable growth in the recent decades. The revolution began in 1960's with the fabrication of the first integrated circuits (ICs). Since then, electronic products in the form of mobile electronic devices, desktop personal computers or large supercomputers have been pervading in our daily world. This rising amount and sophistication of electronics in everyday life makes it most important to ensure that static charges are not built up or that they are controllably dissipated, i.e. protection against electrostatic discharge (ESD), and spurious signals are kept out, i.e. electromagnetic interference (EMI) shielding. But before a problem can be solved, it should be first defined.

2.1.1 Electrostatic Discharge (ESD)

Electrostatic charge (ESC) occurs due to sliding, rubbing, or separating a material, which is a prime generator of electrostatic voltages, e.g. plastics, rubber, textile. ESD of this voltage will eventually occur via an arc or a spark when the material comes in contact with a body of a sufficient potential difference. Consequences of ESD through an electrical component can range from an incorrect reading to permanent damage resulting in costly repair or its total replacement [1].

Providing ESD protection to a device enables it to reduce a high applied voltage (up to 20.000 V) to a level where damage is not caused (often under 1 V). The rate of charge dissipation is governed by the following equation:

$$\tau = \varepsilon_o \varepsilon' \rho \qquad (2.1)$$

where is τ the time constant, called the relaxation time for decay of free charge, ε_o the permittivity of free space ($8.85 \cdot 10^{-12}$ F m^{-1}), ε' the relative permittivity of the material, and ρ the volume resistivity of the material. For metals, τ is so short that is hardly measurable (e.g. for copper is of the order of 10-18 sec), but for conventional polymers, which exhibit very high resistivities, τ can be very long. In other words, polymers can retain charges for very long periods, sometimes several years, and this illustrates an important aspect of their insulating character [2].

A material is able to protect against ESD when it is not as insulating as plastics. Moreover the material should be able to control the discharge and thus the high conductivity values of metals are also undesirable. An optimal range of electrical conductivity for such kind of applications is estimated between 10^{-9} and 10^{-6} S/cm. Practical examples where protection against ESD is required are hospital operating rooms where semiconducting walls and floors are used, and industrial environments where antistatic conveyor belts are employed to eliminate static charges [3].

2.1.2 Electromagnetic Interference (EMI)

Almost every electrical/electronic device is a source of electromagnetic signals. If intense enough, and of a frequency affecting the performance of another device, those signals are termed as electromagnetic interference (EMI). The effect of EMI can range from minor nuisance, e.g. snow on TV or hiss on radio, to serious consequences, e.g. corruption of data in large-scale computers or interruption of medical devices such as pacemakers [1,4].

In order to reduce EMI by reflection and/or absorption, shielding can be applied to different areas of the electronic equipment using conductive materials. Shielding performance is a function of the properties and configuration of the shielding material (conductivity, permeability and thickness), the frequency, and the distance between the source and the shield. The shielding effectiveness, *SE*, of a material, measured in decibels (dB), is given by the logarithmic ratio of the electric (magnetic) field with and without the shield:

$$SE = 10 \cdot \log \frac{P_1}{P_2} \tag{2.2}$$

where P_1 and P_2 denote the incident power and transmitted power, respectively. Most common EMI problems occur in the radio frequency range of the electromagnetic spectrum (1 kHz to 10 GHz). Radio frequency interference (RFI) shielding problems in this spectrum can often be solved with conductive materials having as little as 20 dB of shielding effectiveness. More sophisticating problems as those in military may require levels of 50-80 dB or higher.

In applications where EMI shielding is important, highly conductive materials are required. Theoretical estimation indicates that a moderate shielding effectiveness of around 35-40 dB requires a volume resistivity of less than 1 Ω·cm.

2.1.3 From Metals to Conductive Polymers

Metals, as inherently conductive, have been traditionally the material of choice for facing such problems. Polymers, on the other hand, classified like electrically insulating materials, have been mostly used as dielectrics or encapsulants [5]. Their low degree of conductivity make them transparent to EMI, while built-up charges tend to remain localised on their surface thus creating high ESD danger. However, polymers are desirable in many applications as they exhibit a number of advantages compared to metals. These include:

- Good physical properties, e.g. corrosion resistance,
- Low density, resulting to weight reduction,
- Low cost versus life,
- Ease of shaping, etc.

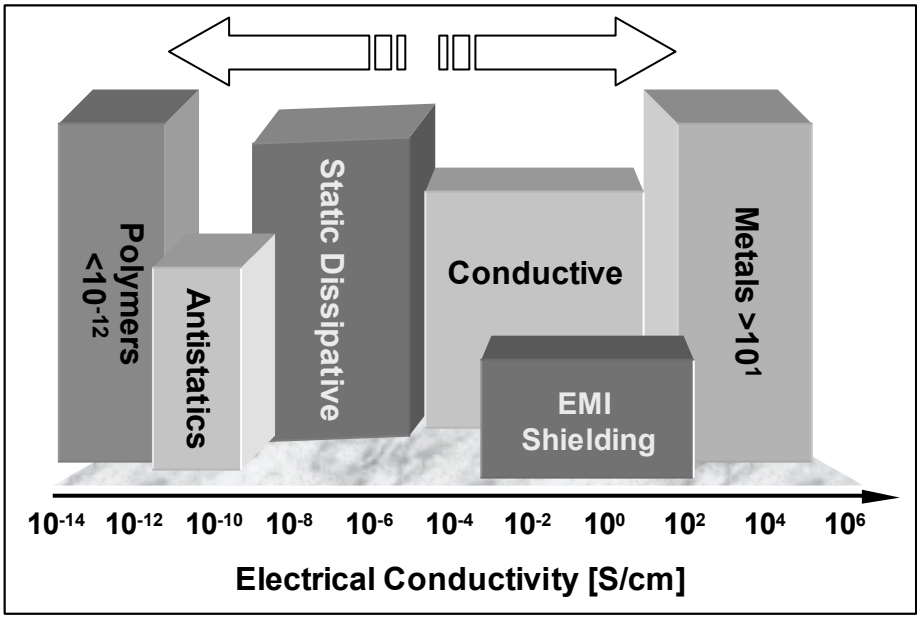

Figure 2.1: Schematic presentation of material categories between polymers and metals, regarding their degree of electrical conductivity.

Furthermore, there has been a demand of materials which can fill the electrical conductivity gap between the insulating polymers and the highly conductive metals

(Figure 2.1), and whose electrical properties can be tailored to the target value. All these factors and considerations have led to a tremendous interest in developing electrically conductive polymer composites.

2.2 Electrically Conductive Polymers and Polymer Composites

2.2.1 Conductive Coatings

A traditional way to obtain polymer parts suitable for electrical applications is applying a conductive coating on their surface. The three most popular conductive coatings in the electronic industry today are electroless plating, vacuum plating, and conductive paints [6,7].

- Electroless plating starts with etching the plastic, then immersing it in a fluid, where the plating materials, usually copper, bonds to the plastic. This is usually followed by an overcoat of nickel to provide corrosion resistance. The result is a highly conductive, stable and durable surface. This process is limited to those plastics that can be etched.
- During vacuum plating a treated plastic is placed in a vacuum chamber where a metal, usually aluminium, is evaporated on to the plastic. It is the most environmentally friendly process as no solvent is needed and no harmful products are produced. The coatings have a smooth metallic appearance and are highly ductile. Vacuum plating can been done on a variety of plastics.
- Conductive paints are the mixture of a conductive phase with a nonconductive carrier. Almost any metal can play the role of conductive part, with most common copper, nickel, silver, and their combinations. They have lower conductivity than the other types of coatings, depending mainly on the contacts of many small conductors with each other. They are applied in the same manner as common paints, using a spray gun or even a brush, and can be applied to any surface that can accept paint.

As it can be figured out from the short description of the above techniques, the application of a conductive coating consists an extra step in processing conductive polymers in this way. Therefore, this technique exhibits a disadvantage of time

consuming and high cost. Moreover, conductive coatings often show serious shielding performance problems, e.g. due to scratches on the coating, delamination during thermal cycling or other adhesion problems. The use of conductive coatings includes also many limitations to the shape and size of the polymer parts.

2.2.2 Conductive Fillers

Another method to develop conductive polymers, which can avoid the problems existing in coated structures mentioned above, is to incorporate fillers of high intrinsic conductivity into the conventional polymers. This concept originated from the conductive rubber filled with carbon black in the latter part of the 19^{th} century [8]. A lot of publications dealing with heating elements developed from conductive polymers began to appear around 1940. Since the 1950s systematic attempts have been made to employ conductive fillers, such as metal powders, foils and fibres, having mostly as goal the enhancement of the mechanical performance of polymers. Conductive polymer composites were not highly investigated and commercialized until the late 1960s, when the electrical/electronics industry boomed.

It is well known that polymers containing electrically conductive fillers exhibit a distinctive dependence of conductivity on filler volume fraction, i.e. a polymer composite can change from insulator to semiconductor or conductor over a very narrow range of filler concentration. A degree of conductivity is achieved when the concentration of the fillers is high enough in order to form a conductive network within the polymer matrix. At low filler concentrations the fillers are distributed homogenously in the insulating matrix and no contacts between adjacent filler particles take place. At a critical concentration, which is called the percolation threshold, V_c, each filler makes contact with at least two neighbouring fillers [2,8,9]. Due to the formation of continues conductive pathways, the electrical conductivity of the composite increases sharply by many orders of magnitude when this percolation threshold value is reached. Once the first conductive network is developed, the electrical conductivity increases slowly by further addition of fillers. This can be explained with a slightly improved quality of the conductive network. This trend is displayed in Figure 2.2, which shows the three main regions of a typical conductivity curve of a composite material.

Electrical conduction in materials can occur through the movement of charge carriers according to the following equation [2]:

$$\sigma = e \cdot n \cdot \mu \tag{2.3}$$

where σ is the conductivity, *e* the charge, η the carrier concentration and μ the mobility of the carriers. In the electrical conductive polymers, the formation of a conductive network, and the nature, concentration, and mobility of the charge carriers depend strongly on the filler characteristics, such as filler type, geometry and morphology, their distribution, and the processing conditions [3, 8-10].

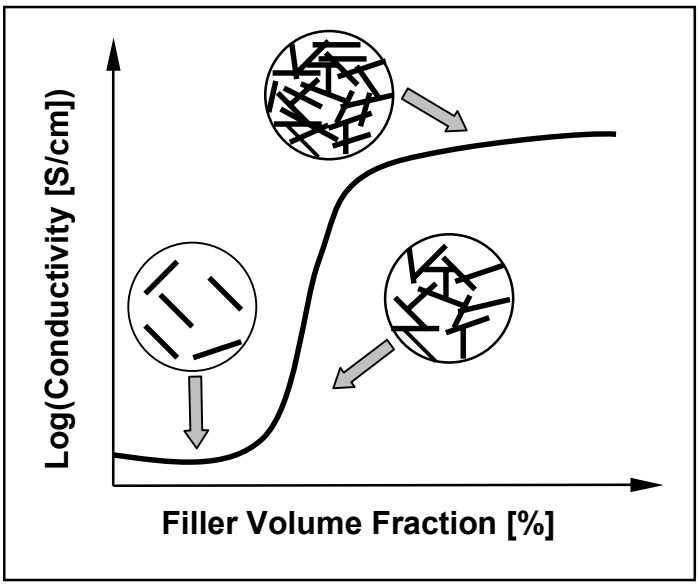

Figure 2.2: Dependence of electrical conductivity on the filler volume fraction.

Different types of conductive filler materials in various geometrical forms, such as particulate, flake and fibre, are available for developing conductive polymer composites [9,10]. The inherent conductivity of the fillers controls the upper bound of the percolation curve. Conductive fillers can be divided into two basic types based on their action in the composites, i.e. enhancing and additive type [10]. The first category includes fillers such as carbon fibres (CF), graphite fibres and stainless steel fibres, which can lead to both increased electrical and mechanical properties of the polymer matrix. Additive type fillers such as carbon black, aluminium flakes and copper powders generally lower the strength performance of the base polymer.

2.2.2.1 Types of Conductive Fillers

Carbon blacks (CB) have been widely employed as conductive fillers in plastics [11-14]. Commercial conducting composites using these fillers are the most popular in practical applications because of the enhanced electrical conductivity and cost effectiveness. The high surface area of conducting CB facilitate the contact probability of aggregated CB by decreasing the particle-to-particle distance. Generally, addition of CB leads to reduction of the mechanical and physical properties. The excessive sulphur contained in some CB may also corrode the electrical contacts. Another drawback of CB lies in the fact that carbon powders may come off the product surface and this could be catastrophic in certain applications.

The use of fibres of carbon and graphite in making conductive polymer composites has been also of great interest [15-19]. Both pitch- and PAN-based carbon fibres (CF) or graphite fibres provide uniform conductivity and significant mechanical improvement [18]. Due to their high aspect (length/diameter) ratio, usually a lower loading of fibres, compared to conductive particles, is necessary for achieving the desired levels of conductivity. Nickel-coated graphite (NCG) fibre is a version of modified graphite fibre with greatly increased electrical conductivity, which combines lightweight, high strength and modulus of the core fibre with the high electrical conductivity of the nickel coating [20]. The conductivity of carbon fibre can also be improved by electroplating a thin layer of nickel on its surface. Nickel-coated CF provide more effective EMI shielding and allows the use of a lower fibre concentration compared to common CF [21]. The major disadvantage of these kind of fibres relates to its reduced reinforcing efficiency. Stainless-steel fibres are not so brittle as the CF but they are more inclined to curl during processing. They exhibit lower percentage loadings compared to CF: for ESD, about 3-5 wt.%, and for 30 to 50 dB shielding, 5-7 wt.%.

Metallized microballons are also available from several suppliers, as well as copper and aluminium particles and flakes, with silver metallization [22]. The main disadvantage of these kind of fillers is the inevitable high loadings resulting from their low aspect ratio. Metallized microballons are mainly used in thermosets, as they

would not withstand thermoplastics processing. Typical loading for ESD protection is 10-15 wt.%, while for EMI applications at least 40 wt.% is needed.

Lately, the carbon nanotubes (CNT) have been used as electrically conductive fillers. CNT have extremely small size and a high aspect ratio. The percolation threshold was determined to be between 0.02 and 0.04 wt.% for untreated catalytically grown CNT in epoxy matrix [23].

2.2.3 Intrinsically Conductive Polymers

Intrinsically conductive polymers (ICPs) are a different class of materials from the conductive polymer composites described in the above paragraph, which are merely a physical mixture of an insulating polymer matrix with conducting fillers. Polyacetylene (PA) was the first organic polymer, which, in 1977, became intrinsically conductive, by a process called “doping” [24]. The doped form of polyacetylene had a conductivity of 10^5 S/cm, which was higher than that of any previously known polymer. As a comparison, teflon has a conductivity of 10^{-16} S/cm and silver and copper 10^8 S/cm.

ICPs tend to have the electrical, magnetic, and optical properties of a semiconductor or metal and, on the other hand, polymeric properties such as low density and processibility [25]. The discovery of the “metallic” polyacetylene was followed by the discovery of a whole group of similar conductive polymers. Many other polyaromatic-based polymers showed the same electrical properties: polypyrrole, polythiophene, polyaniline (PANI) and others. The chemically repeated units of these polymers are shown in Figure 2.3. For the discovery and development of these new polymers Drs. A.J. Heeger, A.G. MacDiarmid, and H. Shirakawa were awarded the Nobel Prize in Chemistry in 2000.

The common electronic feature of undoped conductive polymers is the π-conjugated system, which is formed by overlap of carbon p_z orbitals and alternating carbon-carbon bond lengths [25-27], as shown schematically in Figure 2.4. However, the conjugated double bonds are not enough for achieving advanced electrical properties. The conductivities of the ICPs are transformed from insulating to

conductive through doping, which is a redox process [25-28]. Oxidation via *p*-type (electron accepting) dopants or reduction via *n*-type (electron donating) dopants of the chain, by chemical or electrochemical means, results in the formation of a charge-transfer complex, with stacks or sheets of counterions along the polymer chain. In this way, high levels of conductivities are achieved.

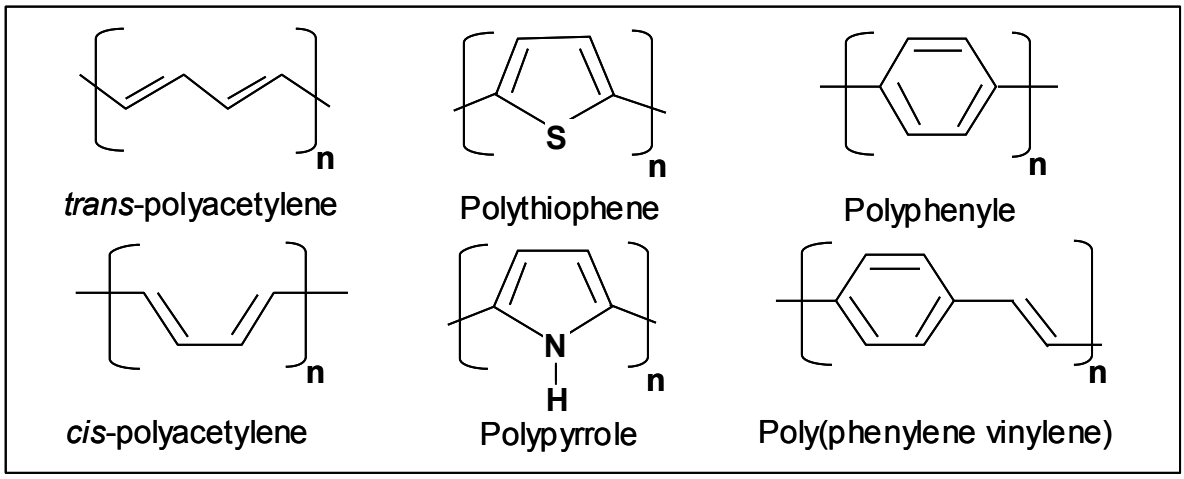

Figure 2.3: Repeat units of some conjugated polymers.

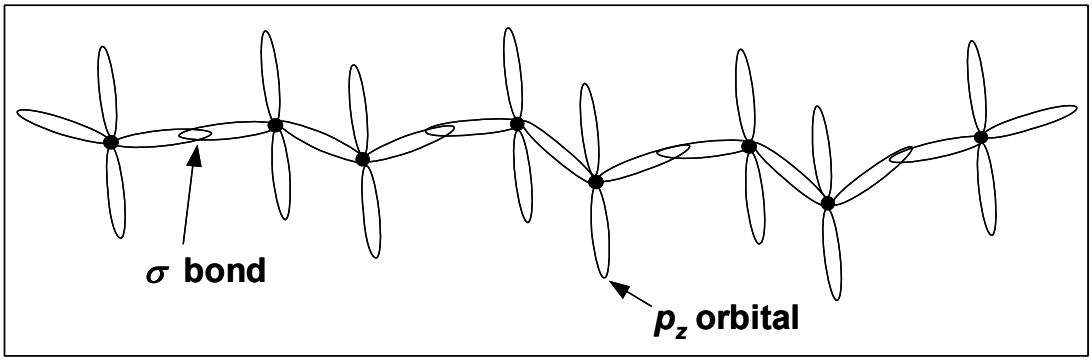

Figure 2.4: Schematic view of the carbon backbone of *trans*-polyacetylene showing the σ bond formed by the overlap of the sp^3 orbitals of adjacent carbon atoms, and the p_z orbitals which form the π- and π^*-bands that give rise to the electronic properties of semiconducting and metallic states of polymers [27].

2.2.3.1 Polyaniline (PANI)

PANI is one of the most promising candidates among the ICPs. It is a relative old material, but it had been not intensively studied until the discovery of polyacetylene resurge the interest in conductive polymers. PANI exists in three different oxidation

states: leucoemeraldine (fully reduced), emeraldine base (EB, partially-oxidized) and perigraniline (fully oxidized) (Figure 2.5) [25-29]. In contrast to the *n*- and *p*-type doping process applied to polyacetylene, polypyrrole, leucoemeraldine base etc., the EB form of PANI, can be rendered conductive by a non-redox process [25-29]. In this protonation process, EB is treated with a protonic acid, e.g. dodecyl benzene sulfonic acid (DBSA) and camphor sulfonic acid (CSA), leading to a nine- or ten-order of magnitude increase in conductivity. The resulting material is called emeraldine salt (ES).

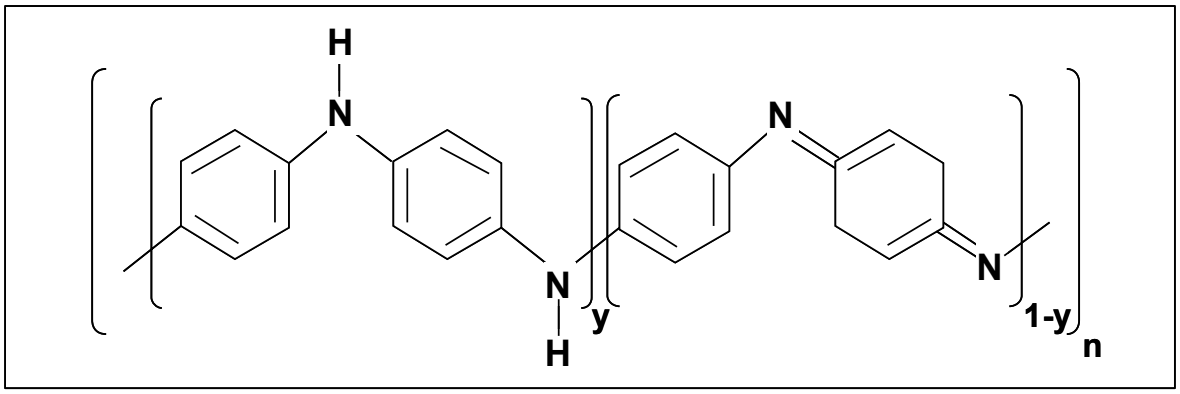

Figure 2.5: Polyaniline: leucoemeraldine (y=1), emeraldine (y=0.5), and penigraniline (y=0).

During the protonation process, no addition or removal of electrons takes place but the conductivity is achieved by a internal redox reaction [29-31]. Figure 2.6 shows schematically the protonation of EB to form the conductive ES. Initially, the hydrogen ions from the acid attach themselves to the quinoid nitrogen atoms. Due to the high energy of these structures, they are extremely unstable. As a consequence, the C==N bonds of the quinoid imine structure break transforming the quinoid ring into a more stable benzenoid ring with lower energy, thus creating the bipolaron structure of doped PANI. The new benzenoid ring, although more stable than previously, still has relative high energy due to the repulsion forces from the adjacent positive charges. In order to stabilize this structure, the positive charge of one of the hydrogen ions attracts electrons from the neighbouring benzene ring therefore neutralizing the charge. This creates a new positively charged nitrogen group with a neutral nitrogen atom between the two positive ones. The increased distance between the two positive charges results in the polaron structure, which has a lower energy level than

the bipolaron one. Doping by protonation can be reversed by treatment with a base [28].

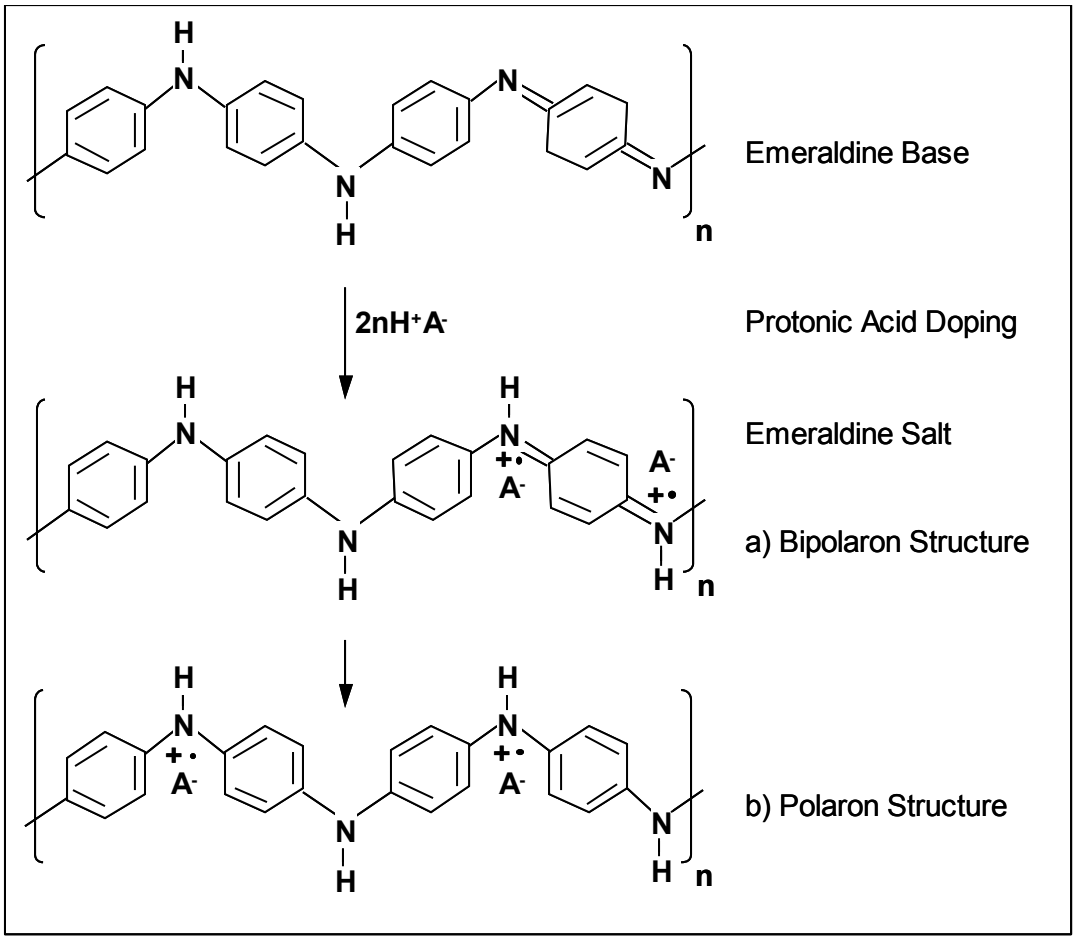

Figure 2.6: Schematic presentation of the emeraldine base form of PANI by protonic acid.

When functionalized protonic acids are used as dopants, protonation of high molecular weight PANI can be achieved and, additionally, the resulted conductive form of PANI can be solved in many common nonpolar or weakly polar organic solvents [32,33]. A functionalized protonic acid can be denoted as $H^+(M^-R^-)$, where the counter-ion species (M^-R^-) contains the functional group R that can be chosen to be compatible with nonpolar or weakly polar organic solvents. The ability to achieve conductive PANI complexes, which are soluble in common organic solvents, gives the opportunity to create a variety of conductive polyblends where PANI is mixed with bulk polymers [33]. The ideal case would then be the existence of a solvent in which both the conductive PANI complex and the polymer are soluble.

2.2.3.2 Polyaniline-Blends with Polymers

PANI in the form of electrically conductive salt has poor mechanical properties and that makes it inappropriate for many applications. In order to overcome this difficulty, PANI-blends with different polymers can be developed, via solving, mixing or melting procedures. This way, materials with desirable electrical and mechanical properties can be designed.

PANI-blends with different thermoplastics have been intensively investigated. In most studies these blends were prepared in solution [33,34] or by melt processing [35-36] using various polymer matrixes, such as polypropylene (PP) [37], polycaprolactone (PCL), polystyrene (PS), and linear low-density polyethylene (LLDPE). In both cases an additional amount of the functionalized acid (plasticizer) is usually essential in order to enhance the solubility or the processibility of the conductive salt. Several factors affect the percolation behaviour of the blends and the viscosity of the matrix polymer, e.g. the level of the plasticizer in the PANI-salt.

The trend of ICP-blends has also been recognized by manufacturers, who are actively investing in order to move ICPs from the laboratories to the industry. For example, at the annual European conference “Commercializing Conductive Polymers”, which takes place since 2002, innovative commercial applications of ICPs are discussed among some leading companies [38]. Recently, the RTP company was the first material supplier who commercially manufactured melt-processable ICP thermoplastic compounds. In order to cover the needs of its clients, RTP has used these compounds for developing electronic packaging for dissipating static charges [39], and carriers for wafer transport [40].

Limited research has been made in the field of PANI blends with thermoset polymers and more specifically with epoxy resins. Nevertheless, the few studies which can been found in the literature on this subject show quite promising results. Peltola et al. [41] prepared electrically conductive epoxy adhesives based on PANI-CSA, which showed conductivities in the antistatic range (10^{-8}-10^{-3} S/cm) with less than 2 wt.% of the conductive salt. An alkyl-substituted phenol was used as solvent for the PANI-salt in order to form a low viscosity solution. However, this system was found to be highly

plasticized due to the relatively large amount of alkyl phenol present in the blend. A patent introduced by Laasko et al. [42] was directed towards a method of producing electrically conductive thermoset mixtures. According to this invention, different thermosets e.g. phenol-formaldehyde resin, melamine-formaldehyde resin or polyester resin, could be converted into electrically conductive materials by using a conductive component of polyaniline that is protonated by a protonic acid containing at least one hydroxyl group. Protonated polyaniline with such acids was able to act in the thermoset composition not only as a conductive component, but also as a curing agent. Particularly, phenol-4-sulphonic acid protonated PANI was easily dissolved in resin, resulting to homogeneous and uniform thermoset compositions.

Aiming to similar results, i.e. electrically conductive thermoset compositions, researchers have directly mixed epoxy resin and polyaniline protonated with different acids, such as *p*-toluenesulfonate (PTSA), hydrochloric acid (HCl), and DBSA [43-45]. The percolation values in these cases were at concentrations above the 15 wt.% of the conductive polyaniline salt. Another interesting approach was attempted by Wang et al. [46] on the synthesis of conducting semi-interpenetrating (INP) network composites from polyaniline doped with acidic phosphate ester and melamine-urea resin. A perfect network of the polyaniline salt in these composite was observed, and the percolation threshold of the system was about 1.86 wt.% of the polyaniline salt. An overview of these previous efforts, together with a few others that can be found in the literature [47,48], show that many parameters are responsible for the properties of the developed polymer composite, such as the dopant of polyaniline, the epoxy system, and the mixing procedure. However, the curing of an epoxy system is itself a complicated procedure, which can easily affect as well as be affected by the presence of the polyaniline salt.

2.2.4 Modelling Aspects for Conductive Polymer Composites

Whether the conductive additive in the insulating polymer matrix is a conductive filler, as those described in paragraph 2.2.2.1, or an ICP, as discussed in paragraph 2.2.3.2, both cases represent a mixture of an insulating and a conductive phase. With respect to the mechanisms of conductivity in such mixtures, usually two scenarios

can be considered. One deals with the formation of the conductive network within the polymeric matrix, and the other examines the movement of charge carriers along these pathways. Both mechanisms are closely related to the concentration of the conductive fillers.

Generally the transition in conductivity is attributed to the percolation phenomenon, which is based on the fact that the conductive fillers are able to come in contact with each other when the filler content exceeds the percolation threshold value, as it was mentioned in paragraph 2.2.2. It has been experimentally proved that the critical filler content depends upon the structure, inherent conductivity, geometry, and distribution of the fillers in the polymer. Further factors are the rheology and the thermal behaviour of the polymer, and the thermodynamic interaction between filler and polymer. Hence, many researchers have tried to predict the critical filler concentration and the electrical conductivity based on these aspects. The models found in the literature can be divided into four main categories: statistical, thermodynamic, geometrical, and structure-oriented. A few examples of each category are summarised in this section. For a more detailed review of available models one can refer to the work of Lux [49] and Clingerman [50].

2.2.4.1 Statistical Percolation Models

A persuasive theoretical approach used to study the percolation behaviour of an insulating polymer containing random distributed conductive fillers has been developed by Kirkpatrick [51] and Zallen [52]. According to the theory, a composite is regarded as a lattice of conductive phases joined by resistive bonds and the conductivity of the composite above the percolation threshold follows a power law dependence of the form:

$$\sigma \propto (V_f - V_c)^t, \text{ for } V_f > V_c \qquad (2.4)$$

where σ is the conductivity of composite, V_f the filler volume fraction, V_c the percolation threshold, and t a critical exponent, depending on the dimension of the lattice. For statistically distributed ideal spherical mono-dispersed particles that are non-interacting with the polymer matrix the theoretical values of V_c and t are equal to 0.16 and 1.6, respectively. However, attempts to use the statistical percolation

approach for the description of real binary mixtures has concluded that these theoretical values of the critical parameters (i.e. t and V_c) are not in agreement with the experimental ones. The disagreement is due to the fact that the conductivity is significantly influenced from the geometric parameters of the fillers, the quality of their contacts, and the interactions between the matrix and the fillers. These facts have not been taken into account in the purely statistical percolation theory. The particulate-filled composites, such as those reinforced with CB and silver particles, have resulted in t values ranging from 1.5 to 2.0. For samples reinforced with fibres, t values as high as 3.1 have been determined, due to the greater aspect ratio of fibres compared to particulate fillers.

2.2.4.2 Thermodynamic Models

The surface properties of the polymer and filler are parameters, which also affect the conductivity of the composite by influencing the interaction between them. How well the polymer wets the surface of the filler can be quantified by the difference between the surface energies of the two materials. Smaller differences between the two surface energy values lead to a better wetting of the fillers by the polymer matrix. Better wetting corresponds to larger amounts of polymer covering the filler surface and finally to an advanced distribution of the fillers in the matrix. This will increase the percolation threshold and the resistivity of the composite, as larger concentration of fillers will be needed before the particles will come in contact with each other. Therefore, a slightly larger difference between the surface energy of the two materials is desirable.

Sumita et al. [53] and Wessling et al. [54] proposed thermodynamic percolation models for the cases where CB and ICP were used as conductive additives in polymers, due to the serious disagreements between the experimental results and the predictions of the statistical percolation models. Both models emphasize the importance of the interfacial interactions at the boundary between the individual filler particles and the polymer for formation of the conductive network. As a consequence, these models interpret the percolation phenomenon as a phase separation process. The experimental results of these researchers were in agreement with the predictions of the models. Furthermore, Mamunya et al. [55] evaluated the influence of factors

such as the filler and polymer surface energies and the polymer melt viscosity on the conductivity of polymer composites. The calculated values also showed good agreement with the experimental data for a number of different polymers filled with CB [55].

2.2.4.3 Geometrical Percolation Models

This class of percolation models was proposed in order to explain the percolation phenomenon in different dry-premixed, non-sintered structures of mixtures of conductive and insulating powders. A well-known model in this class is the one proposed by Malliaris and Turner [56]. There are two equations used to predict two volume fractions: one to calculate the percolation threshold and the other for the volume fraction at the end of the conductivity increase. These equations use the diameter of the particles, the probability for the occurrence of infinitely long bands of conductive particles on the surface of the insulating particles, and the arrangement of the conductive particles on the surface of the insulating ones. Comparison of experimentally determined percolation values with predicted ones using this approach showed that the assumptions of this model were not sufficient to predict the percolation concentrations in conductive binary mixtures. Bhattacharya and Chaklader [57] proposed an enhancement of the above model, but the disagreements were still typically $\pm$ 15%-20% (with respect to the experimental value).

2.2.4.4 Structure-Oriented Models

The physical construction of composites is the basis for the prediction of their electrical conductivity according to the structure-oriented models. The electrical properties of composites are affected by its final structure, and in consequence by the filler's aspect ratio, orientation and contacts to each other. Taking this idea in consideration, Weber and Kamal [58] constructed a fibre-contact model (FCM) for the prediction of the volume resistivity in fibre reinforced composites. The final equation is:

$$\rho = \frac{\pi d^2 \rho_f X}{4 V_p d_c l \cos^2 \phi} \tag{2.5}$$

where ρ is the composite volume resistivity, ρ_f the filler resistivity, d the fibre diameter, l the fibre length, d_c the diameter of circle of contact, X a function of the number of contacts m, and V_p the volume fraction of fibres participating in strings. A good agreement between the prediction of this model with experimental results was found for polypropylene composites reinforced with nickel-coated graphite fibres [58] and with polyaniline and carbon fibres [59]. Further reference to this model takes place within Chapter 5 and in Appendix.

2.3 Functionally Graded Materials

2.3.2 Demand for New Functional Materials

In recent years the environments in which materials are used have become more demanding. Therefore the development of new materials that can withstand certain conditions and exhibit specific properties is of great importance. In developing such materials two different avenues can be followed. One path is the design of materials that differ totally from those that already exist. The other one is to invoke new functions for already existing materials.

A general requirement for industrial materials is uniformity in material properties. The requirements for homogeneous conductive polymer, as those mentioned in paragraphs 2.2.2 and 2.2.3, are no exception. For this reason, most effort in polymer composites in the past has been put into determining how to uniformly mix the additives in the matrix. From a macroscopic point of view (Figure 2.7a) these materials are regarded as homogeneous because their mechanical properties and other characteristics do not change within the samples (as functions 1. and 2. different material properties can be assumed, such as Young's modulus, electrical conductivity, thermal expansion coefficient, regarding the type of materials A and B).

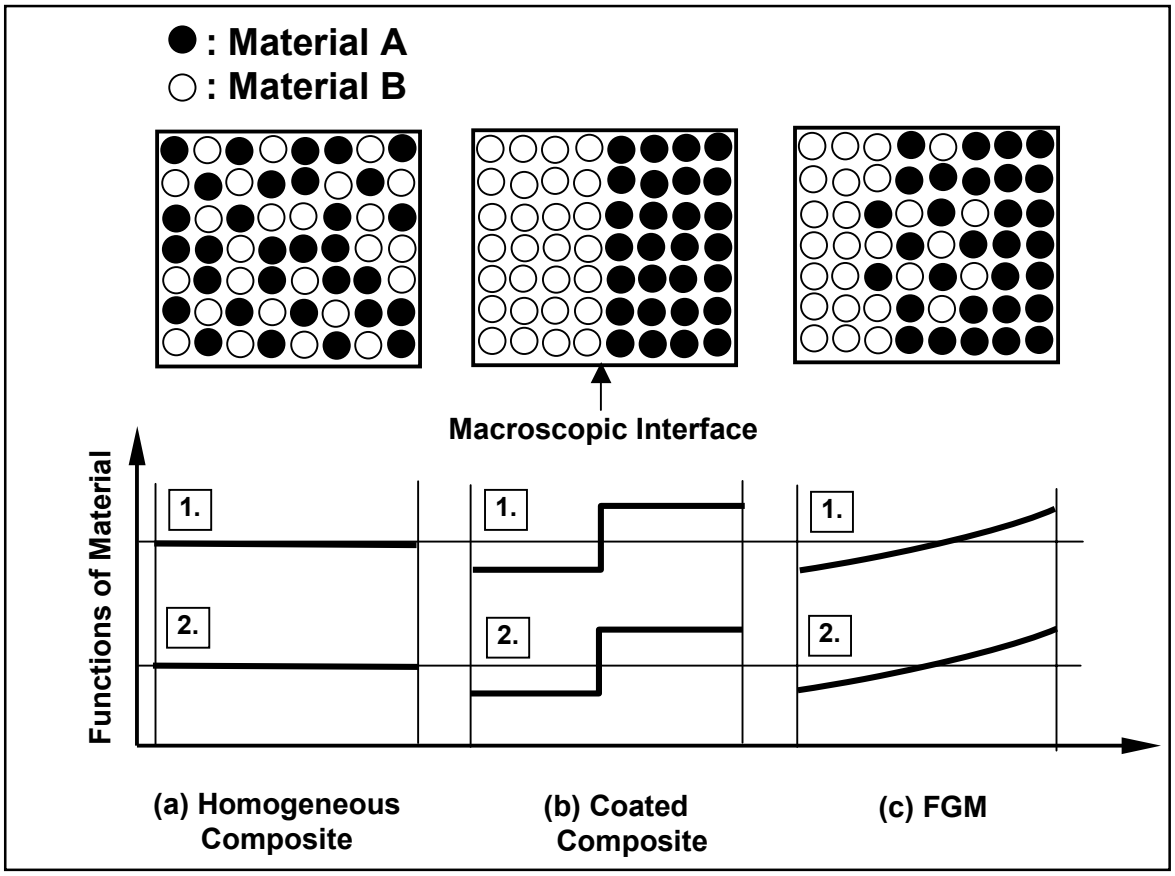

Figure 2.7: The compositional and functional differences between conventional composites and FGM`s [61].

In contrast, studies are also being done to design materials that have different functions within their structure. An example of such a material is coated structures as those mentioned in paragraph 2.1.1. However these inhomogeneous materials process sharp boundaries, as shown in Figure 2.7b. The boundary exhibits often various undesirable properties caused by the existence of discontinuities in the material's mechanical, physical, and chemical characteristics at the boundary. For these reasons a new class of materials aimed at eliminating the macroscopic boundary has been proposed : the *functionally graded materials* (FGMs) [60,61].

2.3.2. Characterization of Functionally Graded Materials

FGMs are materials in which the composition and/or the microstructure varies in one specific direction, resulting in corresponding changes in the properties of the material [60-62] (Figure 2.7c). Those gradients in the material properties are engineered,

meaning intentionally altered and quantitatively controlled in order to achieve improvement in mechanical or other properties of the final component. The concept of FGMs originated in Japan in 1987 in the form of a proposed thermal barrier material capable of withstanding a surface temperature of 2000 K and a temperature gradient of 1000 K along a length of less than 10 mm.

Following this first step, the FGM research area has been spreading into the fields of mechanical, electrical, nuclear, and optical applications as well, where gradients of other properties become important [63,64]. For example, Nishida [65] designed and fabricated a new composite dielectric substrate, in which the external part was designed with low conductivity while the internal part was conceived with a high conductivity area. Such graded substrates allow minimization of long-frequency signal loss, while ensuring the availability of a large substrate width for circuit printing. Furthermore, FGM concept is actively extended from ceramic/metal materials, where it was initially introduced, to organic composite materials.

There are several approaches to attain graded compositions. Gases, liquids, and solids can be used as starting materials to be treated either physically or chemically to obtain the desired distribution. Specifically, for the preparation of bulk continuous FGMs, some of the methods reported in the literature are controlled powder mixing, electrophoretic deposition, slipcasting, sedimentation forming and centrifugal forming [60].

2.3.3 The Centrifugation Method

In the centrifugation method, a centrifugal force is applied to a mixture of a liquid phase with solid particles. The particles are arranged gradually along the radial direction (centrifugal direction) due to the density difference between the matrix and the fillers. The centrifugal technique has already been applied to aluminium alloy melts containing ceramics particles, and alumina fibres [66], as well as to epoxy resin containing carbon fibres [67,68].

Although the centrifugal method has the advantage of possible application to mass production, accurately controlling and understanding the distribution of particles remains a difficulty. The motion of solid fillers in viscous liquid under centrifugal force can be determined from Stoke's law [69,70]. The radial velocity of fillers, *dx*/*dt*, can be expressed as:

$$\frac{dx}{dt} = \frac{\left|\rho_f - \rho_m\right| G g d^2}{18\eta} \tag{2.6}$$

where ρ_f is the density of the filler, ρ_m the density of the matrix, *d* the filler diameter, η the apparent viscosity, and *g* the acceleration due to gravity. The *G* parameter is given by the equation:

$$G = \omega^2 R / g \tag{2.7}$$

where *R* is the radius of the cast tube (m), ω the mould rotation rate (1/s).

It is known that the viscosity of a suspension becomes higher when the number of fillers in it is increasing. The Brinkmann equation [71] expresses this change in viscosity as:

$$\eta = \frac{\eta_o}{\left(1 - \frac{V_f}{V_t}\right)^{2.5}} \tag{2.8}$$

where η_o is the viscosity of the liquid matrix without fillers, V_f the filler volume fraction, V_t the maximum packing fraction.

Substituting Equation (2.7) into Equation (2.6)

$$\frac{dx}{dt} = \frac{\left|\rho_f - \rho_m\right| G g \left(1 - \frac{V_f}{V_t}\right)^{2.5} d^2}{18 \cdot \eta_o} \tag{2.9}$$

Based on this equation, attempts have been made to study and simulate the motion of fillers in a liquid matrix under centrifugal force [69,72]. The results of the simulations were in reasonable agreement with the experimental data.

3. Objectives of the Study

In Chapters 1 and 2 the need for the development and use of electrically conductive polymer composites was presented. Forced from this need, polymers have long since exceeded the limits of insulating applications and broadened their use in fields where traditionally only metals were occupied.

In Chapter 2 the different ways for developing conductive polymer composites were reviewed. It was shown that the most promising manufacturing method for this kind of materials comprises of the addition of conductive fillers in the insulating polymer matrix. For this purpose traditional conductive filler such as carbon fibres (CF) can be used as well as ICPs, i.e. polyaniline. In both cases, the creation of a conductive network within the polymer matrix is desired in order to observe increasing electrical conductivity. Each type of conductive additives has different properties and therefore different impact on the electrical and mechanical properties of the resulting polymer composites. In the frame of this work, various CF, a polyaniline (PANI) salt and a combination of them were studied as conductive additives in an epoxy (EP) matrix, for the purpose of a better understanding of the behaviour of the different conductive fillers.

The concept of FGMs was introduced in paragraph 2.3 and their unique properties compared to the traditional homogeneous composite materials were shortly characterised. As it can be observed from Figure 2.7, FGMs exhibit some similarities to the coated structures, which are usually used for ESD and EMI applications. However, FGMs due to their graded microstructure are able to avoid problems of discontinuities present in coated structures. In this way, FGMs containing conductive fillers could be a promising alternative to the conductive coatings. In order to realise this concept, a centrifugation method was used in this study for creating graded distributions of the conductive fillers within the EP matrix.

Based on the above background and ideas, the present work was divided into three parts concerning the type of conductive filler used. The main concerns and aims for each part are summarised in the following paragraphs.

Carbon Fibres

In the case of CF, more effort was made to develop gradients in the fibre distribution within the EP matrix, and study the functional properties of the resulted graded materials. The more important points under investigation for this part of the work were:

- To investigate the influence of different processing parameters, i.e. centrifugation speed, and fillers characteristics, i.e. aspect ratio, on the developed graded distributions.
- To study the affect of the CF aspect ratio on the electrical conductivity of the materials.
- To determine the possible gradients in the electrical and mechanical properties of the graded materials and examine any correlation between them.

Polyaniline

As it was mentioned in section 2.2.3.2, PANI-salts have been mostly used as conductive fillers in the case of thermoplastic matrixes, and only few attempts have been made to incorporate PANI-salts in thermosets. Aiming to bring more light in this field, this work dealt with the use of a PANI-salt as conductive filler for an EP matrix. Most attention was paid to:

- The development of an appropriate process for the preparation of PANI-salt blends with EP.
- The compatibility of a PANI-salt with the EP system.
- The effect of PANI-salt on the curing of the EP system.
- The influence of PANI-salt on the thermal, electrical, and mechanical properties of the blends.

Combination of Carbon Fibres and Polyaniline

Clearly there is no limit in the use of only one conductive filler in a polymer composite. Therefore in the present work the two previously described fillers were conjointly added in the EP matrix. Topics that were systematically examined were:

- The effect of CF on the thermal, mechanical and electrical properties of the EP/PANI-salt blends.

- A possible synergy effect between the PANI-salt and the CF regarding the electrical properties of the materials.
- The creation of gradients in the conductive fillers distributions, and consequently in the functional properties of the materials, by the use of centrifugation method.

A critical question for designing conductive polymer composites is how the electrical conductivity changes with the content of the conductive filler. For this purpose various models can been found in the literature, which attempt to predict the electrical conductivity of composites based on numerous factors (cf. paragraph 2.2.4). It was therefore a further aim of this study to apply different models to the developed conductive polymer composites described above, and compare the predicted values with the experimental data. This part of the research was mainly focused on the structure-oriented models, since they can better describe the conductivity versus filler concentration curves.

4. Experimental

4.1 Materials

4.1.1 Epoxy System (EP)

The epoxy system used for the fabrication of the CF/EP samples consisted of a mixture of bisphenol A and bisphenol F epichlorohydrin epoxy resin (Harz L, R&G Faserverbundwerkstoffe, Germany) and an amine curing agent (Härter L, R&G, Faserverbundwerkstoffe Germany). The density of the cured epoxy system was 1.16 g/cm^3. For the development of conductive blends with the polyaniline salt, a bisphenol F epichlorohydrin epoxy resin (Epikote 826, Resolution Performance Products, Nederland) was chosen. Different curing agents were tested for the polymerization of these blends since the nature of the hardener was found out to influence greatly the final electrical properties of the cured samples. The properties of each curing agent and its compatibility with the polyaniline salt is discussed in detail in section 5.2.1.

4.1.2 Carbon Fibres (CF)

In order to investigate the effect of the different aspect ratios on the electrical conductivity and the formation of the graded structures, three different types of pitch-based carbon fibres were tested. In Table 4.1 the properties of these fillers are summarized (S-, M-, and L-, denote small, medium, and large CF, respectively).

4.1.3 Electrically Conductive Polymer

From the category of intrinsically conductive polymers, a conductive polyaniline-dodecylbenzenesulfonic acid (DBSA) salt was selected (Panipol F, Panipol Ltd., Finland). The doping was made in a molar ratio of 1 to 1.1 to polymer repeat unit PhN (overdoped state). The density of this PANI salt was evaluated at about 1.0-1.1 g/cm^3. Its physical form was green, dry powder, and its pH value 2-3. The producer specified the decomposition temperature at around 200°C. The electrical conductivity of the PANI-DBSA powder was measured on thin pellets produced under high

pressure, and it was determined at 1 S/cm. Figure 4.1 compares scanning electron micrographs of the PANI-DBSA powder and the MCF.

Table 4.1: Specific properties of CF.

	SCF	**MCF**	**LCF**
Brand Name	M101 S	M107 T	DONACARBO S246
Manufacturer	Kureha Chemicals Japan	Kureha Chemicals Japan	Osaka Das Japan
Density [g/cm^3]	1.65	1.65	1.65
Length [μm]	130	700	1200
Diameter [μm]	14.5	18	13
Elastic Modulus [GPa]	32	32	40
Tensile Strength [MPa]	720	720	800
Electrical Conductivity [S/cm]	67	67	100

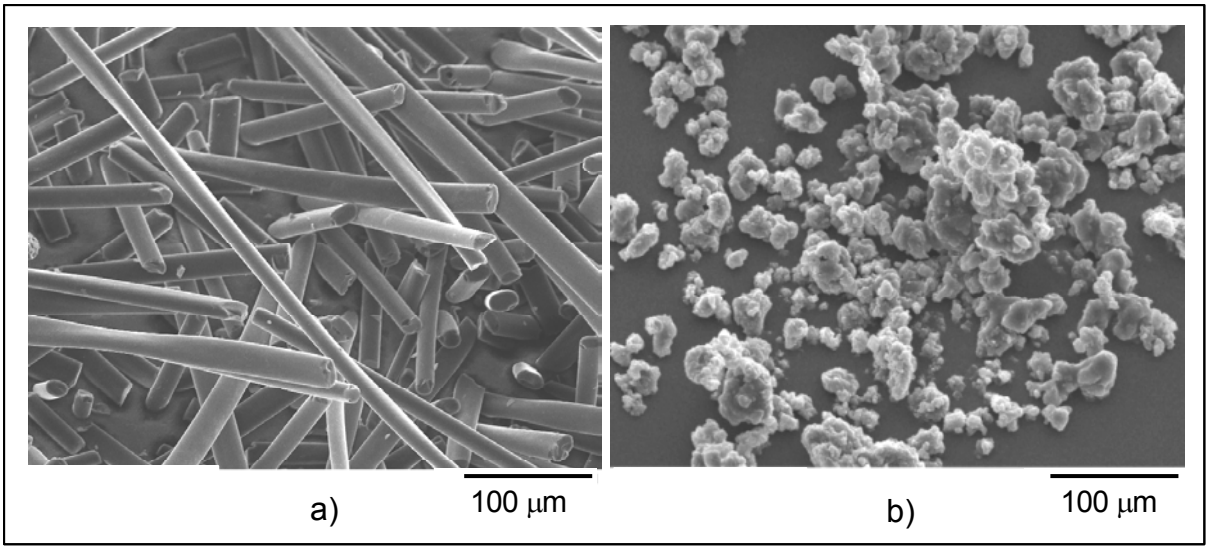

Figure 4.1: Micrographs of a) MCF and b) PANI-DBSA.

4.2 Samples Preparation

4.2.1 Carbon Fibre/Epoxy Matrix Composites

CF were mixed with the EP matrix using a simple mixing stirrer (RW20, IKA-Werke GmbH & Co. KG, Germany); air was removed from the samples under reduced pressure. Samples with different total volume fractions were developed (from 1 to 20 vol.%). For the preparation of the graded samples, the isotropic CF/EP mixtures were filled in aluminium forms and centrifuged in a centrifuge machine (Centrifuge Biofuge stratos, Heraus Instruments, Germany). The distance between the rotor axis and the bottom of the samples was 162 mm. The rotor was accelerated to a maximum rotation speed and this speed was maintained for 10 min before the experiment was stopped. Five different centrifugation speeds were tested: 0, 500, 1000, 2000, and 5000 rpm. The graded samples were cured at room temperature for 24 h. For each set of parameters, 2 samples were fabricated in order to ensure reproducibility.

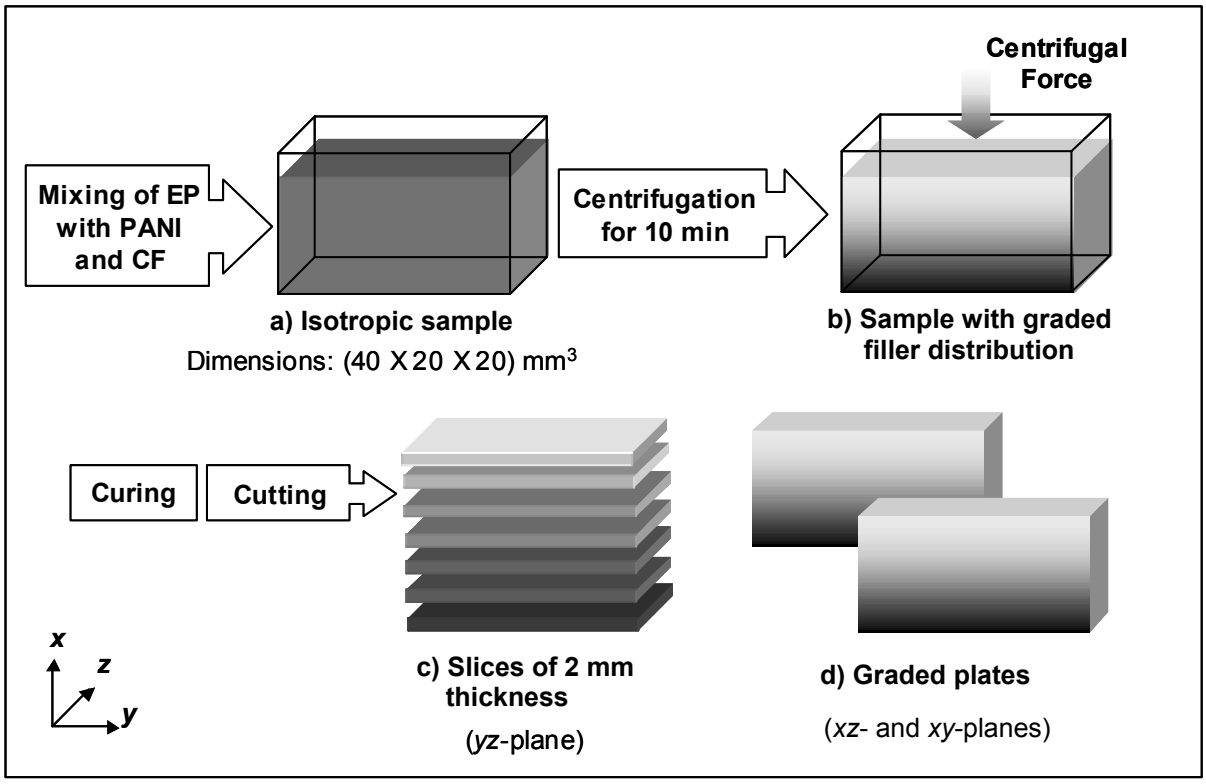

Figure 4.2: Samples preparation: (a) isotropic sample, (b) sample under centrifugation, (c) slices of 2 mm, and (d) graded plates.

One sample was cut into thin slices of about 2 mm thickness perpendicular to centrifugal force, using a microtome with rotating diamond-coated saw blade

(SP1600, Leica). These slices (Figure 4.2c) were used for the determination of the fibre volume content by means of density measurements. Additionally, their volume resistivity and flexural properties were estimated, as described below. In this way a possible connection between the fibre concentration and the electrical and mechanical properties of the graded samples was investigated. From the other sample two plates were obtained by cutting them parallel to the *x*-direction (Figure 4.2d). These plates were polished and used for measuring the surface resistance (in *xy*-plane) and the fibre orientation and microhardness (in *xz*-plane) along the *x*-axis of the samples.

4.2.2 Epoxy/Polyaniline Blends

The preparation time of EP/PANI-DBSA samples was longer and the process more complicated compared to the CF/EP ones. Samples containing 0 to 11.1 vol.% PANI-DBSA were fabricated. PANI-DBSA was first dried at 40°C under vacuum for about 16 h. The dried powder was added slowly in toluene in order to create a 5 % solution and mixed together with a magnetic stirrer for 48 h. In order to improve the mixture quality this was treated in an ultrasonic bath for about 3 h and at the end a green transparent low-viscosity polymer solution was obtained. In consequence, the PANI-DBSA solution was mixed with the EP which was before warmed for 1 h at 50°C. The blend was stirred under vacuum at 50°C with stirring speeds of 500-2000 rpm until toluene was evaporated. This procedure lasted over 3 h and took place in a dissolver device (Dispermat AE, VMA-Getzmann GmbH, Germany). The EP/PANI-DBSA blend was eventually mixed with the curing agent at room temperature for 10 min. The samples were cured in a forced-air circulating oven (Thermicon P, Heraus) at temperatures up to 130°C.

4.2.3 Carbon Fibre Reinforced Epoxy/Polyaniline Blends

In the case where a combination of the two conductive materials was studied, the procedure started by preparing the EP/PANI-DBSA blend as described above. The CF were added and mixed under vacuum at 50°C until the blend was free of air and a homogeneous mixture was obtained. Isotropic and graded samples were developed and cured as described above.

4.3 Microstructure

4.3.1 Determination of Filler Fraction

The filler content was determined from density measurements according to Archimedes' principle [DIN 53 479, 1991]. For this purpose, the 2 mm thick slices (Figure 4.2c) or small pieces of the isotropic samples were used. After the determination of the slice density (*D*), the content of fillers was calculated according to the following equation:

Volume fraction [vol.%]:
$$V_f = \left[1 - \left(\frac{D_f - D}{D_f - D_m}\right)\right] \cdot 100 \qquad (4.1)$$

where D_m and D_f are the density of matrix and filler, respectively.

4.3.2 Light Optical Microscopy

A light optical microscope (Aristomet, Leitz) was used in order to observe the polished surfaces of the graded plates (Figure 4.2d). The samples were adjusted on the microscope's moving table, and images were taken every 2 mm along the *x*-axis starting from the bottom of the samples. In this way the graded distribution of the fillers could be visually studied. In addition these images were utilized for the determination of the fillers orientation. For this purpose an image analyzer was connected to the microscope. The in-plane orientation angle, ϕ, which was defined with respect to the *z*-axis, could be determined directly from the *xz*-plane in the image analysis (cf. Figure 4.3) [73].

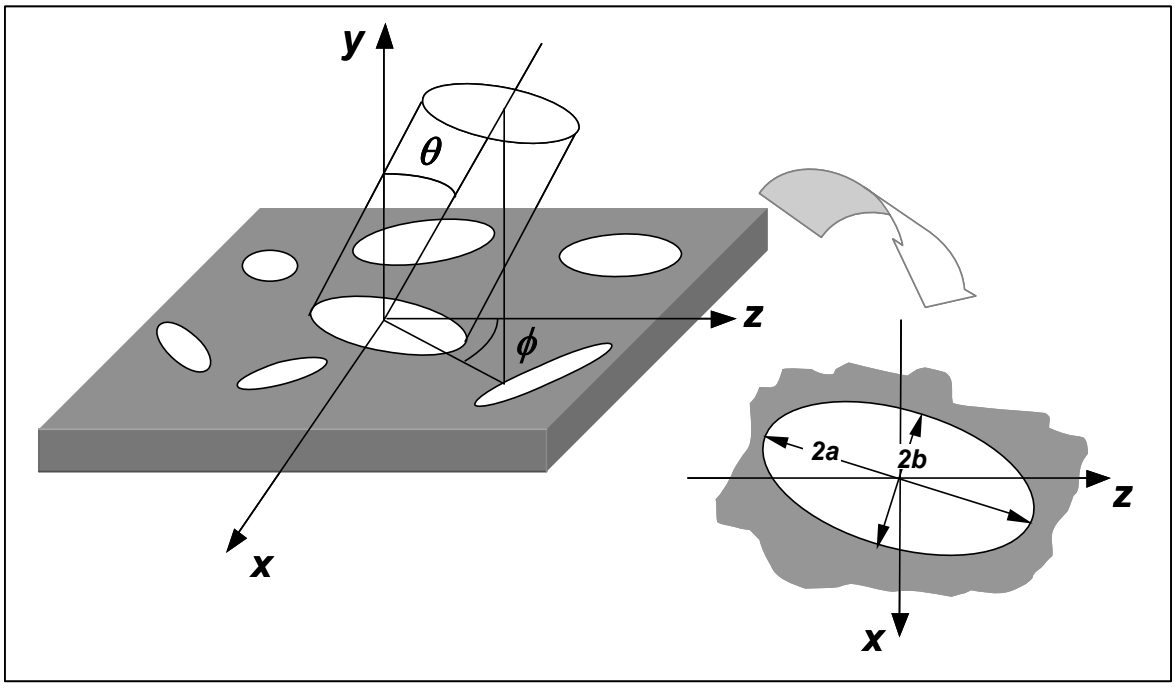

Figure 4.3: Definition of the orientation angle.

The out-of-plane orientation angle can be determined from the geometry of the ellipse (Figure 4.3) since:

$$\theta = \cos^{-1}(b/a) \tag{4.2}$$

where 2*b* is the diameter of the fibre (*d*) and 2*a* is the length of the major axis of the ellipse. These were both experimentally measured by the image analysis.

4.3.3 Transmission Optical Microscopy

Fibre length was determined for the three different types of CF before mixing, using a transmission optical microscope, TOM (Diaplan, Leitz). No further breaking of the fibres was assumed to take place during the mixing procedure. The length of about 200 fibres for each of the three types was measured and the number average fibre length was calculated as:

$$l_m = \frac{\Sigma N(i)}{\Sigma N} \tag{4.3}$$

where *N(i)* is the number of fibres of length *l(i)* [73].

Furthermore the solubility of the PANI-DBSA in different solvents and later in epoxy was inquired by TOM. Films were cast onto glass microscope slides and dried at room temperature.

4.3.4 Scanning Electron Microscopy

The fractured surfaces of the samples were studied in a scanning electron microscope, SEM (JSM 5400 of Jeol, Tokyo, Japan). The surfaces were first sputtered at sputtering device (SCD-050, Balzers, Liechtenstein) for 150 sec with a Pt/Pd alloy. This conductive coating was essential in order to obtain stable images. Through it, the charges deposited on the sample surfaces by the electron beam were able to leak away to earth. The use of SEM was effective in order to investigate the adhesion between fillers and matrix and to estimate the fracture mechanisms.

4.4 Electrical Properties

4.4.1 Graded Surface Resistance

Surface resistance (R_s) is the ability of a material to leak away localised charges across the surface, and it is closely related to the electrostatic discharge control. In order to measure the surface resistivity at different points of the graded samples, a measuring device was constructed (Figure 4.4). A resistivity meter (Hiresta UP) and a mini 2-pin probe (UA Type) were both obtained from Mitsubishi Chemicals, Japan. This resistivity meter was able to carry out accurate measurements of surface resistivity in the range of 10^4-10^{14} Ohms. The 2-pin probe had an inter-pin distance of 20 mm, pin points of 2 mm diameter each, and a spring pressure of 240 g/pin. The graded samples (Figure 4.2d) were adjusted on a moving table, which could be moved in small steps across the *x*-axis of the samples. In this way measurements of the surface resistivity were carried out in 2 mm steps, starting from the bottom-side of the samples. The graded samples were first polished in order to obtain a better contact between the measured surfaces and the electrodes. They were afterwards dried overnight in a vacuum oven at 40°C and then stored in a desiccator. The mini probe and the sample were enclosed in a metal box in order to shield the measurements from external interference.

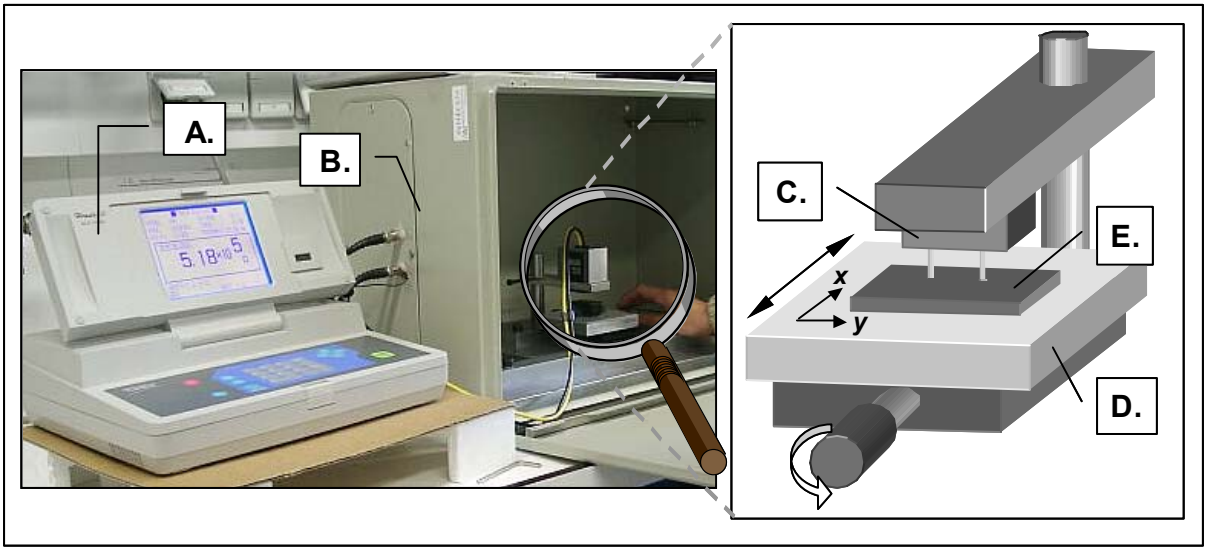

Figure 4.4: Device for the measurements of the graded surface resistivity: A. Resistivity meter, B. Protective metal box, C. Mini 2-pin probe, D. Moving table, E. Graded sample.

4.4.2 Electrical Conductivity

The volume resistance (ρ) describes the ability of a material to promote the leakage of developed electrostatic charges through its thickness. The electrical conductivity (σ) can be directly calculated from the volume resistivity by the following equation:

$$\sigma = \frac{1}{\rho}. \tag{4.4}$$

For the measurements of the volume resistivity, the 2 mm thickness slices (Figure 4.2c) were used. The surfaces of these samples were polished and cleaned with appropriate cleaning liquids in order to create a better contact with the electrodes. The samples were additionally dried over night in oven at 40°C under vacuum, and then kept in dried environment, for the elimination of moisture effect. The resistivity meter described above was used once more, this time in connection with a ring probe (UR-SS Type, Mitsubishi Chemicals, Japan) and a measuring stage (Resitable UFL, Mitsubishi Chemicals, Japan) (Figure 4.5). Samples were placed on the metal surface of the measuring stage and the probe electrode was pressed upon them. The suitable voltage was then impressed through the thickness of the sample. The volume resistivity was measured on both surfaces of the slices, and the average value was obtained.

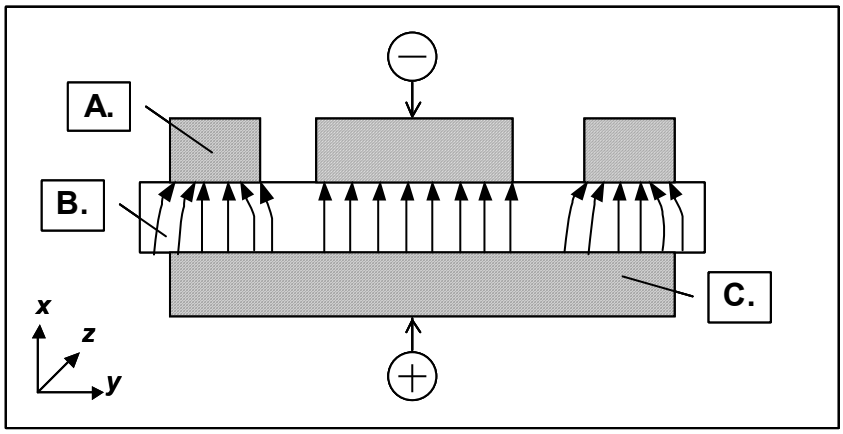

Figure 4.5: Configuration for the volume resistivity measurement: A. Ring probe, B. Sample, and C. Measuring stage.

4.4.3 Dielectric Measurements

The above described d.c. electrical measurements are able to show the effect of the addition of a conductive phase to the insulating matrix. However, frequency dependent measurements can provide additional information about the mechanisms controlling the electrical response of the system.

The dielectric properties of the cured samples were measured by an Eumetric® System III microdielectrometer (Micromet Instruments, Inc.). A midconductivity inter-digitated electrode sensor (IDEX) was attached onto the samples surface, and values of the dielectric constant ε' (or relative permittivity) and loss factor ε'' were determined over the frequency range from 0.075 to 10^6 Hz. The dielectric constant is a measure of the energy stored in a sample during cyclic electric excitation. The dielectric factor is a measure of the energy loss in a system during cyclic electric excitation. The lost energy is typically due to the viscous drag of moving dipoles and ions within the sample.

4.5 Mechanical Characterisation

4.5.1 Flexural Tests

The stiffness or rigidity of composites when subject to bending is of great importance for their use in engineering and structural applications. The flexural properties were measured on a Zwick™ 1485 or 1445 (Ulm, Germany) universal testing machine.

The samples were submitted to three-point bending tests (DIN 178). A load cell of 10 kN and a crosshead speed of 1 mm/min were applied to all materials.

4.5.2 Microhardness Tests

Indentation is a quick and non-destructive method of valuating the mechanical properties of a material. For this test isotropic samples or the graded plates (Figure 4.2d) were used. The microhardness was measured at room temperature at every 1-2.5 mm along the thickness of the samples (*x*-axis) starting from the bottom-side of the graded samples. An ultramicrohardness tester (Simatzu DUH-202) was employed to carry out the measurements. A continuous load-displacement monitoring was possible, as the indenter was driven into and out of the samples surfaces. The measurements were performed with a Vickers indenter, i.e. a square–based diamond pyramid. A load range of 1.5 N was chosen in order to produce large indentations. In this way both matrix and fillers were taken into account and an average microhardness value of the composite was obtained. A loading and unloading speed of 70 mN/sec was used. For each step five measurements were made across the *y*-axis and were then averaged. Two values were obtained from each measurements: a) the universal (or dynamic) microhardness (*HU*), and b) the Vickers microhardness (*HV*).The universal microhardness was calculated by following equation:

$$HU = \frac{P}{26.43 \cdot h^2} \tag{4.5}$$

where *P* is the applied test force, and *h* the indenter penetration depth.

The Vickers microhardness is defined as the load/surface area of impression which can be shown to be:

$$HV = \frac{1.854 \cdot P}{d^2} \tag{4.6}$$

where *P* is the maximal load applied, and *d* the distance across the diagonal of the impression. *HV* considers only the irreversible plastic deformation of the material, while *HU* represents the strength characteristics including both plastic and elastic deformations.

4.5.3 Fracture Toughness Tests

Fracture behaviour of the different samples was investigating by means of the compact tension (CT) method according to the ESIS testing protocol [74]. The test were carried out on a Zwick^{TM} 1445 (Ulm, Germany) universal testing machine and the fracture toughness K_{IC} and fracture energy G_{IC} were determined. The CT specimens (dimensions: 35 X 35 X 3 mm^3) were notched by sawing. The notch root was sharpened by a razor blade. The specimens were placed into a jig and tested at a crosshead speed of 1 mm/min.

4.6 Analytical/Thermal Characterisation

4.6.1 Differential Scanning Calorimetry, Thermogravimetric Analysis

Heat capacity of the fabricated materials (mainly of the EP/PANI-DBSA samples) was examined by differential scanning calorimetry (DSC) in a DSC 821 device (Mettler Toledo, Germany). Cured samples were heated up to 270°C, with a heating rate of 20°C/min, then cooled and finally heated again. In this way the glass transition temperature (T_g) was estimated and a consensus was reached regarding their cured status. For a better understanding of the curing process, uncured samples were subjected to dynamic heating from 25 to 200°C with 10°C/min. The total heat of the reaction was estimated by drawing a straight line connecting the baseline before and after the peak, and integrating the area under the peak.

Thermogravimetric analysis (TGA) was used for the determination of the materials weight loss versus temperature. A TGA40 (Mettler Toledo, Germany) device was occupied to heat up small samples up to 600^{o}C, with a heating rate of 10°C/min, in nitrogen atmosphere. In this way the degradation of the materials could be studied.

4.6.2 Dynamic Mechanical Thermal Analysis

The viscoelastic response of the composites fabricated was studied by dynamic mechanical thermal analysis (DMTA). An Eplexor^{TM} 150N (Gabo Qualimeter, Ahlden, Germany) DMTA device was employed to carry out the tests. The specimens were subjected to oscillating dynamic loading consisting of a static preload of 4N on which a sinusoidal wave of 2 N at a constant frequency was superimposed. Viscoelastic

parameter such as the mechanical loss factor, $tan\delta$, and the complex Young's modulus, E^*, were measured. The measurements were made under three point bending loading. Heating occurred at a rate of 2°C/min and in a temperature range between –50 to 260°C. The testing frequency was 10 Hz.

4.6.3 UV-Visible Spectroscopy

Transmission spectra of the EP/PANI-DBSA blends were recorded at room temperature on a UV-vis scanning spectrophotometer (UV-2101PC, Shimadzu). Dilute solutions of the polymer samples in toluene were used. The transmission spectra of the solutions was measured in the range of 800-300 nm.

5. Results and Discussion

5.1 Carbon Fibres/Epoxy Matrix Composites

Carbon fibres (CF) have been one of the most common fillers used for the purpose of enhancing the electrical properties of polymers [15-17,19,75,76]. Different types of CF have been mixed with a variety of polymers, and the properties of the resulting composites have been intensively studied. In the majority of these cases, isotropic composite materials were developed, and a good understanding of the influence of the components characteristics, as well of the processing parameters on the consequent electrical properties, has been achieved. In order to broaden this already well-investigated category of polymer composites to new fields, this part of the present work is merely focused on developing graded CF/EP composites by the use of a centrifugation method. In the next paragraphs the parameters influencing the created graded CF distributions, and subsequently the functional properties of these materials will be examined and discussed.

5.1.1 Microstructure

5.1.1.1 Graded Fibre Distribution

As it was shown in paragraph 2.3.3, the motion of solid fillers in viscous liquid, in this case of CF in the liquid EP system, under the centrifugal force can be expressed by Stoke's law (cf. Equation 2.6). The different parameters that influence the fillers velocity and therefore the resultant graded distribution according to this equation are summarized in Table 5.1.

The motion of the fillers can be controlled by changes in the centrifugation process (e.g. speed, time), but also by the use of fillers and matrices with different characteristics (e.g. size, density). Since all these various factors significantly influence the graded distribution of the dispersed fillers during the FGMs fabrication, an accurate control of the fillers movement is difficult to take place.

In this study a part of the above-mentioned parameters was kept constant in order to simplify and obtain a more clear view of this complex process. Therefore, the sample thickness was in all cases 20 mm, the density for every type of CF 1.65 g/cm^3 and the

centrifugation time 10 min. In the following paragraphs the influence of centrifugation speed, average fibre length, total fibre content, and viscosity of the matrix on the graded CF distribution is discussed.

Table 5.1: The effect of processing parameters on the graded distribution of the dispersed fillers [61].

Processing Parameter	Graded Distribution Gentle ←…→ Sharp
Centrifugation Speed	Low ←…→ High
Total Filler Concentration	High ←…→ Low
Fillers Size	Small ←…→ Large
Difference in Density between Liquid Matrix and Fillers	Small ←…→ Large
Viscosity of Liquid Matrix	High ←…→ Low
Centrifugation Time	Short ←…→ Long
Sample Thickness	Thick ←…→ Thin

The variation in the volume fraction of CF across the thickness of the graded samples (direction of centrifugal force) was determined by density measurements of the 2 mm thickness slices, as described in detail in paragraph 4.2.1.

Effect of Centrifugation Speed

Figure 5.1 compares the graded distribution profiles of samples with total volume fraction of 10 % SCF, centrifuged under different centrifugation speeds. The abscissa in this figure represents the relative position in the normalized thickness direction of the sample, where 0.0 and 1.0 corresponds to the bottom- and top-side, respectively. Samples prepared without centrifugation (0 rpm) exhibit almost constant values of fibre content along the thickness of the sample. Nevertheless, this changes when centrifugal force is applied. A gradient in the fibre concentration is created over the thickness of the sample, with maximum value at the bottom-side. This value increases with an increase in the centrifugation speed from 25 vol.% for 500 rpm to 32 vol.% for 5000 rpm. After a certain speed value, the maximum volume fraction does not change significantly anymore, as the fibres have already reached a closely-

packed state. No further movement of the fibres can be permitted at the bottom-side of the samples in these cases. CF volume fraction shows the tendency to decrease along the thickness of the sample. This decrease becomes sharper with the application of higher rotation speeds (>2000 rpm). CF are packed near the bottom of the samples, and almost no fibres exist along the remaining sample thickness. It was observed that the centrifugation speed influences the distribution of the MCF and LCF within the EP matrix in a similar way.

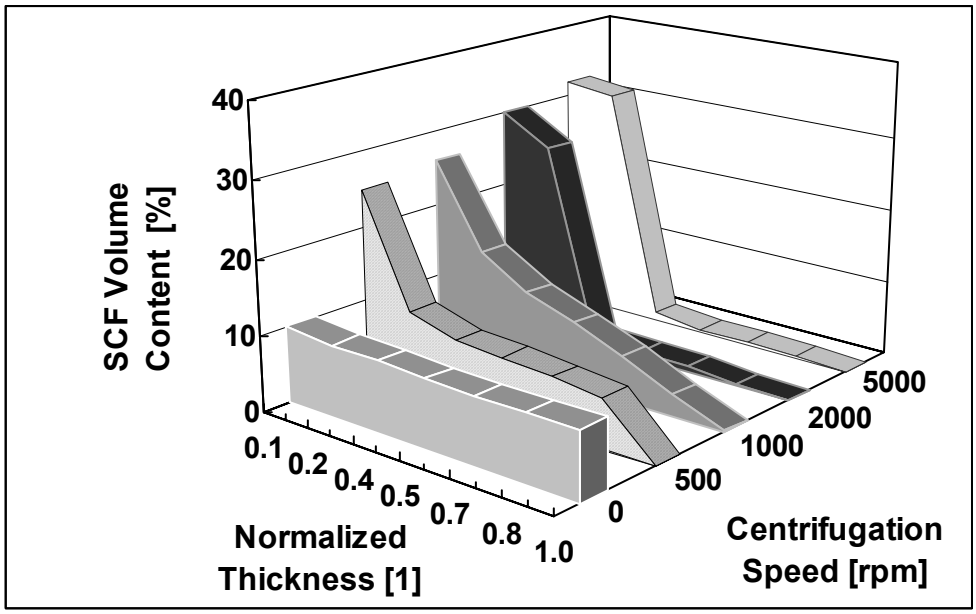

Figure 5.1 Graded distributions of SCF/EP samples as a function of the centrifugation speed. Total SCF content: 10 vol.%.

The graded microstructure profiles of the fabricated samples were observed by the light optical microscopy. Figure 5.2 illustrates the profiles of the same graded samples analysed in the previous paragraph. Comparable conclusions can be derived from these images, as well as by the density analysis of the samples. High centrifugation speeds lead to sharper changes of the microstructure across the thickness, *x*, and force the majority of the fibres to be packed at the bottom side of the sample.

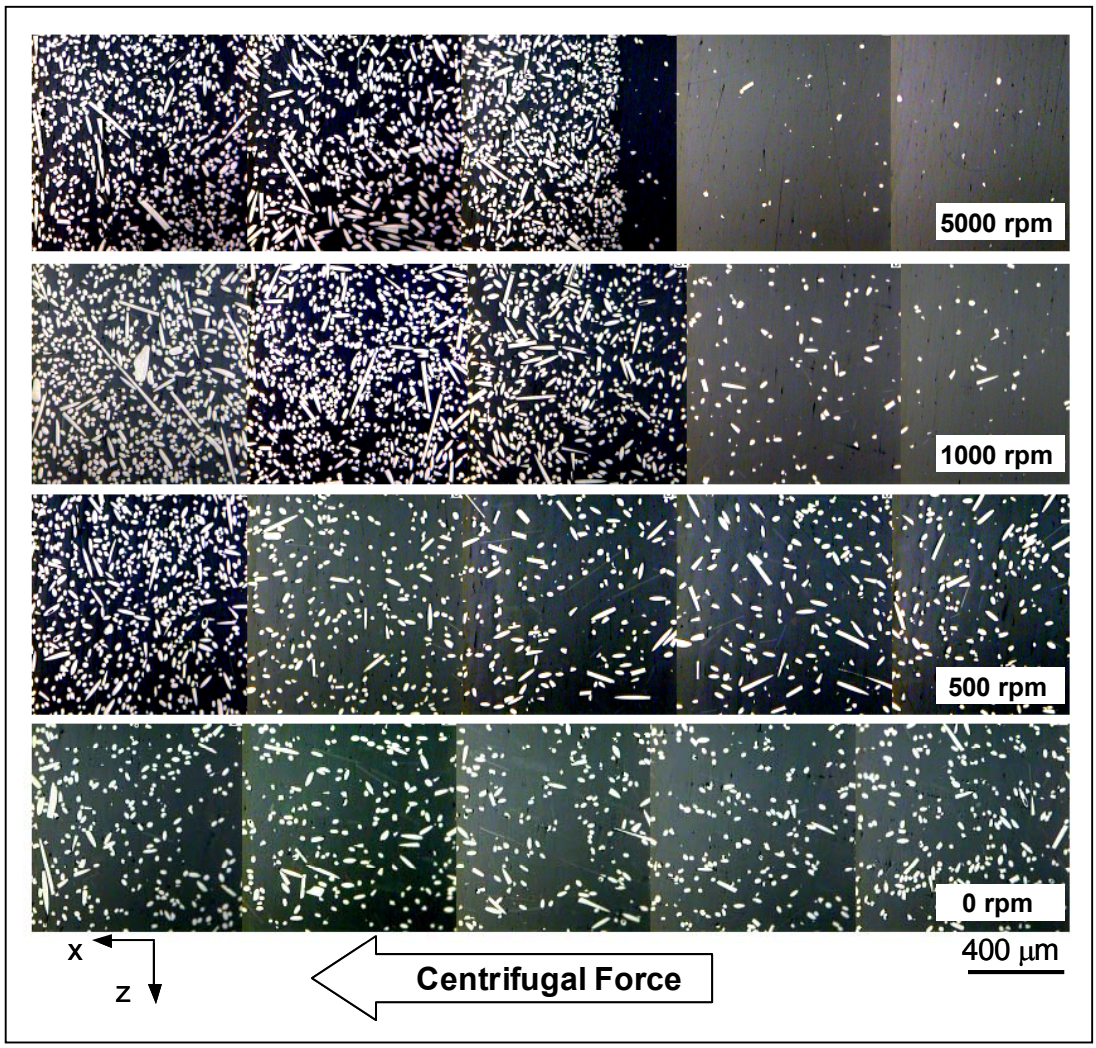

Figure 5.2: Images by light optical microscopy, showing the graded profiles of samples centrifuged under different rotation speeds. Total SCF content: 10 vol.%.

Effect of the Average Fibre Length

During the mixing of the CF with the resin and its subsequent centrifugation, no significant breaking of the fibres is assumed to occur. The average fibre length, determined from the samples before mixing, was 107 μm for SCF, 269 μm for MCF, and 399 μm for LCF. These values were found to be much smaller than those stated by their manufacturers (Table 4.1), especially for the MCF and LCF. Figure 5.3 shows the fibre length distribution of the different CF. For fibres with longer length (i.e. MCF and LCF) a broader distribution is observed.

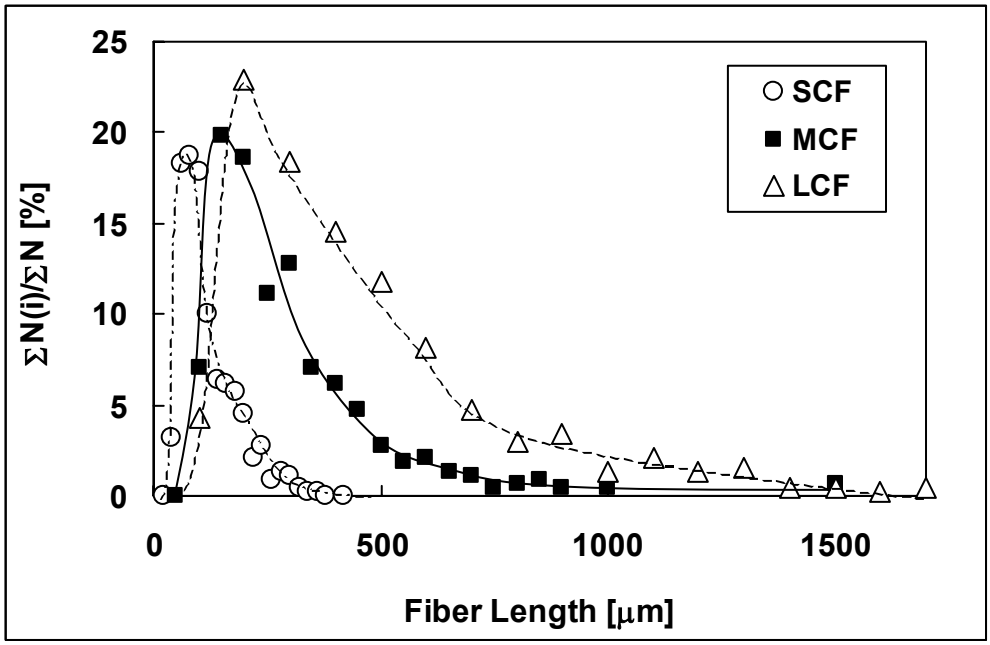

Figure 5.3: Fibre length distributions for SCF, MCF, and LCF.

Figure 5.4 depicts the volume fraction profiles for the three different types of CF. The total volume fraction and centrifugation speed for the preparation of each sample were 5 % and 1000 rpm, respectively. It is obvious that the SCF/EP system exhibits the highest value of volume content and shows the largest concentration difference. With increase in the fibre length, much lower CF concentrations at the bottom-side of the sample are observed. This suggests that the length of the fibres has a great influence on the maximum packaging density if a randomly close-packed state is considered. As the fibre length increases, fibres can easily come in contact to each other enclosing larger spaces of neat epoxy between them. This indicates that in the system with longer fibres, lower values of the maximum fibre content should be expected. Furthermore, the longer fibres with a broader distribution, as shown in Figure 5.3, can easily create a linear volume content profile for a given set of parameters. Lee [68] has also observed experimentally this tendency for carbon fibres with smaller length differences (72-156 μm) in epoxy matrix. However, when particles are used instead of fibres the results are quite different. According to Stoke's equation, larger particles can move with higher speed within the liquid matrix, as their speed is proportional to the square of their diameter. This has also been observed experimentally by Watanabe [69], who has observed sharper composition gradients when larger particles were used.

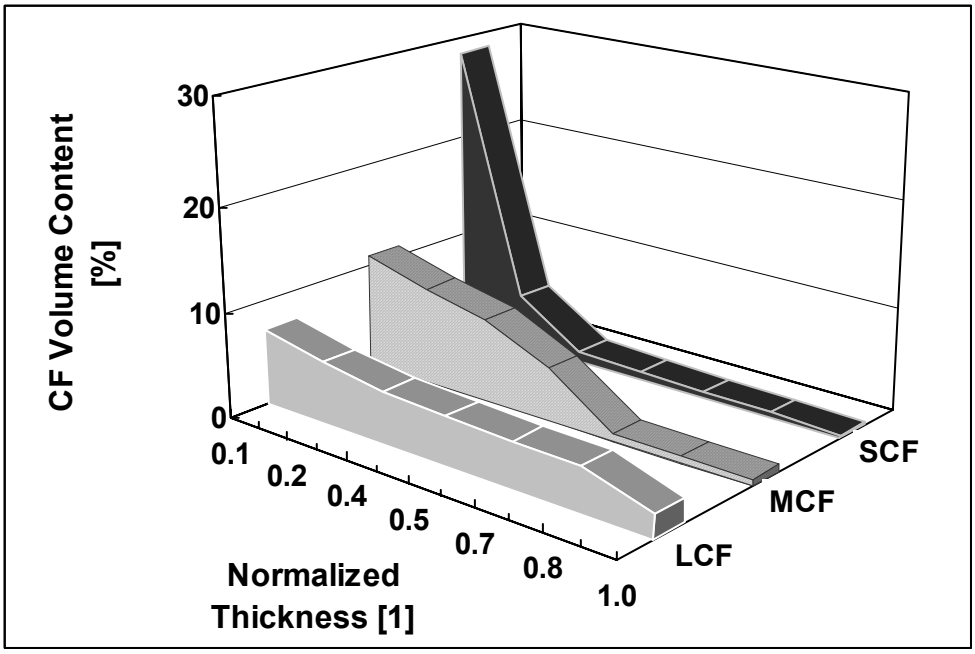

Figure 5.4: Graded distributions for the different CF types. Total CF content: 5 vol.%, and centrifugation speed: 1000rpm.

The maximum filler concentration (V_t), or filler-packing factor, is considered as one of the most important characteristics of a polymer-filler composite [50,77]. The value of V_t is a limit of a system filling, and equal to the highest volume content for a given type of packing. For statistically packed monodispersed spherical particles of any size, V_t is equal to 0.64. Mamunya [78] has cast V_t as a function of the aspect ratio α, in the case where fibres are used as fillers:

$$V_t = \frac{5}{a + \frac{75}{10 + a}} \tag{5.1}$$

According to this equation, the V_t values for SCF, MCF, and LCF are 0.43, 0.28, and 0.15, respectively. In order to experimentally determine the maximum packing fraction of the different CF, samples containing each type of fibres were centrifuged at 4000 rpm for 20 min. In this way a maximum concentration at the bottom-side of the samples was achieved as determined by density measurements. As expected, SCF exhibit the higher maximum fibre concentration value (0.37), while for the MCF and LCF this value is clearly smaller (0.23 and 0.10, respectively). These

experimental values are, for every CF type, smaller than those calculated by Equation 5.1, but the tendency is the same. This difference is though quite logical, since the theoretical equation does not take into account the properties of the polymer matrix, such as density and viscosity.

Effect of Total Fibre Content

Figure 5.5 shows the effect of the total CF content on the graded distribution of the SCF/EP composites. The total CF content is defined as the isotropic volume fraction of the fibres before centrifugation. As the CF content increases, the ratio of the length of the fibre-packed region to the total specimen thickness tends to grow, and the fibre volume content difference between the bottom- and top-side of the sample becomes larger. However, it can be seen that for high total fibre content (e.g. 25 vol.%), the maximum volume fraction at the bottom-side of the sample does not increase significantly. The fibres have already reached a closely-packed state at this side of the sample, thus leading to higher CF contents along the whole sample thickness. Therefore, the difference in the fibre volume content between the bottom- and top-side for samples with high total CF fractions tends to decrease.

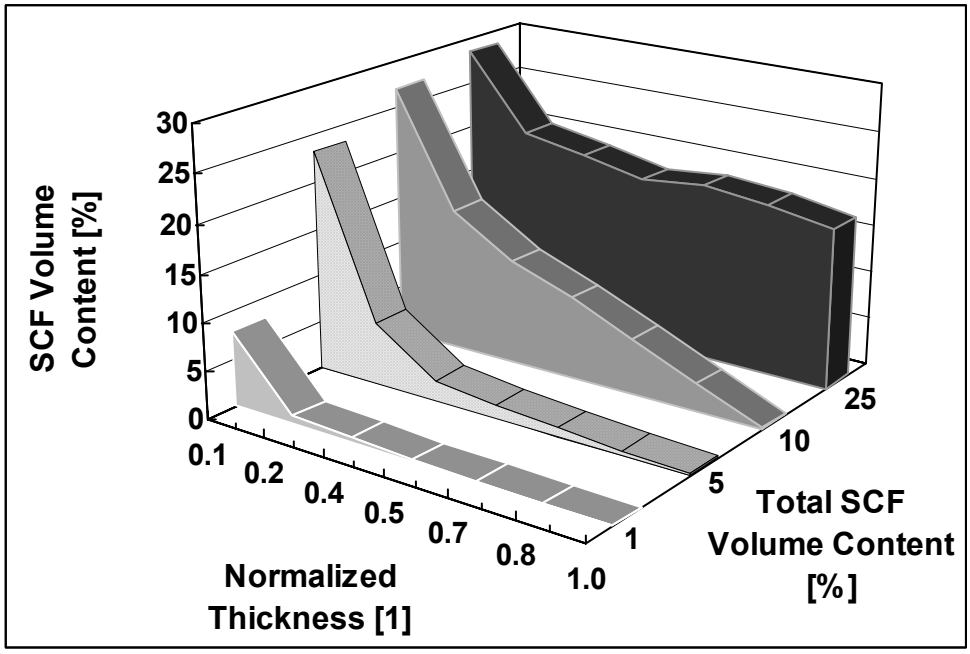

Figure 5.5: Graded distributions of SCF/EP samples as a function of the total weight content. Centrifugation speed: 1000 rpm.

At low fibre content, the movement of CF due to the applied centrifugal force is controlled by Stoke's law. For this system the individual fibres are relatively free to move regardless of the presence of other fibres, in such a way that the longer fibres, having larger equivalent diameter, move faster than the shorter ones. Therefore longer fibres will reach the bottom of the mould first and will be packed there. When the fibre content increases, the interaction between the fibres becomes more intensive and influences the motion of individual fibres together with Stoke's individual diameter. Consequently, a cooperative motion of long and short fibres is likely to occur, a result that increases the packing efficiency of the fibre-packed region at the bottom-side of the specimens.

Viscosity of the EP Matrix

In order to study the effect of the EP viscosity on the movement of CF, the liquid CF/EP mixtures were submitted to centrifugation at different delay times. Delay time is defined as the period between the addition of the curing agent into the mixture and the initiation of the centrifugation process

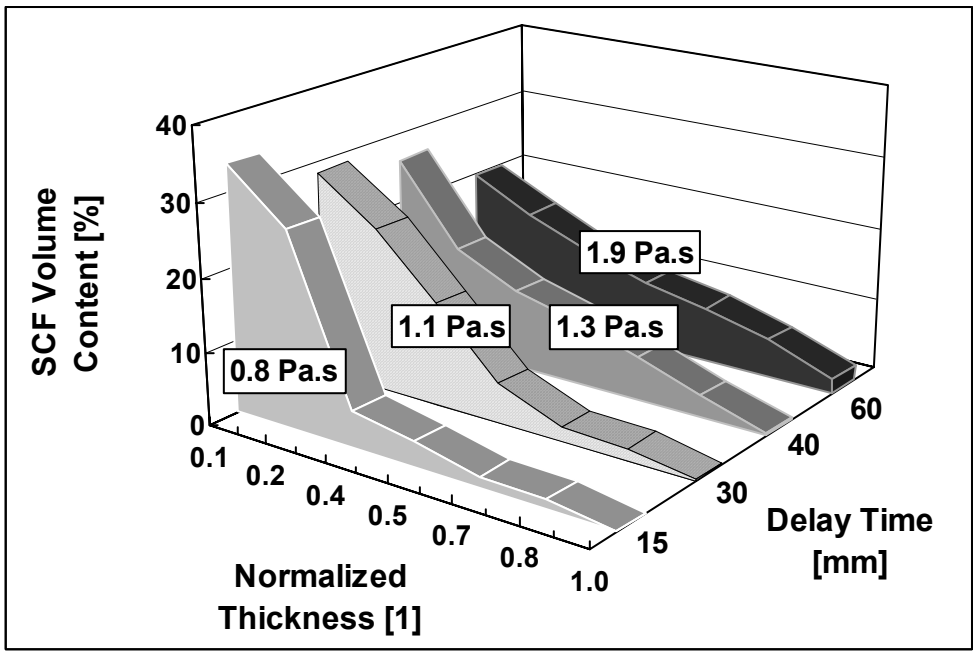

Figure 5.6: Graded SCF distributions as a function of delay time. Total SCF content: 10 vol.%, and centrifugation speed: 1000 rpm.

It is expected that after the addition of the curing agent, the curing reaction of the EP system begins and therefore the viscosity of the mixture increases. The viscosity of the unfilled liquid EP system was measured after the corresponding delay times using a plate-plate rheometer (V-10, Suck, Germany) at room temperature.
Figure 5.6 shows the graded SCF distributions for different delay times. For all cases the initial SCF content was 10 vol.% and the centrifugation speed 1000 rpm. Delay time is strongly connected to the viscosity of the blends. When the samples are centrifuged after a short delay time (e.g. 15 min), the viscosity of the mixture is still low and the fibres can reach high terminal velocities. In this manner, sharply graded distributions of the fibres are created. On the other hand, when the delay time is longer, the obtained concentration profile is almost linear. Reduced velocities lead to a lower packing rate near the bottom-side, and this accounts for the smoother fibre content distributions.

5.1.1.2 Fibre Orientation

According to Funabashi [67], during the centrifugation process most of the fibres tend to align perpendicular to the direction of the centrifugal force due to the rotation of the single fibres in the liquid matrix and the depression of the fibre network in the centrifugal direction. Watanabe [79] offered a different explanation attributing this phenomenon to the viscosity changes within the liquid mixture. The viscosity of the mixture increases towards the centrifugation direction due to the increased fibre concentration. Since the velocity of the mixture at the bottom-side is higher than in the top-side, the fibres are subjected to a moment. Thus fibres are aligned with their length nearly perpendicular to the centrifugal force direction.
In order to obtain a detailed picture of the microstructure across the thickness (*x*-direction) of the CF/EP composites, the fibre orientation was characterized in various areas along the samples thickness (*x*-*z* plane), as described in detail in paragraph 4.3.2. Additionally, the fibre orientation on the *y*-*z* plane which is vertical to centrifugal direction was investigated. The comparison of the two pictures in Figure 5.7 indicates that most of the fibres tend to lie in random directions in the plane *y*-*z*, while in the vertical *x*-*z* plane the cross sections of fibres are mostly visible. To obtain a more clear view of the orientation trends, the distribution of the in-plane angle ϕ (*x*-*z* plane)

at the bottom side of samples containing 10 vol.% SCF and centrifuged under different speeds is shown in Figure 5.8a.

Maximum distributions are observed for values near 0° and 180°, especially for the highest centrifugation speed. This is an evidence that the majority of the fibres are aligned perpendicularly to the centrifugal direction in *x*-*z* the plane. The sedimented sample (0 rpm) shows an almost random in-plane distribution, and therefore the observed maximum ϕ values for 1000 and 5000 rpm should be attributed mostly to the centrifugal force. The out-of-plane angle θ exhibited a maximum value of 50° with respect to the *y* axis for all samples. This implies that the fibres are about 40° out of the *x*-*z* plane.

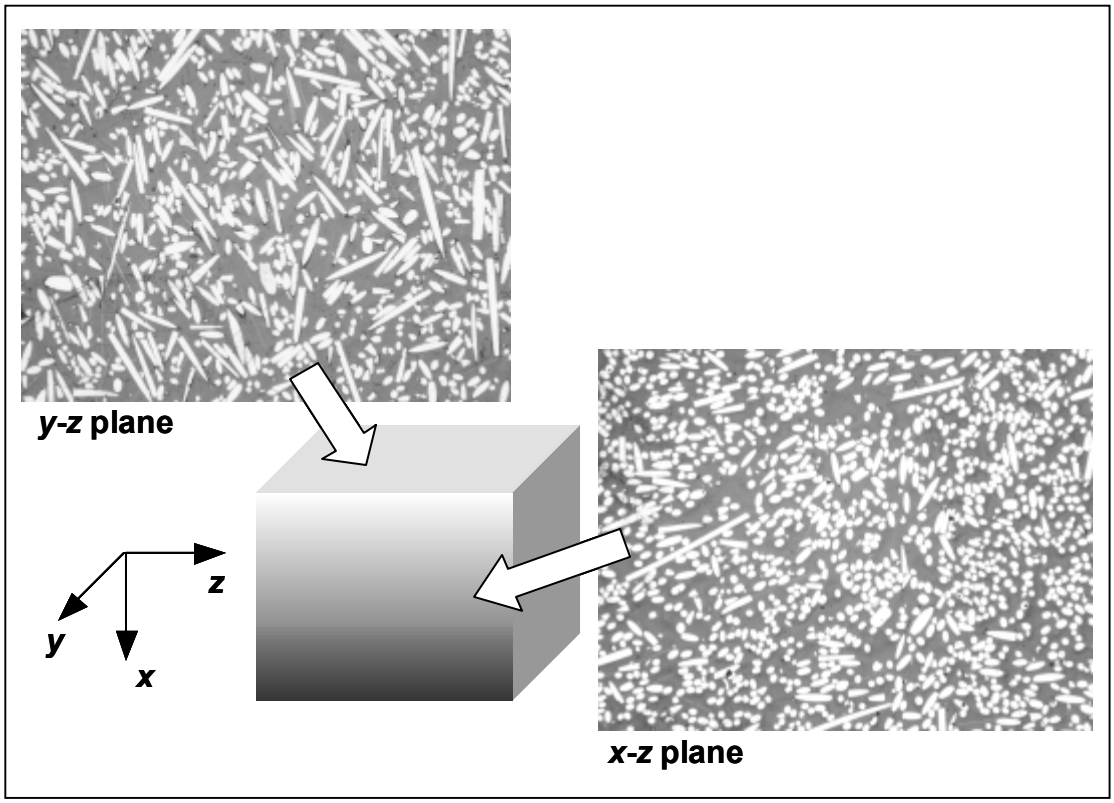

Figure 5.7: Investigation of the fibre orientation in the *y*-*z* and *x*-*z* planes.

In Figure 5.8b the distribution of the in-plane angle (*x*-*z* plane) is illustrated at areas near the top-side of graded samples with a total content of 10 vol.% SCF. In this case a nearly uniform ϕ distribution is observed for all samples, indicating a random in-plane orientation of the fibres in these regions. Again a maximum at 50° was observed for the angle θ, showing that the out-of-plane orientation of the fibres does not change along the sample thickness. The same tendencies were observed at the

fibre orientation of MCF/EP and LCF/EP graded samples. Similar conclusions can be drawn from images of very thin slices (*y*-*z* plane), obtained by transmission optical microscopy (Figure 5.9).

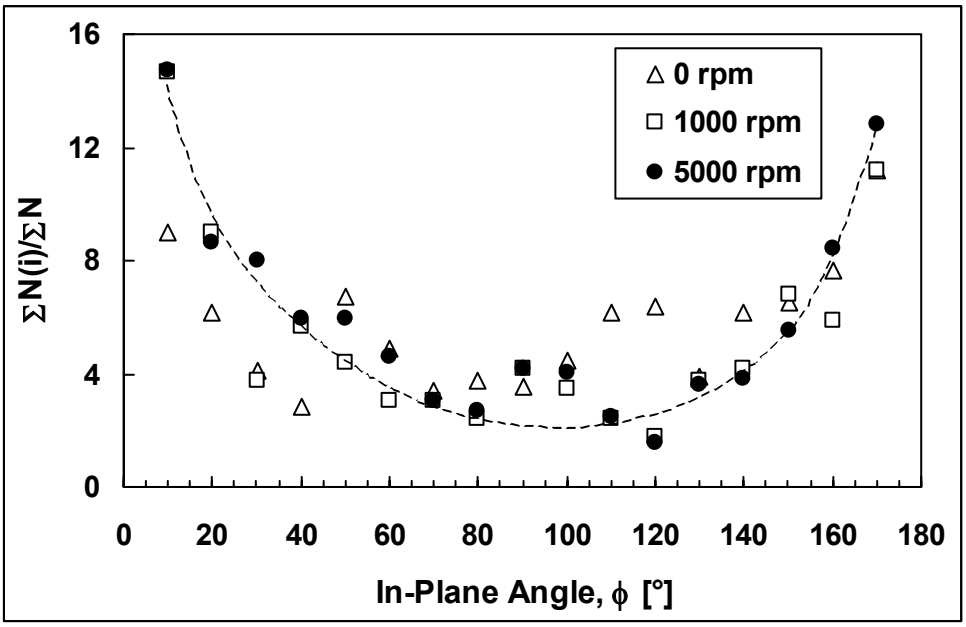

a)

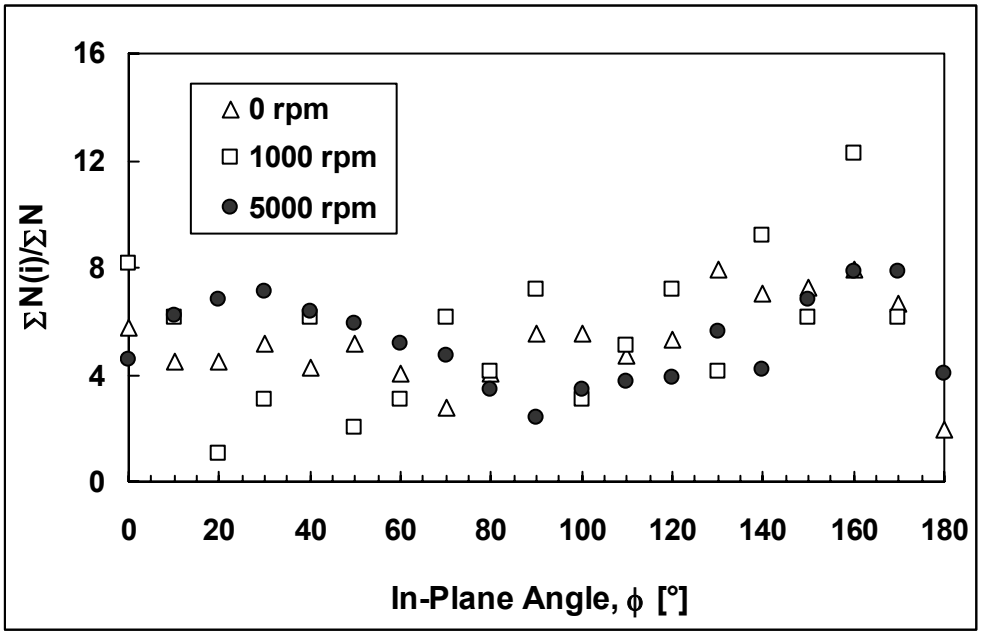

b)

Figure 5.8: In-plane fibre orientation at the a) bottom- and b) top-side of SCF/EP composites (*x*-*z* plane).

Although some orientation tendencies are detected, the absolute alignment of the fibres in the plane vertical to centrifugal force, as it has been reported in literature

[67,68,77], is not verified for the developed graded samples in this study. A high interaction between the fibres is evident, preventing a large number of them to move and orientate only under the influence of the centrifugal force.

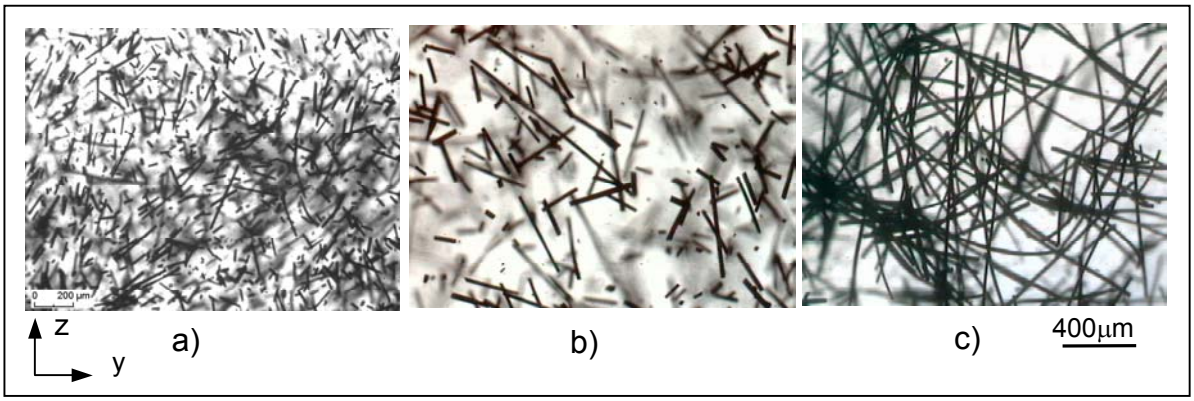

Figure 5.9: Transmission optical microscopy images: a) SCF, b) MCF, and c) LCF (*y*-*z* plane).

5.1.2 Electrical Properties

5.1.2.1 Graded Surface Resistance

The results presented in the previous paragraphs showed that gradients in the CF distributions can be created in the EP matrix by the use of the centrifugation technique. As CF are inherent conductive fillers, they are anticipated to lead to graded electrical properties along the direction of the centrifugal force. In order to investigate this possibility, the surface resistance along the *x*-axis of the sample was measured, as previously described in section 4.4.1.

The surface resistance was found to decrease along the thickness of the samples in the direction of the centrifugal force, following the increase in CF concentration. This trend is to be expected since the electrical properties of polymers filled with conductive fillers are closely related to the fillers concentration. The gradients of the surface resistance are affected from the same parameters which influence the CF concentration profiles, as seen Figure 5.10. Using higher centrifugation speeds, larger fibre contents are achieved near the bottom of the sample, resulting in very low values of surface resistance. The conductive part of the sample thickness, i.e. the

part with low resistance values, becomes larger for centrifugation speeds higher than 1000 rpm, while for the isotropic sample (0 rpm) with the same total CF content, the surface resistance remains to the high values of the neat EP matrix (Figure 5.10a). Similar trends are observed in the case where different total CF contents are used, as shown in Figure 5.10b. A low total CF concentration is not sufficient to enhance the electrical properties of the insulating matrix. However, further addition of CF can lead to a sharp decrease of the surface resistance near the bottom-side of the samples. As the total fibre content increases, the part of the sample thickness with low surface resistance is also increasing. Furthermore the fibres with different lengths result in different gradients in the surface resistance (Figure 5.10c).

The comparison of the different samples, illustrated in Figure 5.10, indicates that sharp changes in the surface resistance take place along the thickness. The low resistance at the bottom-side returns quite rapidly to insulating values. Even though the surface resistance follows in all cases an opposite trend to the fibre concentration (i.e. an increase in fibre content corresponds to a decrease in surface resistance), this variation does not occur in a smooth way, as for the CF concentration. Electrical conductivity is not a linear function of the filler content. For each CF type a specific concentration threshold should be reached, in order to result in the enhanced electrical properties. This fact can therefore explain the abrupt profiles of surface resistance.

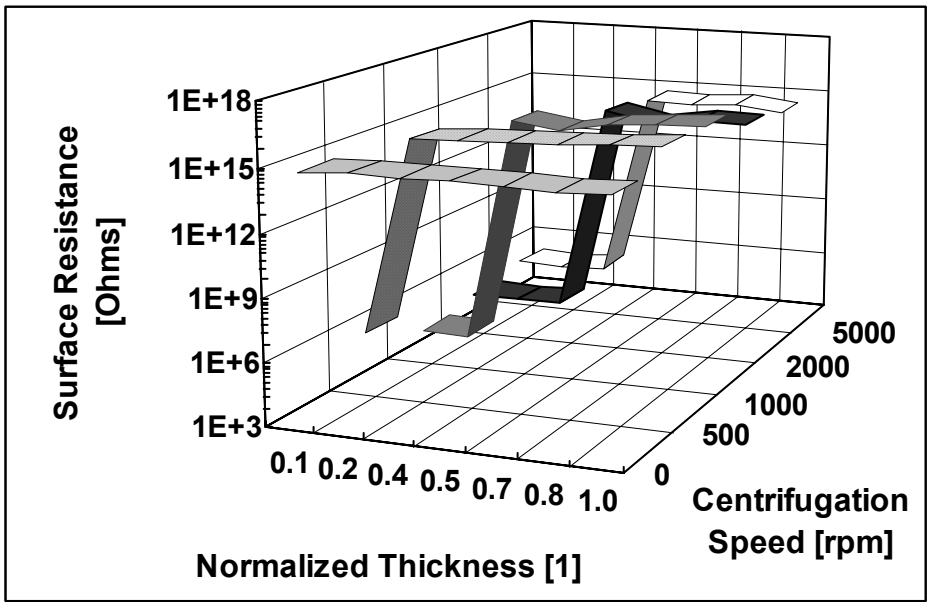

a)

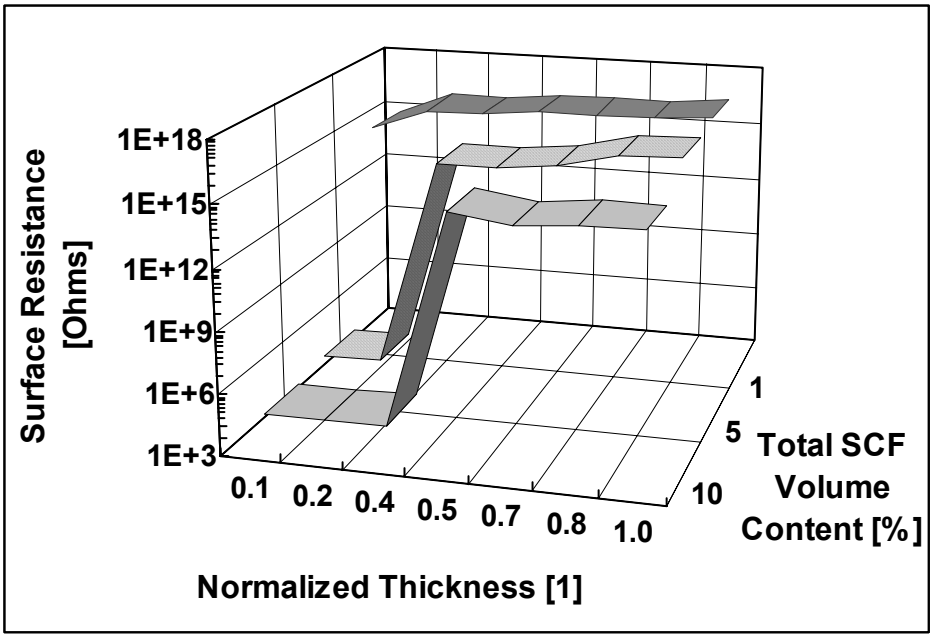

b)

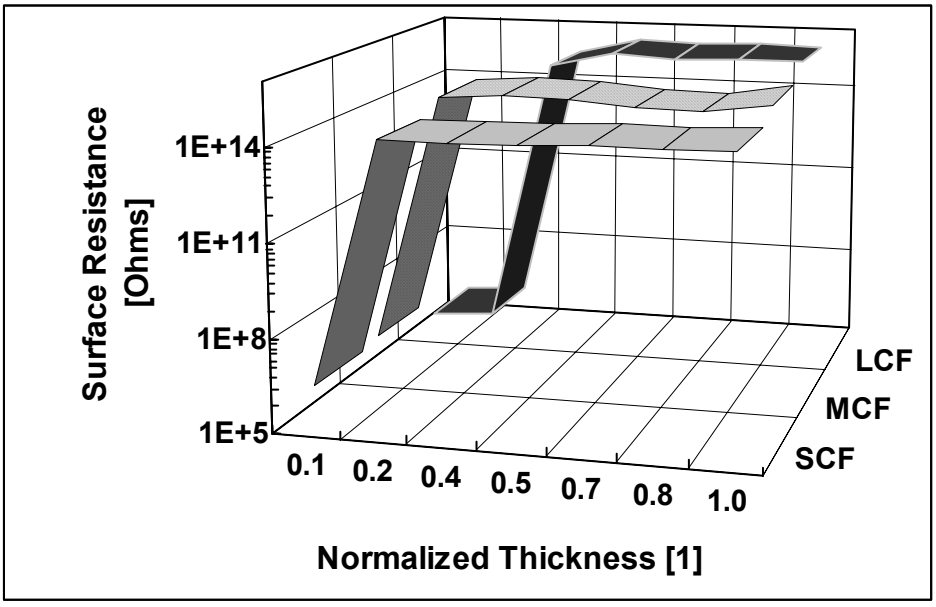

c)

Figure 5.10: Surface resistance along the thickness of graded samples with different fabrication parameters: a) Various centrifugation speeds. Total SCF content: 10 vol.%, b) Various total SCF content. Centrifugation speed: 2000 rpm, and c) Different CF types. Total CF content: 1 vol.%. Centrifugation speed: 1000 rpm.

5.1.2.2 Electrical Conductivity

Figure 5.11 illustrates the influence of the volume content of the different fibre types on the electrical conductivity, as it was determined by volume resistivity

measurements. A steep conductivity increase is evident for each CF type. The percolation threshold is determined at about 23.6, 10, and 3.3 vol.% for the SCF, MCF, and LCF, respectively. At lower concentrations the fibres are separated and thus no conductive pathways can be created throughout the insulating EP matrix between the neighbouring fibres. The transport of charge carriers is inefficient and therefore the overall conductivity of the composites remains at low levels. The conductivity rises steeply when effective contacts are made among the fibres and a continuous conducting chain on macroscopic level is built. Physical contact is not necessary in order to observe a conductivity enhancement, but the distance between the fibres must be small enough (about 10 nm) in order to permit electron hopping across the gap [80]. This behaviour is represented by the non-linear current-voltage dependence of these materials. During the experimental measurements, lower volume resistivity values were obtained for higher voltages especially for low fibre contents. With increasing intensity of the applied electric field the probability of charge transfer through the insulating gap of matrix rises resulting to lower resistivity values. However, increasing filler content results in nearly linear *I-U* characteristics, implying that the conductivity obeys the Ohm's law. Therefore, for high fibre contents ($V_f > V_c$) conduction is achieved through fibre contacts.

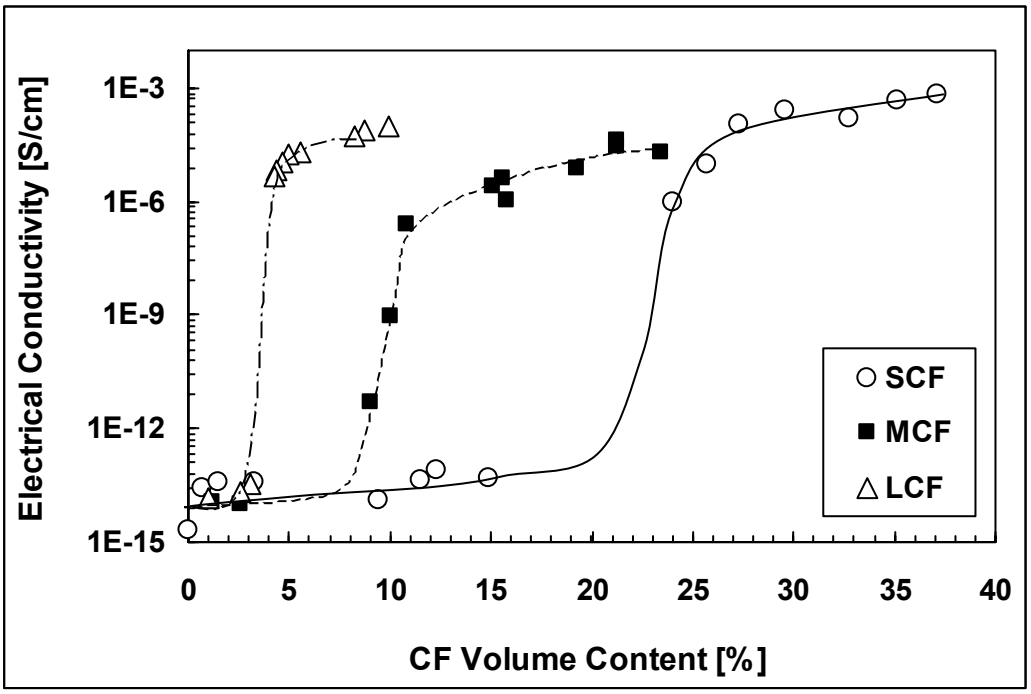

Figure 5.11: Percolation curves for the different types of CF.

The percolation threshold is highly dependent on the geometry of the fillers, as observed from the experimental curves (Figure 5.11). Longer fibres have a high probability of making effective contact with neighboring fibres in order to form the required path for electrical conduction, and therefore the percolation threshold is shifted to lower values. Other investigators have also previously confirmed a close relationship between the fibre aspect ratio and percolation threshold [59,81]. Figure 5.12 shows the relationship between aspect ratio and critical fibre concentration needed to induce conductivity. The relationship is linear on a log-log plot, and shows the dramatic effect of fibre aspect ratio on the critical volume content, V_c. Bigg [82] found that the percolation threshold is inversely proportional to the 0.6 power of the aspect ratio for randomly dispersed fibres in the matrix, a finding which is in a rather good agreement with the experimental data of the present study.

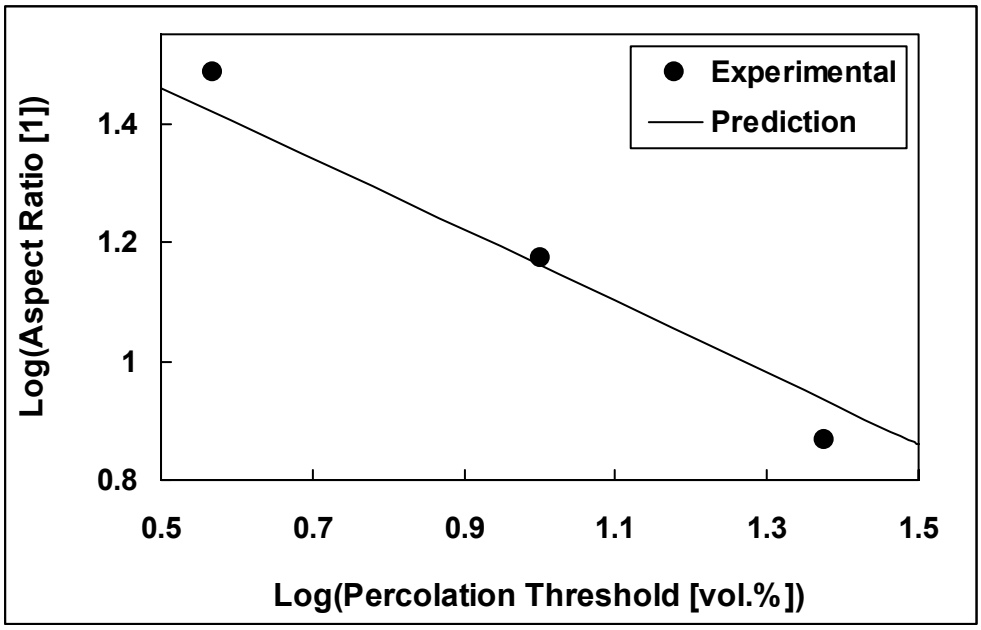

Figure 5.12: Fibre aspect ratio versus percolation threshold: Experimental data and calculated values after Bigg [82].

5.1.3 Mechanical Properties

5.1.3.2 Flexural Properties

In order to study the flexural properties of the graded CF/EP composites, an extra set of samples with 3 mm thickness was fabricated under the same conditions mentioned in paragraph 4.2.1, and subjected to bending. The reason was the

following: to compare the two cases in which the samples are loaded either at the fibre-poor surface (Type I) or at the fibre-rich surface (Type II) (Figure 5.13). For comparison, isotropic samples were also prepared.

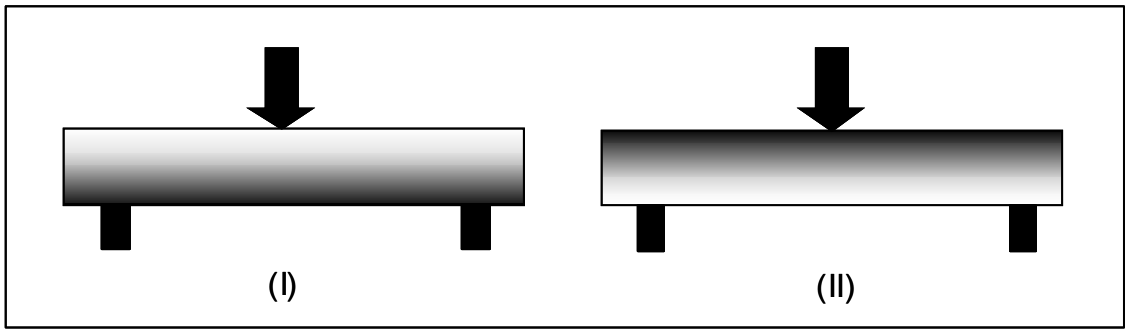

Figure 5.13: Flexural test of graded CF/EP composites.

Table 5.2 shows the flexural properties of these specimens along with those of the isotropic and neat EP samples. Type I specimens exhibit the lowest values of flexural strength while Type II the highest ones, for every type of CF. In case of the flexural modulus, the different CF/EP composites exhibit similar values and evident improvement over the neat resin. A tendency can be also observed in the values of the elongation at break values: the larger values correspond to the Type II samples, while the smaller to the Type I samples. However, the elongation at break is in all cases lower to that of the neat EP matrix. These results indicate that the mechanical properties of the lowest area of the specimen, which is submitted to tensile stresses, plays a significant role in the flexural behaviour of the CF/EP composites. The absence of CF in the Type II specimens on the opposite side of the centre loading point, leads to a greater elongation at break, while the richness in CF at the loading side improves the resistance to compression failure. These two phenomena are deemed responsible for the higher flexural strength and elongation at break values of the Type II specimens.

In Figure 5.14 the fracture surfaces of graded SCF/EP and MCF/EP specimens are presented. The arrow shows the direction of the centrifugal force. For the SCF/EP sample a large dissimilarity between the two different fracture surfaces can be observed: the left side appears to be rich in fibres, while at the right side only neat resin is visible. In contrast, the MCF/EP surface shows no significant variation in the fillers concentration across the centrifugal direction. The different microstructures of

these specimens can also explain the observation of higher values in flexural strength and elongation at break for the Type I specimen with MCF compared to that containing SCF (Table 5.2).

Table 5.2: Flexural properties of graded CF/EP composites. Centrifugation speed: 1000 rpm.

	EP	SCF 10 vol.%			MCF 10 vol.%			LCF 3 vol.%		
		Isotropic	Type I	Type II	Isotropic	Type I	Type II	Isotropic	Type I	Type II
Flexural Strength [MPa]	106.6	92.5	90.2	127.0	103.5	100.7	126.4	104.7	92.2	118.9
Flexural Modulus [GPa]	3.1	4.1	4.2	4.8	3.6	4.2	4.2	3.7	3.3	3.7
Elongation at Break [%]	4.5	2.3	2.0	4.0	3.2	2.5	3.6	3.2	3.0	3.8

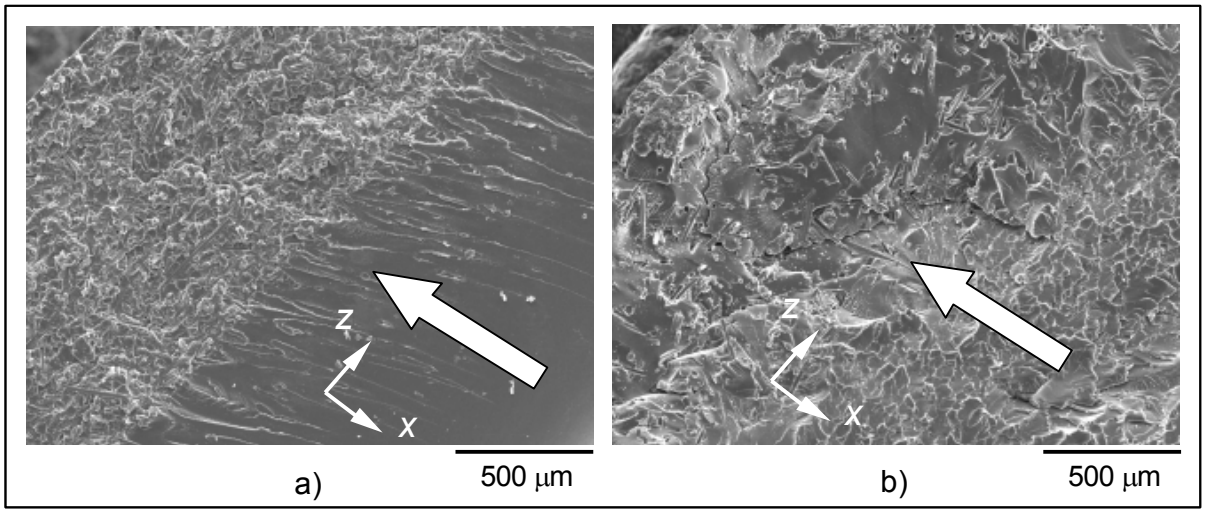

Figure 5.14: Fractures surfaces of graded samples containing a total content of 10 vol.% a) SCF and b) MCF. Centrifugation speed: 1000 rpm.

In a second step to characterise the mechanical properties of the graded CF/EP materials, the 2 mm plates cut perpendicular to the centrifugal force (cf. Figure 4.2c) were submitted to flexural test. In this way, possible gradients in the mechanical

properties of the specimens can be investigated. Figure 5.15 presents the different values of CF concentration and flexural modulus along the thickness of samples having a total content of 10 vol.% SCF or MCF, and centrifuged under 1000 rpm. As the volume content of the fibres decreases, the flexural modulus is also reduced. It is also clear that the changes in the materials stiffness are smoother when a gradual variation in the fibre concentration exists within the specimen. The controlling of the graded fibre distribution by the parameters mentioned in the above paragraphs can also lead to tailored mechanical properties across the thickness of the specimen.

A correlation can be made by comparing the graded profiles of flexural modulus with those of surface resistance (c.f. Figure 5.10). Both functional properties are strongly connected to the local CF concentration. Flexural modulus increases, while surface resistance decreases as the fibre content becomes larger along the sample thickness. However, the flexural modulus exhibits smoother profiles, indicating that this property is enhanced gradually with addition of CF.

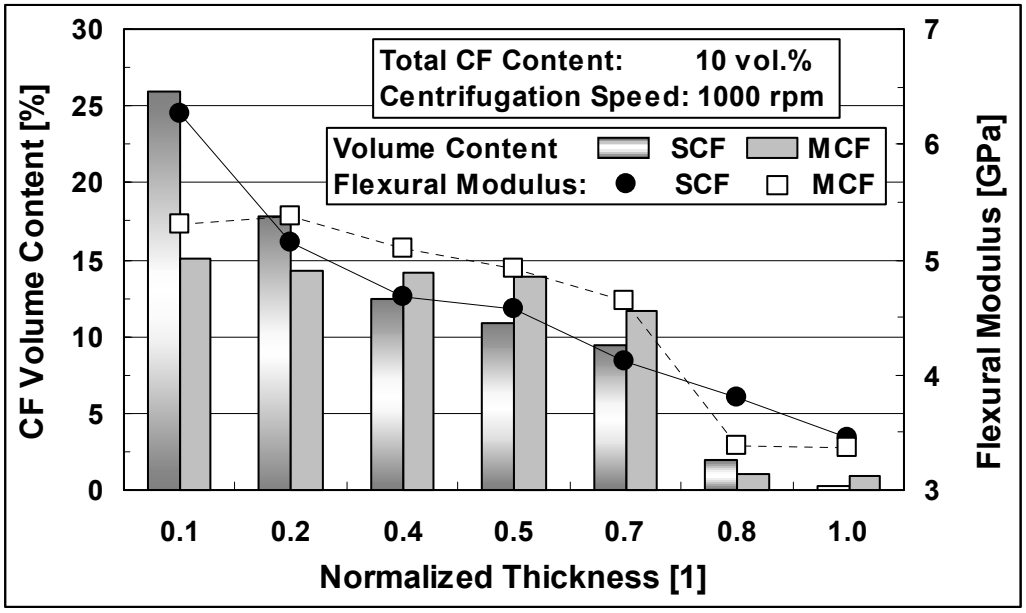

Figure 5.15: Variation of CF content and flexural modulus along the thickness of graded CF/EP samples.

Figure 5.16 shows the flexural modulus as a function of volume fraction of the different CF types. These results are summarised from many values obtained for a large number of graded samples. The value of E_f is constantly increasing with an increase in the CF volume fraction, while for the same concentration the longer CF

result in higher E_f values. The general trend was that CF led to an increase in stiffness, but a reduction in the ultimate elongation of the composites. The flexural strength was not significantly influenced by the addition of the CF.

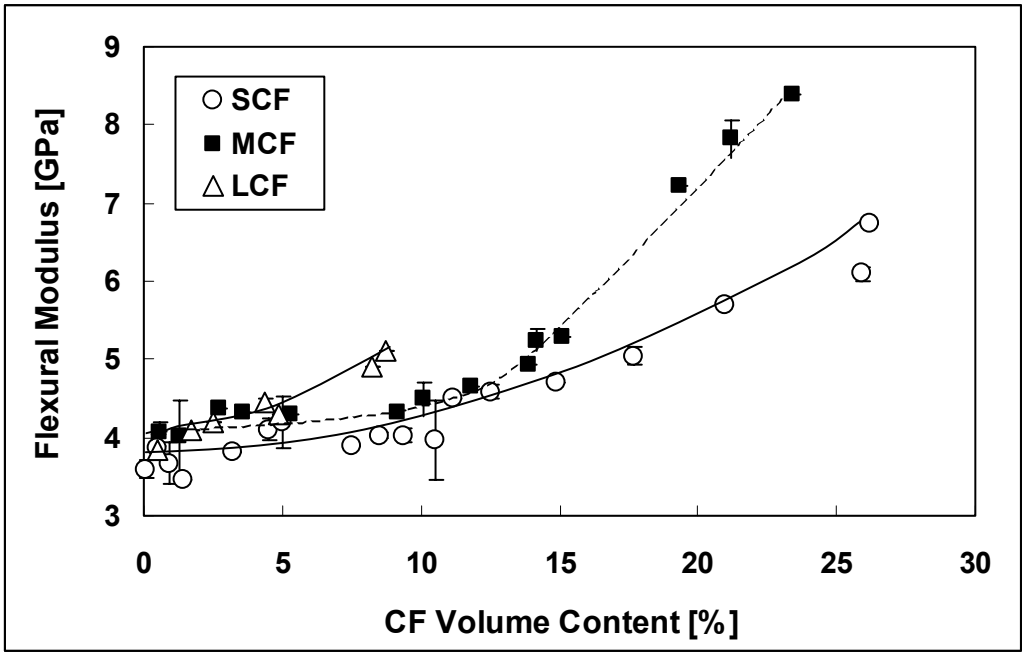

Figure 5.16: Influence of the fibre content on the flexural modulus of CF/EP composites.

5.1.4.2 Microhardness

Along with the density measurements or optical observations, described in the previous sections, some other simple methods are previously reported in the literature for the evaluation of the composition gradients in FGMs [61,83]. The mutual relation among hardness and volume fraction naturally satisfies the hypothesis that hardness is proportional to the composition gradients.

The distributions of the Vickers hardness and SCF volume content across the thickness of two different graded samples are presented in Figure 5.17. It is apparent that the microhardness follows the decrease in fibre concentration across the sample thickness. Very high *HV* values are reported for the side of maximum particle concentration, while low values are measured for the fibre-poor side. A quite sharp transition is observed between these two zones. The curve of Universal hardness showed similar tendencies, with maximum and minimum values of 305 and 145 MPa, respectively. Measurements of hardness can occur in very small steps, and therefore

a more detailed impression of the graded structure can be obtained by this procedure compared to that derived from density measurements.

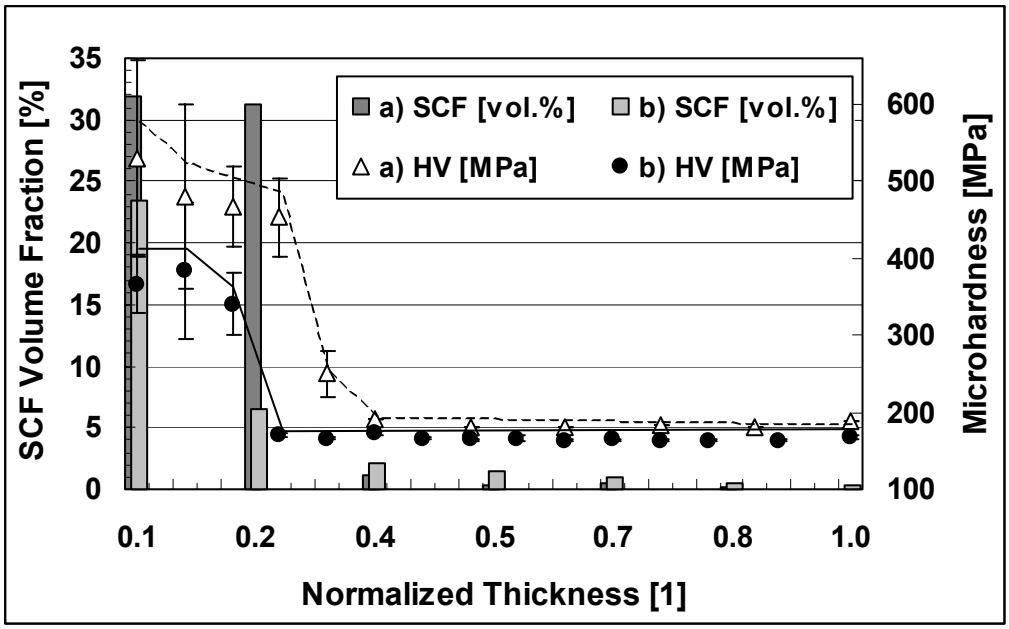

Figure 5.17: Variation of Vickers hardness and the SCF volume content along the thickness of graded samples: a) total SCF volume fraction 10 %, centrifugation speed 5000 rpm, and b) total SCF volume fraction 5 %, centrifugation speed 1000 rpm.

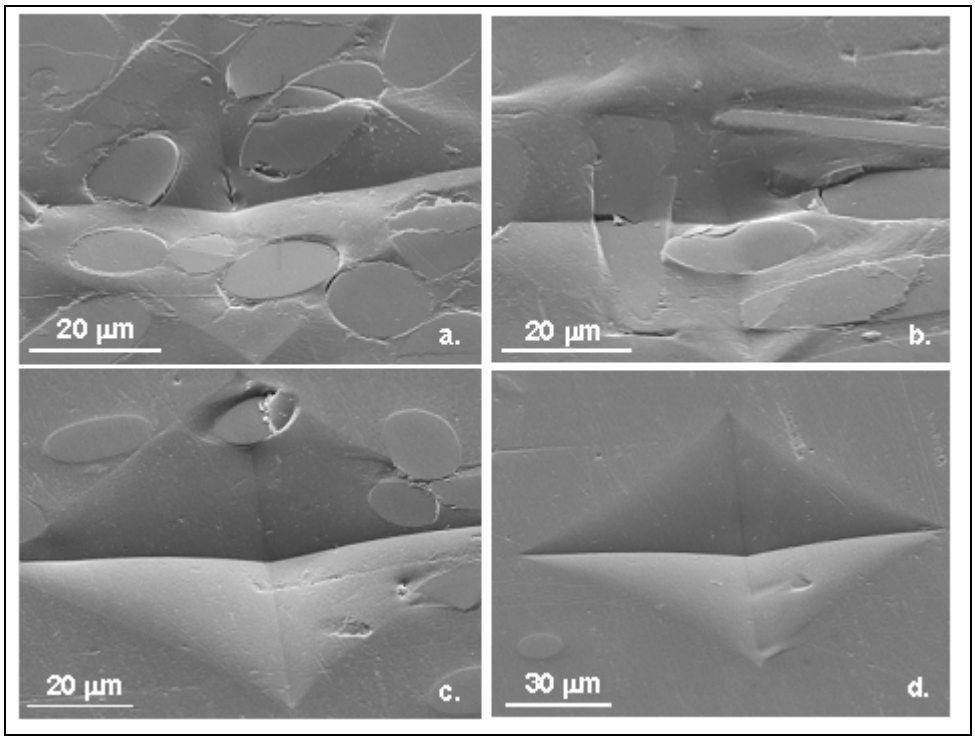

Figure 5.18: SEM micrographs of the indentations on an SCF/EP graded sample a) near the bottom-side, b) the middle of its thickness, and d) near the top-side.

The indentations were observed by scanning electron microscopy in order to attain a better understanding of the samples behaviour during the microhardness test. For the fibre-rich areas (Figure 5.18a, b) the fibres are deformed in different ways depending on their location and orientation with regard to the tip of diamond. Some of them were broken, while others seemed to be only pushed into the softer EP matrix.

It has been suggested [84] that for a number of glassy and semicrystalline polymers, copolymers and blends, microhardness obeys the following additivity law:

$$HV = \sum_i HV_i \cdot V_i \qquad (5.2)$$

where V_i is the volume content, and HV_i the microhardness of each component. In Figure 5.19 the Vickers hardness is plotted versus the SCF volume fraction. A nearly linear relationship can be observed. The extrapolation to V_f =100% leads to a *HV* value of about 1126 MPa for the CFs. This result agrees with the published microhardness value for graphite (1 GPa) [85], which is probably the limiting lower value for the microhardness of CFs.

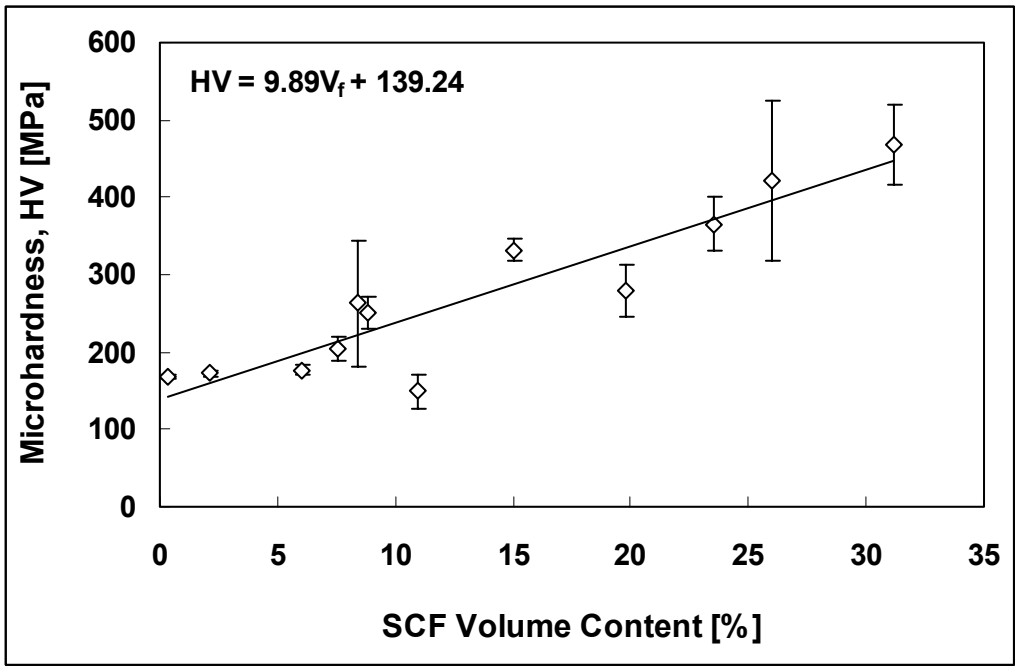

Figure 5.19: Dependence of the Vickers hardness on the SCF volume content.

The slope of the unloading curves obtained during Universal hardness (*HU*) testing has often been regarded as a measure of the materials mechanical properties

[86,87]. In Figure 5.20 a typical load-depth curve of a *HU* test is illustrated. The elastic modulus, *E*, can be obtained by the procedure proposed in [86] via:

$$E = \left(\frac{\pi}{A}\right)^{0.5} \frac{S}{2}\left(1-\nu^2\right) \tag{5.3}$$

where $S=dP/dh$ is the initial unloading stiffness, $A=24.5h^2$ is the projected area of contact between indenter and sample, h the penetration depth of the indenter, and ν is the Poisson's ratio.

According to this method, a power law equation is used to describe the unloading curves:

$$F = c\left(h-h_f\right)^k \tag{5.4}$$

where F is the load, h-h_f the elastic displacement, and c and k are material constants. The value of h_f can then be determined experimentally by the unloading curve. In this work F was plotted versus h-h_f and by power equation fitting the parameters c and k were determined. The initial unloading stiffness S was then obtained by analytically differentiating Equation 5.4 and evaluating the derivative at the maximum displacement.

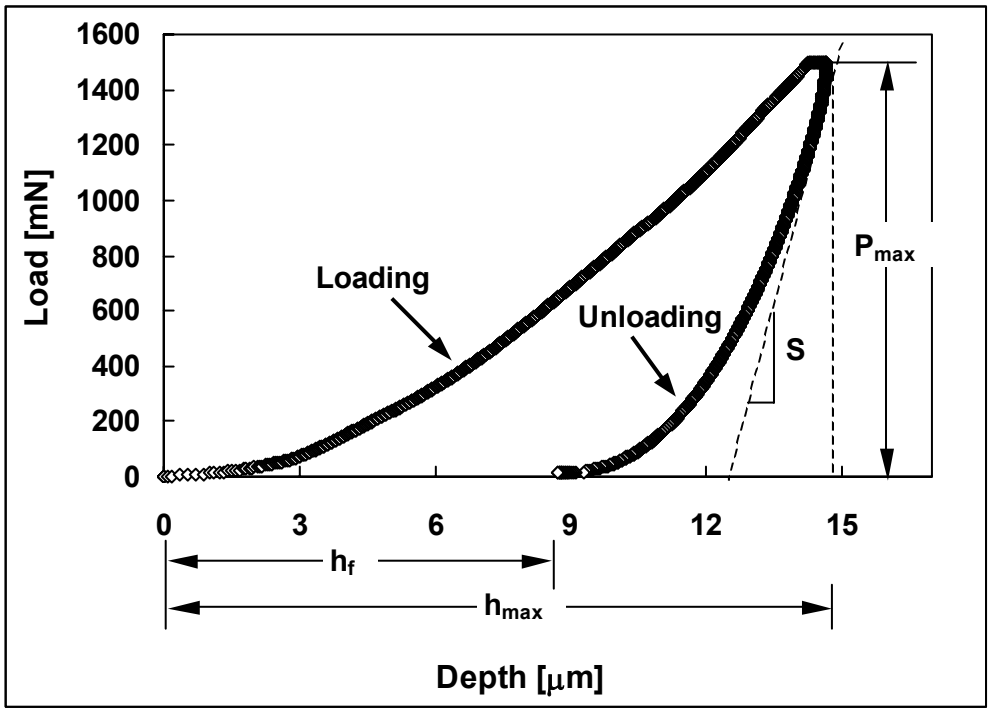

Figure 5.20: Typical load-depth curve obtained during the universal hardness test.

The exact value of E could not be calculated, as the value of Poisson's ratio for the specific system was not available. For this reason, $\nu = 0.4$ was assumed, a value similar to that of the unfilled EP matrix [88]. In Figure 5.21 the estimated modulus by the microhardness test, E_{HU}, is compared with flexural modulus, E_f, for different concentrations of SCF. For low fibre contents a significant difference exists between the two values. In these cases the presence of fibres cannot be easily considered within the small measuring areas where the microhardness tests take place. Most likely the indenter is pushed against neat EP surfaces and therefore the corresponding E_{HU} values are not representative of the overall fibre volume fraction. On the other hand, the flexural test is more capable of taking into account the small amount of fibres in the EP matrix, and thus more realistic values of the modulus can be obtained. For higher fibre concentrations, the E_{HU} values tend to approach the ones for E_f. Since the fibres are present in a larger area of the sample surface, the microhardness test is able to predict the E modulus more accurately. Nevertheless, in order to obtain reliable E_{HU} values, indentations should be performed in many points (at least ten) within the area with the same CF concentration, and then the average value of E_{HU} should be calculated.

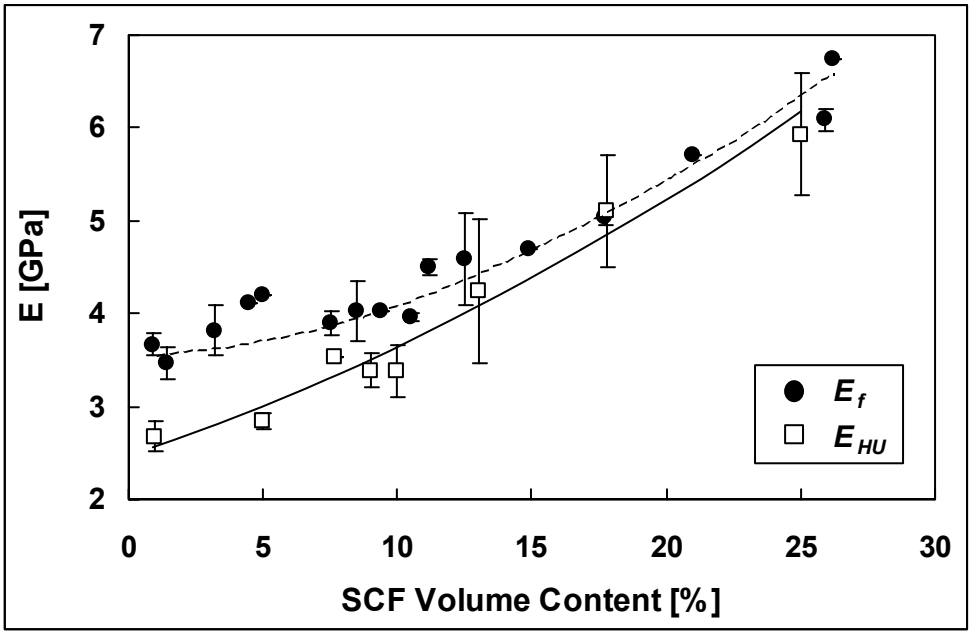

Figure 5.21: Variation of the flexural modulus, E_f, and the estimated by microhardness test modulus, E_{HU}, with the SCF volume content.

5.2 Epoxy Resin/Polyaniline Blends

The conductive polymer composites described in the previous sections correspond to the incorporation of carbon fibres in the insulating EP matrix. In a further effort to enhance the electrical properties of the insulating EP system, a conductive polyaniline salt was tested as a filler. Nevertheless, significant problems were encountered during the preparation of the blends, which commanded to a more detailed survey of their chemical and physical character. The effect of the PANI concentration on the electrical, thermal and mechanical properties of the blends is reported in the following paragraphs.

5.2.1 Processibility of PANI-DBSA

Processing of ICPs, and more specifically of PANI, has been a key problem for basic research and industrial applications. The known methods to produce PANI blends may be essentially reduced to two basic groups [89]: a) synthetic methods based on aniline polymerisation in a polymer matrix, and b) blending methods based on mixing a previously prepared PANI with a polymer matrix. Each of these methods has its own advantages and limitations. The synthetic methods are less expensive due to the use of aniline instead of the costly PANI, while the blending methods seem to be more technologically desirable from the viewpoint of large-scale production. Several of the studies on the preparation of epoxy resin based PANI blends followed the blending methodology [41-45].

As mentioned in paragraph 2.2.1.3, Cao et al. [33] have previously introduced a processing route for the conductive form of PANI-emeraldine salt where, via protonation of PANI by functionalized protonic acids, solubility of the salt can be achieved in non-polar or weakly polar organic solvents. Generally, the organic solvents that dissolve PANI in its conductive form can be divided in two groups [32]. The first group comprises substances with strong hydrogen-bonding groups such as cresols, chloroform, NMP formic acid, and other strong acids. These substances are capable of dissolving at room temperature, PANI-salts that are fully protonated, i.e. have a H^+/PhN ratio of 0.5 [32]. A second class of organic solvents contains those species without or with only very weak hydrogen-bonding ability, such as toluene,

xylene, chlorobenzenes, etc. Fully protonated PANI-salts can be dissolved in this kind of solvents only in the presence of a particular co-solvent. An excess of the same or different functionalized protonic acid (H^+/PhN > 0.5) can also act as co-solvent. This excess amount is hydrogen bonded to the PANI backbone for every 0.5 to 1.0 mole per PANI repeat unit. However it is obviously difficult to find a well-defined boundary between solution systems and nano-scale dispersions. This is rather a problem of definition, and has been a frequent topic of discussions for PANI containing systems [90].

The PANI-DBSA salt used in the present study contains an excess amount of dopant. In order to check the solubility of this salt, simple qualitative solubility tests were carried out using the solvents *m*-cresol, toluene, chloroform, formic acid, xylene, and NMP. PANI-DBSA was found to be either soluble, or partially soluble in toluene, xylene and chloroform, producing dark green solutions. By comparing the solubility parameters (δ) (Table 5.3) between PANI-DBSA and the different solvents, its miscibility in those solvents can be understood. The solubility parameter offers a simple but very approximate method to predict the solubility of polymers, i.e. polymer-solvent with matching solubility parameters can be estimated to be more soluble in one-another than those with more differing solubility parameters. It is should be noted that the solubility parameter of PANI-DBSA reported in this table corresponds to salt without excess DBSA [36]. Since for DBSA δ =18.6 $(J/cm^3)^{0.5}$, a reduced solubility parameter is expected for the overdoped salt used in the present study. Therefore, PANI-DBSA is expected to be soluble in the solvents with δ between 18 and 19 $(J/cm^3)^{0.5}$. For EP, the solubility parameter is around 23, a value not close to that of PANI-DBSA.

For the development of the conductive blends in this study, toluene was chosen as solvent of the PANI-DBSA, and the solutions were prepared according to the process described in paragraph 4.2.2.

Table 5.3: Solubility parameter values for PANI-DBSA, EP, and different solvents.

	Solubility Parameter [$(J/cm^3)^{0.5}$]		Solubility Parameter [$(J/cm^3)^{0.5}$]
PANI-DBSA	20.1	Benzene	18.7
EP	~23	Chloroform	19
Hexane	14.9	NMP	23.4
Xylene	18.2	*m*-cresol	27.2
Toluene	18.3	Formic Acid	27.6

5.2.2 Compatibility of PANI-DBSA with EP Systems

In a first effort to prepare electrically conductive EP/PANI-DBSA blends, the same EP system used as a matrix for the CF was mixed with the conductive salt. The optical observations of these mixtures showed colour changes after the addition of the curing agent, from green to blue. According to the literature [29], green protonated PANI converts to blue nonconductive emeraldine base on direct treatment with alkaline medium. Chiang et al. [30] reported, for example, that emeraldine hydrochloride converts to the emeraldine base by stirring with a dilute aqueous methanolic solution of KOH. Amines on the other hand have a basic character. The nitrogen atom of amine has a pair of electrons, and this gives rise to characteristics of nucleophilicity and basicity. The basic character of the amines can be schematically presented by the following reaction:

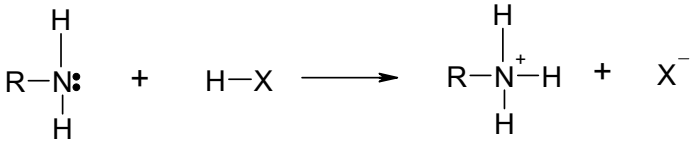

On the other hand, Sertova et al. [91] have presented the deprotonation of the PANI-HCl salt using a base as:

$(EB)H^+Cl^- \rightarrow$ PANI-EB + HCl

It is therefore possible that a reaction takes place between the dopant of PANI, in this case DBSA, and the amine which finally leads to deprotonation of the conductive

salt. Gospodinova et al. [92] have found that the formation of polyaniline salt can be terminated by simply increasing the pH value of the reaction medium from the acidic regime to the alkaline regime, probably indicative of the neutralization of the oligomeric and polymeric radicals or radical cations through the separation of the acidic catalyst. From a similar point of view, several researchers have previously noted the importance of pH on the protonation state of PANI salts [26,30]. As an example, a highly conducting state of the hydrochloride salt can be obtained at low pH, while a low conductivity state is achieved at pH above 4 or 5. However, the sulfonated form of PANI can retain its conductivity up to pH 7 or 8.

In order to investigate the influence of the curing agent's nature on the protonation state of PANI-DBSA, different types of curing agents were tested. In every case the same EP matrix was utilized (Epikote 862, Resolution Performance Products) and blends containing 6.75 vol.% PANI-DBSA were prepared. The mixing ratios and curing schedules for each type of hardener are summarized in Table 5.4. Their chemical structures are illustrated in Figure 5.22. In the case of the anhydride hardener, an accelerator (1-Methylimidazole, DY 070, Ciba-Geiby Ltd.) was used for the initiation of the polymerisation process. The pH value of this component was 11 at 20°C.

Table 5.4: Characteristics of the different hardener types used.

Designation	Amine	Anhydride	Imidazole	BF_3
Brand Name	HY 2954	HY 917	EMI-24	Anchor 1170
Producer	Vantico	Ciba-Geiby	Air Products	Air Products
Composition	Cycloaliphatic Diamine	Methyl Tetrahydrophthalic Anhydride	2-Ethlyl-4-Methylimidazole	Trifluoroboron (4-Chlorobenzene-Amine)
Mixing ratio parts (EP/Hardener)	100/35	100/90	100/4.4	100/10
Cure schedule [hr/°C]	1/80;4/120	4/80; 2/140	3/60; 1/70; 1/100	1/50; 2/70; 0.5/130
pH [at 20°C]	12	3.7	11.5	4

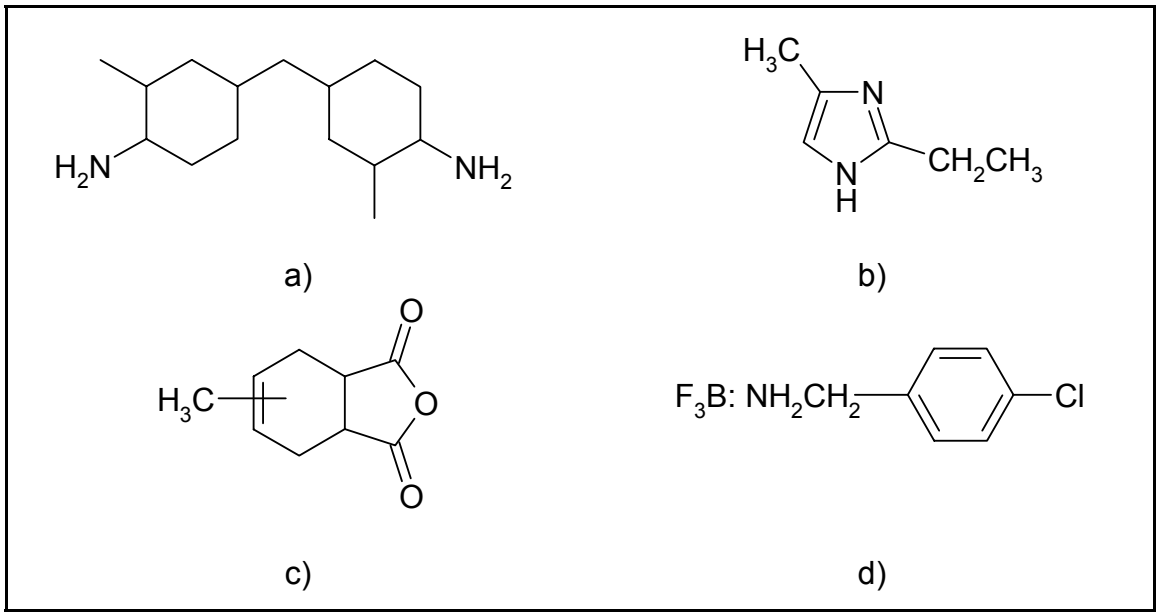

Figure 5.22: Chemical structure of the different types of curing agents: a) amine, b) imidazole, c) anhydride, and d) BF_3.

A change of the blend's colour (from green to blue) was observed in the case of amine and imidazole, while the green colour was retained in the case of anhydride and BF_3. The pH values of the different mixtures were measured before curing by a pH electrode (SenTix 81, WTW) in connection with a measuring system (inoLab Level 3, WTW), at room temperature. In Table 5.5 the determined pH values, together with conductivity values of the cured samples, are presented. It can be seen that the blends with the higher pH values, i.e. the ones containing amine and imidazole, are those who exhibit the lower values of electrical conductivity after curing. In the case of anhydride, an enhancement of the conductivity is observed compared to the neat epoxy, but the material remains in the insulating range. Nevertheless, the use of the BF_3 curing agent, which has a strongly acidic character, leads to an increase in the electrical conductivity by many orders of magnitude. Therefore a strong connection is apparent between the conductivity of the EP/PANI-DBSA blends and the colour and pH values of these blends before curing. These properties on the other hand, are strongly connected to the type of hardener used and thus the choice of curing agent is proved to be a key parameter for the development of conductive thermosetting blends.

Table 5.5: Properties of the mixtures of EP/PANI-DBSA with the different hardeners.

	Amine	Anhydride	Imidazole	BF_3
pH [at 20°C]	10.5	5.9	9.5	1.6
Colour	blue	green	blue	green
Conductivity after curing [S/cm]	$<10^{-14}$	10^{-12}	$<10^{-14}$	$8 \cdot 10^{-8}$

UV-vis spectroscopy is a sensitive tool for studying the protonation state of polyaniline. Transmission spectra of EP/PANI-DBSA blends with the different curing agents were measured, as well as of PANI-EB and the PANI-DBSA for comparison. For the PANI-EB, N-methylpyrrolidone (NMP) was used as solvent and reference, whereas toluene was utilized for the doped polymer. The spectra are presented in Figure 5.23. It should be noted that in this diagram the transmission of the solutions is shown and therefore the minimum values of the curves represent the related peaks. The base polymer shows two characteristic peaks: at 330 nm (A) due to $\pi \rightarrow \pi^*$ transition of the benzenoid amine structure, and at 630 nm (B), corresponding to the excitation of the quinoid imine structure [93]. For the doped PANI-DBSA, the peak at 630 nm disappears. This confirms that PANI is in a fully protonated state [31]. The position of the peak at 330 nm does not change, whereas two new peaks at 450 (C) and 800 nm (D) appear, both stemming from the formation of delocalized polarons [94]. The spectra of the EP/PANI-DBSA blends with anhydride and BF_3 confirm the initial hypothesis that PANI-DBSA remained in its doped state, since the characteristics peaks of the doped polymer are observed. On the contrary, the spectra of the blends with amine and imidazole tend to exhibit the peaks corresponding to the nonconductive PANI-EB, which is in agreement with their poor electrical properties. An interesting observation of the above mentioned results is that the cured anhydride samples did not show significant enhancement of the electrical properties, although the UV-spectra of the blend exhibited peaks similar to those of PANI-DBSA. This may be closely related to the curing state of the final samples. DSC measurements of the blends during curing showed that the exotherm peaks for the systems with amine, imidazole and BF_3 lay within their cure schedule, while for the system with anhydride this peak appears in much higher temperatures. It is speculated that PANI-DBSA negatively influences the curing of this system, leading to a weak cross-linked network with poor electrical properties. Jia et al. [45] had also

observed, by means of DSC analysis, a partial inhibition of the cross-linking reaction of the epoxide groups with anhydride groups due to the presence of DBSA.
It is clear that in order to retain the protonated state of PANI-DBSA, a hardener with acidic character should be chosen. The blends, which will be presented and analysed in the following paragraphs, were cured with the BF_3 curing agent as it led to higher conductivity values.

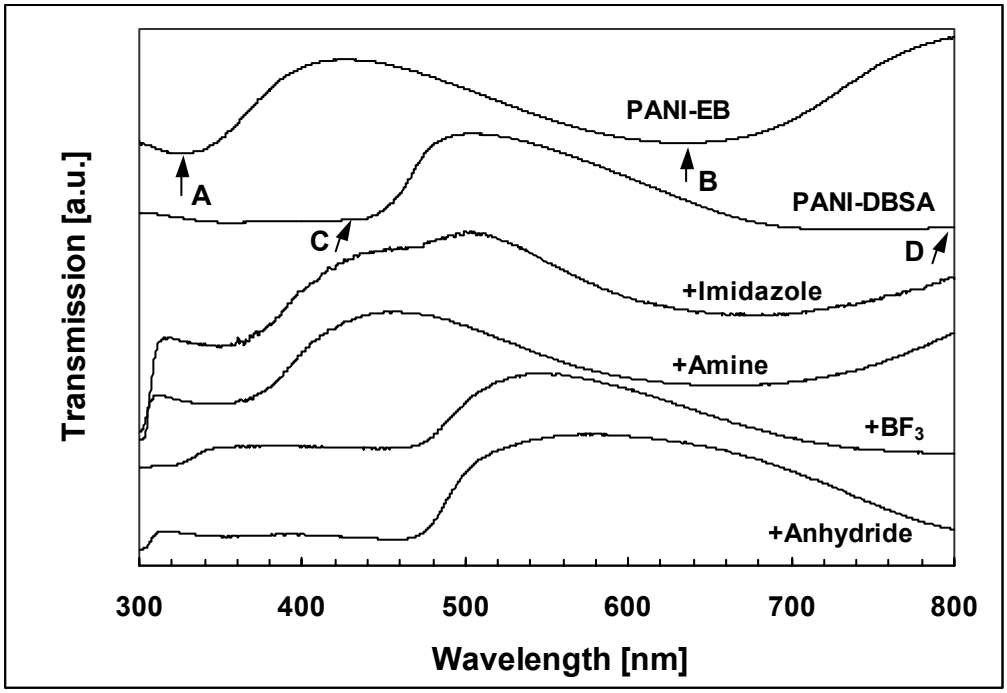

Figure 5.23: Transmission spectra of PANI-DBSA, and its blends with epoxy resin and different curing agents.

5.2.3 Microstructure

The density of the neat EP was found to be 1.240 g/cm^3. The addition of PANI-DBSA led to a decrease in the blends density, which reached a value of 1.206 g/cm^3 at 11.1 vol.% PANI-DBSA. By the measured density values of the different EP/PANI-DBSA blends and the respective volume fractions, the density of the conductive salt was estimated to be around 1.1 g/cm^3.

In Figure 5.24 the three stages during the preparation of the EP/PANI-DBSA blends are illustrated. The final cured blend contained 7.8 vol.% PANI-DBSA. Droplets of the different mixtures were pressed between two glass plates and observed by transmission optical microscopy (TOM). The salt solution in toluene produced green

transparent films (left image) and no particles were visible. The films from the mixtures of EP and PANI-DBSA, after evaporation of the solvent, were also transparent and green in naked eye but their observation by TOM (middle image) revealed the creation of a structure with darker and lighter phases. This structure was retained after the curing process (right image). However, TOM analysis was not able to supply detailed information about the creation of the conductive network and the exact size of the individual particles.

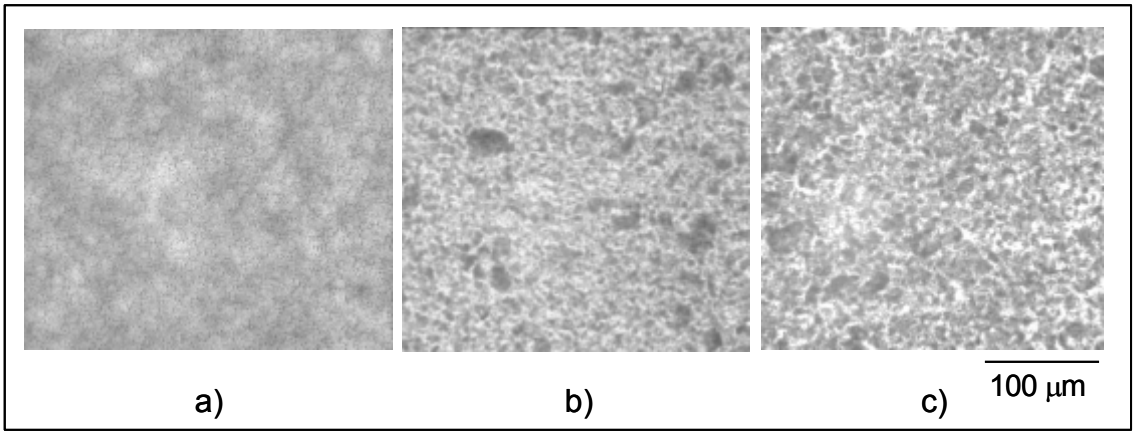

Figure 5.24: TOM images of a) PANI-DBSA solution in toluene, b) mixture of PANI-DBSA with resin, and c) cured EP/PANI-DBSA blend (7.8 vol.%).

In order to obtain a clearer understanding of the state of PANI-DBSA in the EP matrix, a transmission electron microscope, TEM (Philips EM 400), was used. The cured samples were cut in 50 nm thick films using a diamond knife (Leica Ultracut). For the sample containing 2.8 vol.% PANI-DBSA only a small number of agglomerates with diameter less than 50 nm was observed, as illustrated in Figure 5.25a. Moreover, a very fine structure is visible between these isolated agglomerates but it can not be easily defined due to contrast limitations. The existence of this structure was however verified by conductivity measurements (discussed in more detail in paragraph 5.2.5). At this concentration of the conductive salt a significant increase in the electrical conductivity of the blends takes place requiring the formation of conductive pathways.

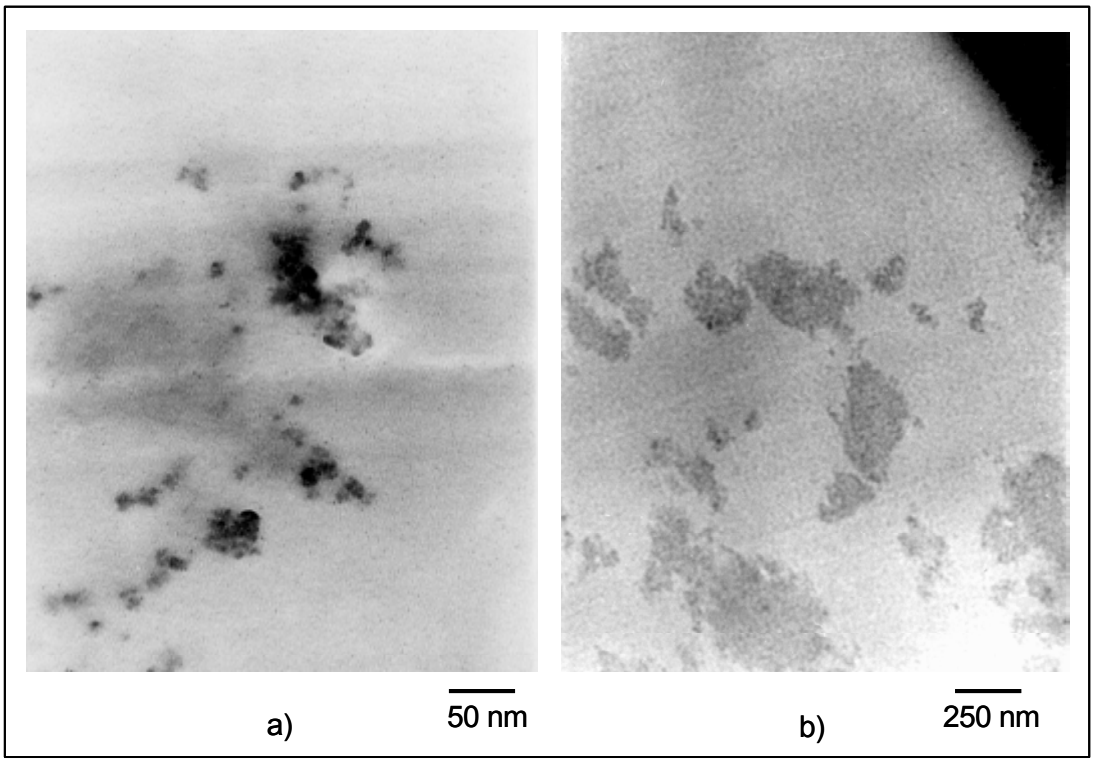

Figure 5.25: TEM micrographs of EP blends with a) 2.8 vol.% and b) 11.1 vol.% PANI-DBSA.

Previous studies on EP/PANI-DBSA blends do not supply much information about the microstructure of these materials [41-45]. Jia et al. [45] using SEM detected PANI agglomerates of 2 μm below the percolation threshold, while for higher concentrations large domains of PANI particles were dispersed in EP, resulting in increased conductivity. Wang et al. [46] observed by means of TEM a perfect network of PANI in melamine-urea resin. Further survey of the literature regarding the microstructure of PANI blends with different polymers, e.g. poly(vinychloride) or poly(methyl methacrylate), indicated the creation of fibrillar PANI networks near the percolation threshold [34, 95-97]. However, the morphology of the present system is undoubtedly different from these PANI dispersions. It is speculated that up to a specific concentration, PANI-DBSA is dissolved in the matrix, forming a translucent conductive network which alters the conductive character of the whole system. This concentartion is estimated between 2.2 and 2.5 vol.% of PANI-DBSA. Above this value the solubility limit is overlapped and the first agglomerates are formed (Figure 5.25a). As the concentration of PANI-DBSA increases, the darker areas are enlarged (cf. Figure 5.25b). These areas may correspond to a more dense PANI-DBSA

network. An interesting observation is that the fine structure visible in the lighter parts of the surface exists also in the darker ones. Therefore, it is not quite clear if the dark spots observed by this TEM analysis represent PANI-DBSA agglomerates or regions with a thicker three-dimensional structure of the conductive salt in the EP matrix.

The microstructure of the cured blends was additionally studied by atomic force microscopy AFM (Nanoscope of Digital Instruments, USA) on surfaces polished and physically ablated ("etched" by Ar+ ion bombardment). The AFM was operated in tapping mode and the related amplitude- and height-contrast images were obtained. PANI-DBSA is expected to be removed from the sample surface via this technique, considering that it is softer than EP. This method has been previously used by Karger-Kocsis et al. [98] for the investigation of vinylester/epoxy-based thermosets of interpenetrating (IPN) structure. Figure 5.26 shows the morphology of blends with different amounts of PANI-DBSA. For the EP system a homogeneous structure is observed. This may depict the developed cross-linked network of EP or simply a pattern created by the etching process. Since the use of AFM method aims at the investigation of the PANI-DBSA distribution and not the structure of EP, this image will be used as reference to compare samples containing the conductive salt. By addition of 3.3 vol.% PANI-DBSA some changes in this structure are visible. Regions with a smoother structure compared to that of the EP system are formed, and few holes (indicated by arrow) attributed probably to PANI-DBSA agglomerates are observed. As the concentration of PANI-DBSA increases, the visible holes are multiplied and the area between them becomes even smoother. In higher magnification (Figure 5.27) the size of the agglomerates can be estimated to be about 200 nm and the fine structure around them can be clearly distinguished. This morphology can be compared to the one obtained by TEM analysis. Both methods revealed the formation of few isolated agglomerates surrounded by a fine network.

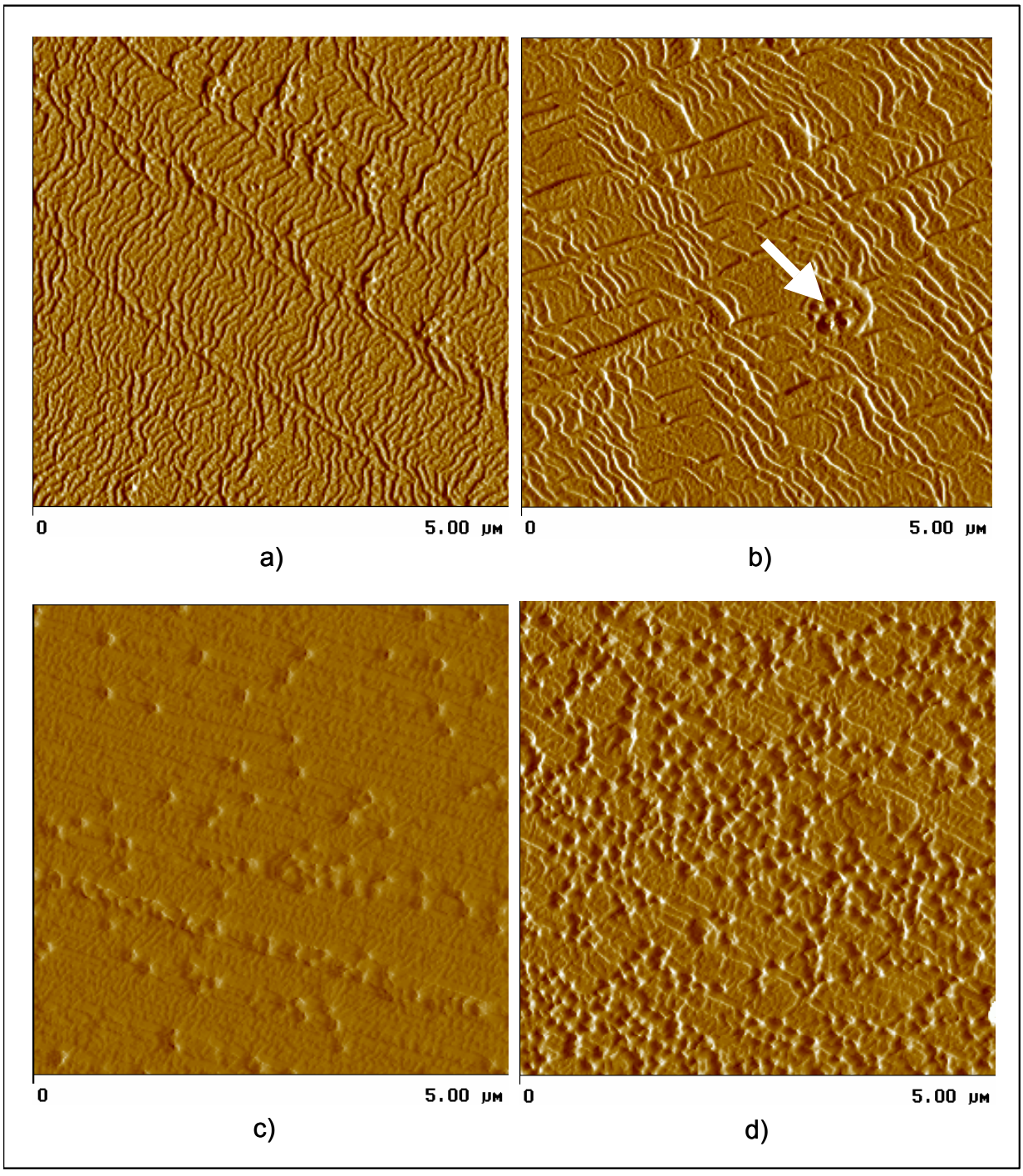

Figure 5.26: AFM amplitude images taken from polished and physically etched surfaces of blends containing a) 0, b) 3.3, c) 7.8, and d) 11.1 vol.% PANI-DBSA.

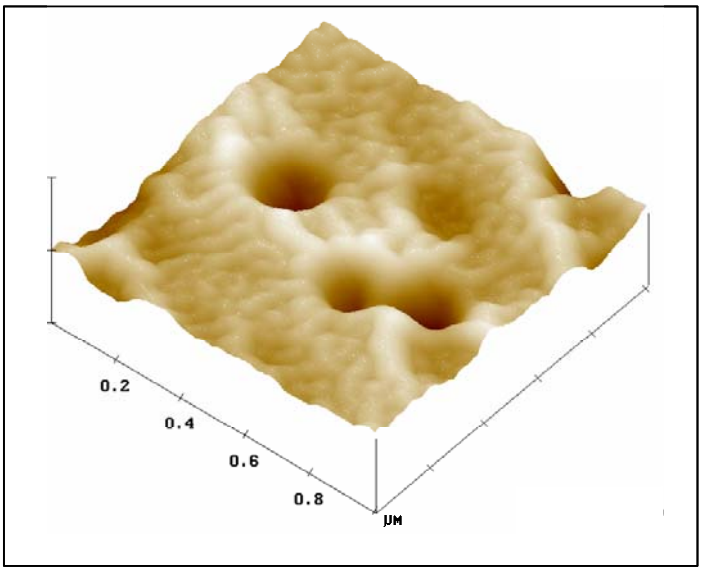

Figure 5.27: AFM height image taken from polished and physically etched surfaces of blends containing 11.1 vol.% PANI-DBSA.

5.2.4 Electrical Properties

The electrical properties of the EP/PANI-DBSA blends were studied by measurements of their volume resistivity, as referred to in paragraph 4.4. Figure 5.28 shows the electrical conductivity versus PANI-DBSA volume content. The expected tendency is observed. Electrical conductivity of the blends rises as the concentration of the PANI-DBSA is increasing, from the value of 10^{-14} S/cm (corresponds to the neat EP matrix) to $2 \cdot 10^{-7}$ S/cm for 11.1 vol. % PANI-DBSA. The percolation threshold is estimated at around 2.4 vol.% of PANI-DBSA. The TEM analysis of the blend with a PANI-DBSA content slightly above the percolation threshold (cf. Figure 5.25a) revealed few individual agglomerates which cannot be the only ones responsible for the enhanced electrical properties of the compound. In this way, the assertion that a translucent conductive network exists among them is verified. By increasing the PANI-DBSA content, a further enhancement of conductivity can be achieved and a plateau value is reached for concentrations above 7.8 vol.% PANI-DBSA. The morphology of such samples is characterised by more rich-in-conductive salt regions (cf. Figure 5.25b). It is alleged that after a certain concentration the presence of these regions cannot result in a further improvement of the electrical properties and the system approaches an upper conductivity limit.

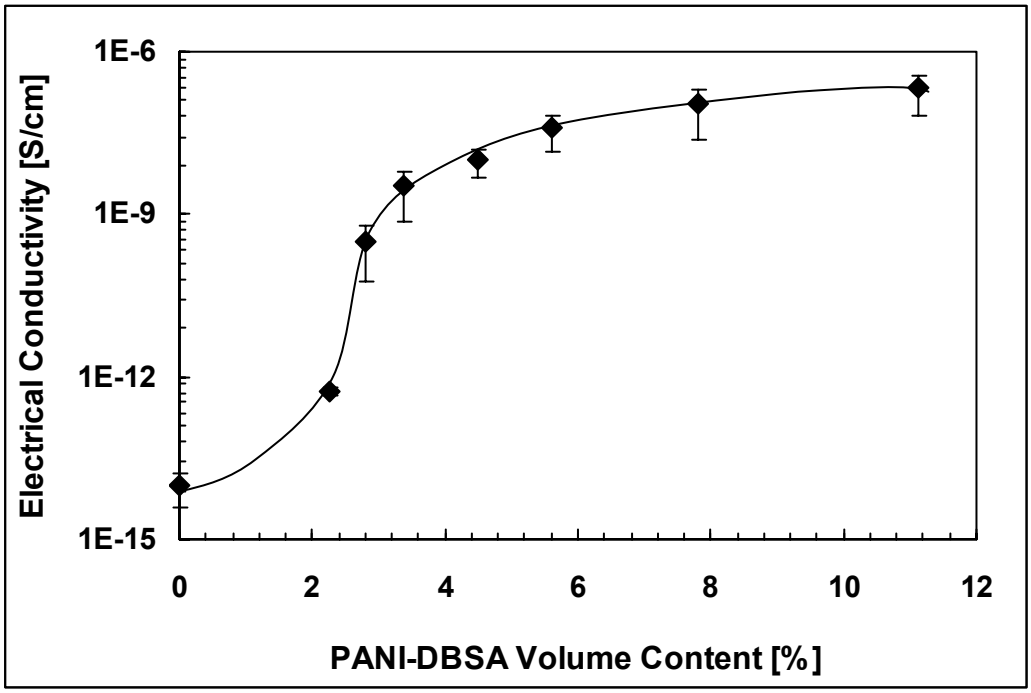

Figure 5.28: Percolation curve for PANI-DBSA.

Comparing the PANI-DBSA percolation curve with those corresponding to the CF/EP composites (Figure 5.29), significant differences can be observed. The percolation threshold is shifted to much lower values in the case where PANI-DBSA is used as conductive filler. It can be also seen that the electrical conductivity values of the EP/PANI-DBSA blends cannot reach the high level of the CF reinforced composites. This stems from the much higher inherent electrical conductivity of the CF compared to the PANI salt, >60 S/cm and 1 S/cm, respectively. Furthermore the conductivity increases smoothly in the range of 10^{-9}-10^{-6} S/cm (optimal range for ESD protection) in the case of EP/PANI-DBSA blends, while for the CF/EP composites abrupt rises of this value occur. Therefore the use of the conductive salt provides the capability to tailor the electrical properties of materials in the target values for this kind of applications. The low inherent conductivity of PANI-DBSA creates however a limit for the highest potential conductivity values of the current EP/PANI-DBSA blends, constituting them unsuitable for EMI shielding applications.

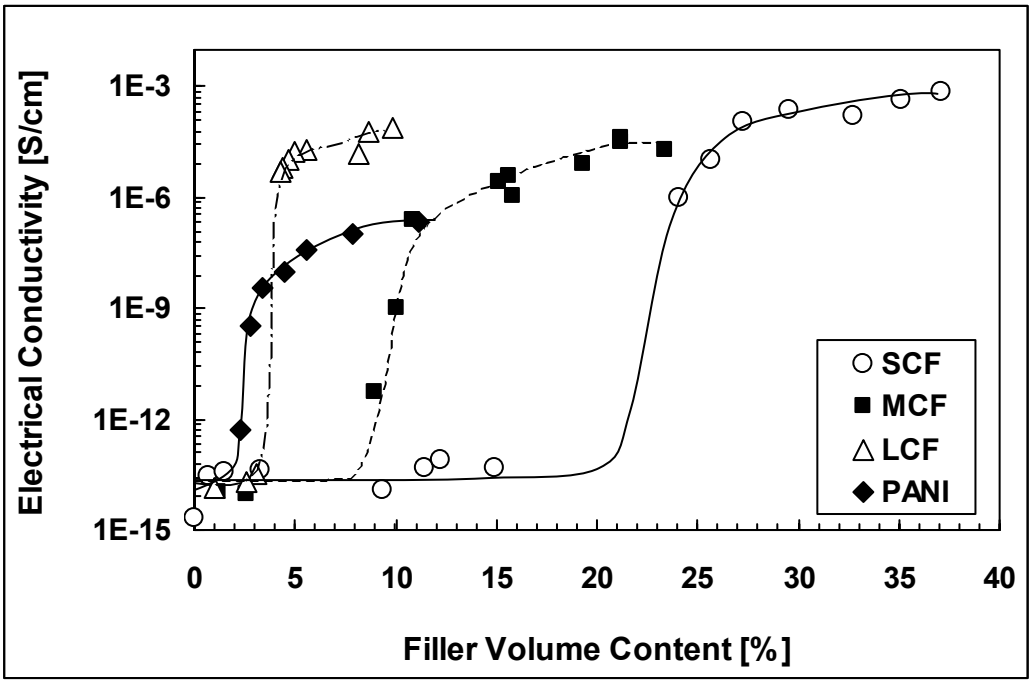

Figure 5.29: Comparison of percolation curves for the different types of CF and for PANI-DBSA.

In a further effort to investigate the parameters which influence the electrical properties of the EP/PANI-DBSA blends, samples were prepared without first dissolving the conductive salt in toluene but directly mixing it with the resin. As it was assumed by the comparison of their solubility parameters (cf. Table 5.3), PANI-DBSA cannot not be straightforwardly dissolved in the EP matrix. Therefore the simple mixing of the two components resulted in a poor dispersion of the conductive salt. The volume resistivity measurements of such blends containing 3.3 and 7.8 vol.% PANI-DBSA showed that they were insulators, in contrast to the blends with the same amounts of PANI-DBSA produced via the solution procedure. It is hence obvious that the quality of PANI-DBSA dispersion is closely related to the final electrical properties of the blends. A poor dispersion means creation of agglomerates which are mostly surrounded by the insulating matrix without being able to come in contact with each other. On the other hand the use of toluene as solvent can lead to a kind of conductive salt solution in the matrix resulting in the formation of a very fine conductive network and consequently to enhanced electrical properties.

5.2.5 Dielectric Spectroscopy

According to a number of experimental observations [99-101], when conductive particles are dispersed in an insulating matrix the dielectric permittivity of the composites or blends increases with the volume fraction of the fillers. In an alternating electric field, the electrical behaviour of materials is characterised by the complex permittivity, ε^*:

$$\varepsilon^* = \varepsilon' - j \cdot \varepsilon'' \tag{5.5}$$

where ε' is the real part (dielectric constant) and ε'' the imaginary part (loss factor) of permittivity.

Figure 5.30 shows the values of ε' and ε'' as functions of frequency for the various EP/PANI-DBSA blends. For PANI-DBSA concentrations below the percolation threshold (< 2.8 vol.%), both values are almost independent of frequency. At higher concentrations ε' and ε'' reach high values at low frequencies, which drop to lower levels as frequency increases, indicating the existence of a dielectric relaxation. This behaviour may be attributed to an interfacial polarization, known as the Maxwell-Wanger-Sillars effect (MWS) [102-104], a phenomenon appearing in heterogeneous media due to the accumulation of virtual charge at the interfaces of the media. However, the loss peaks related to this relaxation are not evident in Figure 5.30.

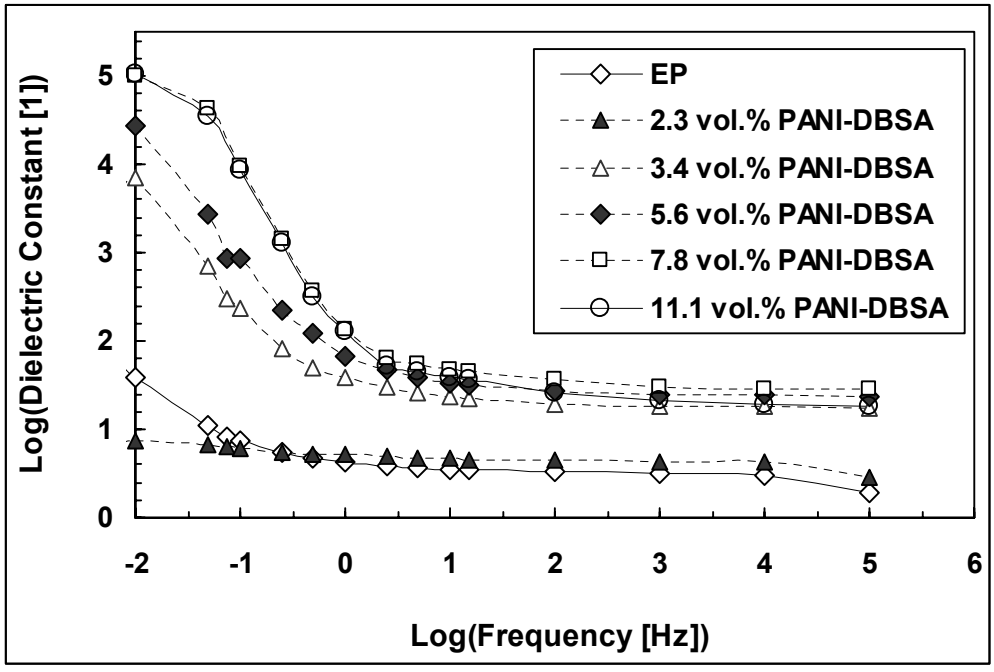

a)

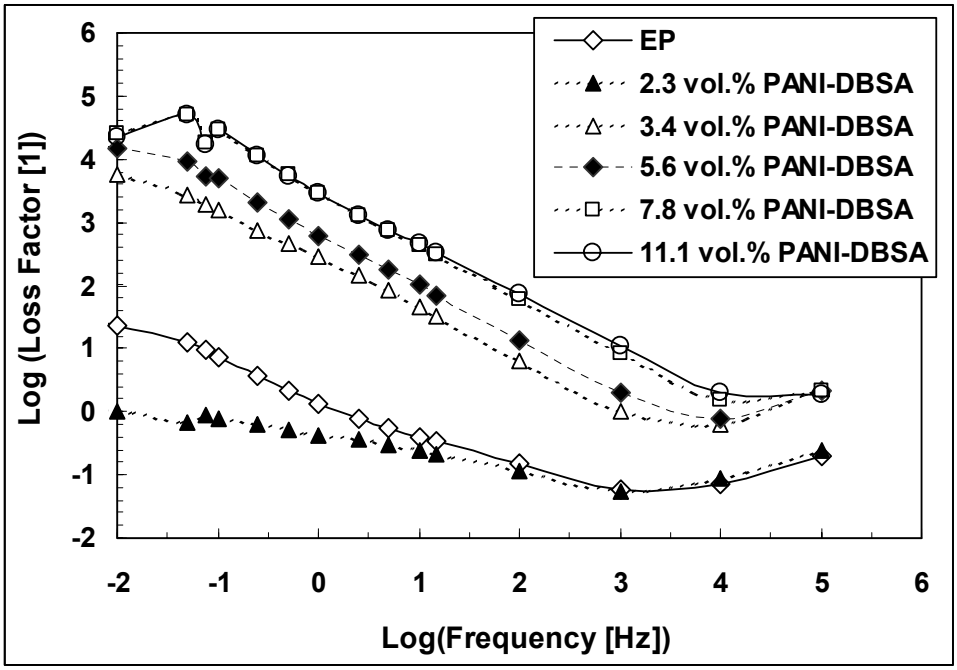

b)

Figure 5.30: Frequency dependence of a) dielectric constant and b) dielectric loss factor for blends with different PANI-DBSA concentrations.

In accordance with the classical percolation theory [105], the dielectric constant of a system with insulating and conductive components should obey the following equation:

$$\varepsilon' \propto \left| V_f - V_c \right|^{-s} \tag{5.6}$$

where V_f is the filler volume fraction, V_c the percolation threshold, and s a critical exponent. This means that before the percolation threshold value (2.4 vol.% PANI-DBSA) a sharp increase of ε' should be observed and after this maximum value it should drop abruptly. However, this behaviour is not evident from Figure 5.31.

The ε' curve can be divided in three different regions:

a. For concentrations up to the percolation threshold, ε' remains constant. The formation of a conductive network is not completed and the behaviour of the system is mainly controlled by the dielectric matrix (capacitance dominated).
b. After the percolation value, ε' increases constantly. For these concentrations ε' is strongly frequency dependent (Figure 5.30a). This behaviour is typical for systems of an insulating matrix with conductive fillers [106]. A conductive network is formed within the insulating matrix, but some unconnected conductive

pathways (e.g. in the form of agglomerates as those observed by TEM analysis) still exist. These pathways cannot participate effectively in the conductive character of the system, and a type of capacitive resistance is developed, resulting in the increase of ε'.

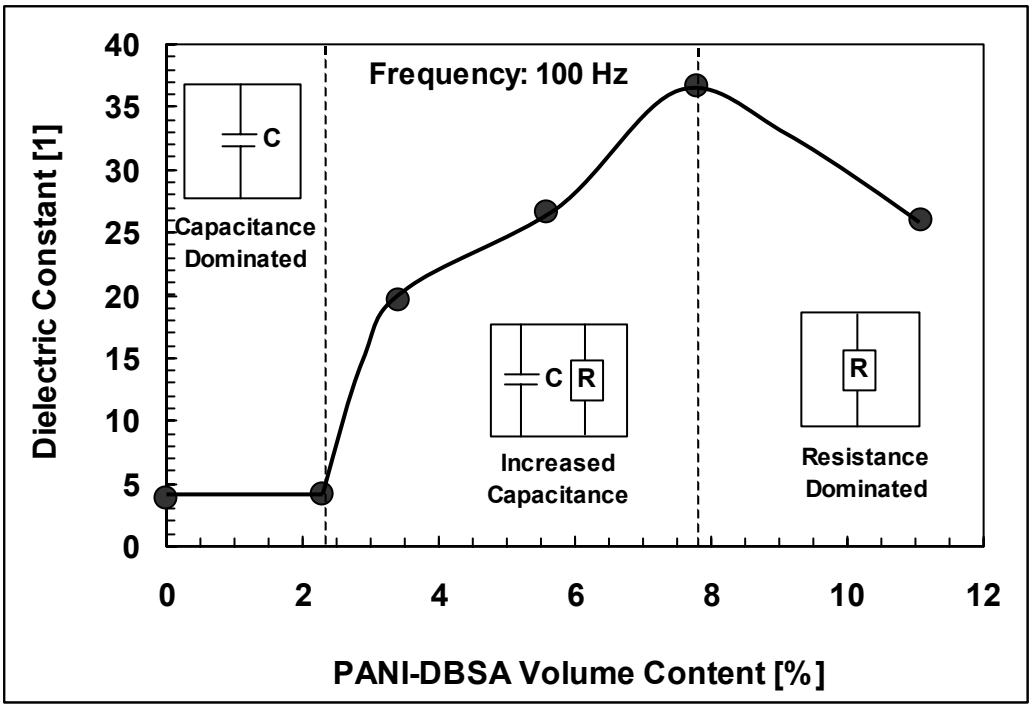

Figure 5.31: Dielectric constant as a function of PANI-DBSA volume content at 100 Hz.

c. ε' drops with further addition of PANI-DBSA. This suggests an almost complete formation of the conductive network, and the domination of a resistance-type behaviour in the system. Recalling the percolation curve at high PANI-DBSA concentrations, one can notice a good correlation between the electric and dielectric properties of the blends. The conductivity plateau corresponds to the reduction of ε'.

Similar curves have been also previously obtained in the case where carbon black was used as conductive filler for EP [107].

5.2.6 Thermal Analysis

Considering the interesting structure of PANI-DBSA within the EP matrix, as it was outlined in the previous sections, it is meaningful to examine the influence of the

conductive salt on the curing process of the different blends and their thermal properties.

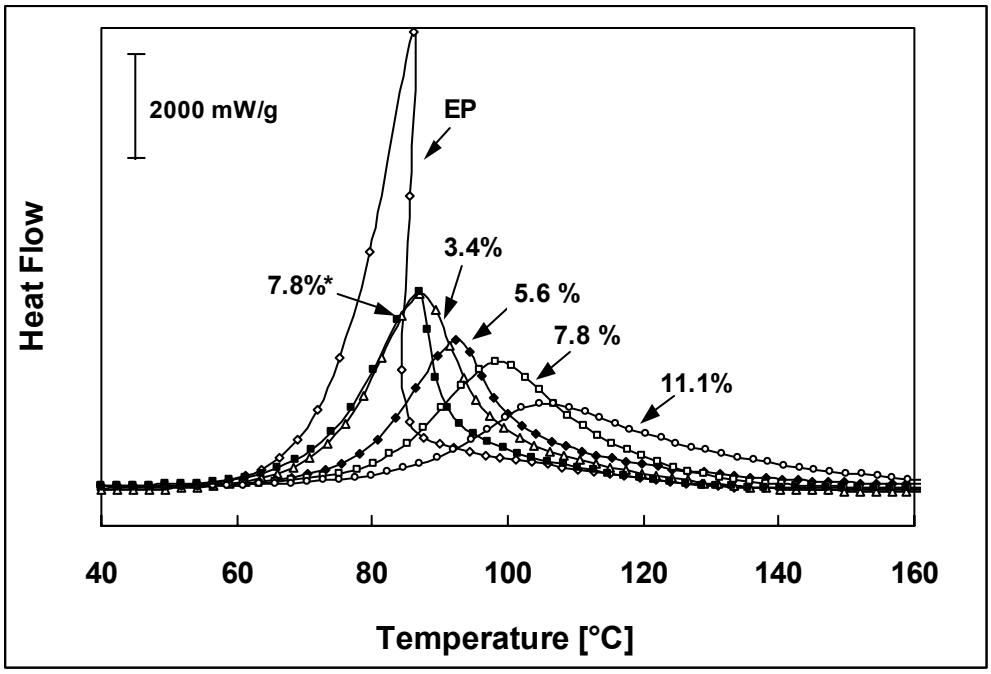

Figure 5.32: Dynamic DSC scans recorded between 40 and 160°C of uncured blends with various PANI-DBSA volume contents. Note: Blend prepared without solution of PANI-DBSA in toluene is denoted by *

The DSC thermograms during the dynamic heating of various uncured EP/PANI-DBSA blends are presented in Figure 5.32. A single exothermic peak is observed for the different concentrations of the conductive salt in the EP matrix, in the region between 40 and 160°C. The maximum peak and the onset of cure, characteristic of each curve, are summarised in Table 5.6. It can be observed that with increasing amount of PANI-DBSA in the blends the maximum peak and the onset of cure are shifted to higher temperatures, while the duration of the reaction becomes longer. Nevertheless, the blend prepared without the solution process (7.8%*) shows a rather different behaviour. The maximum peak and the onset of cure in this case remain at a temperature level similar to EP and the curing time is much shorter compared to the other EP/PANI-DBSA blends. This phenomenon is probably connected to the different microstructures obtained by each method. The nanostructures of PANI-DBSA formed by the solution process have a significant

influence on the curing kinetics of EP, whereas this does not occur for the microparticles (Figure 5.33) produced via the direct mixing process.

Table 5.6: DSC data for the curing reaction of different EP/PANI-DBSA blends, and T_g values determined from the DSC thermograms of the cured samples.
Note: Blend prepared without solution of PANI-DBSA in toluene is denoted by *.

PANI-DBSA [vol.%]	Peak Maximum [°C]	Onset of cure [°C]	ΔH [J/g]	T_g [°C]
0	86	70.6	464	112.5
3.4	87	72.1	432	111.8
5.6	93	78.1	395	110.7
7.8	99	80.6	369	88.4
7.8*	87	68.9	373	77.6 / 99
11.1	106	85.0	337	56.6

The total heat (ΔH) of curing reaction was estimated by connecting the baseline before and after the peak with a straight line and integrating the area under the peak. ΔH decreases with the increase in PANI-DBSA content since the amount of EP in the blends also decreases.

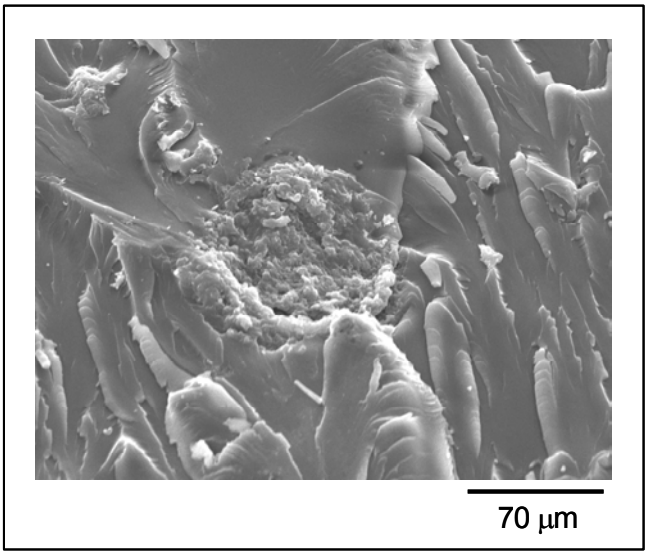

Figure 5.33: SEM micrograph illustrating the size of an agglomerate formed via the directing mixing of PANI-DBSA in EP.

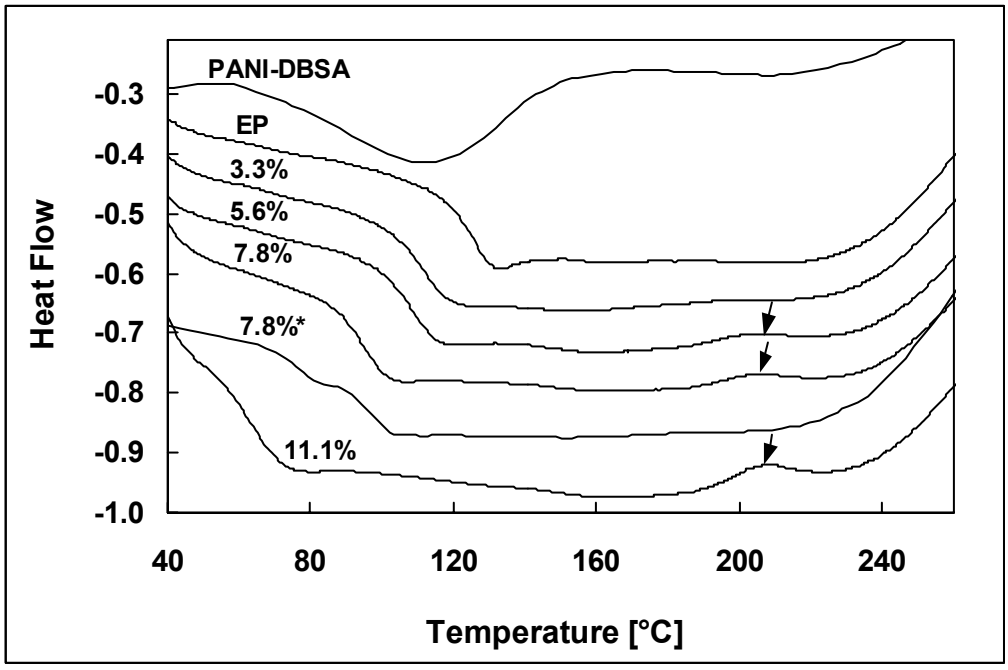

Figure 5.34: Dynamic DSC scans recorded between 40 and 250°C of PANI-DBSA and cured blends with various PANI-DBSA volume contents. Note: Blend prepared without solution of PANI-DBSA in toluene is denoted by *.

Additionally to the analysis of the curing process, DSC was utilised to determine the glass-transition temperature, T_g, of the different cured blends (Figure 5.34). The T_g values, as defined from the first heating of the samples, are presented in Table 5.6. For concentrations up to 5.6 vol.% PANI-DBSA, T_g decreases slightly with the addition of the conductive salt in the EP matrix. The presence of PANI-DBSA has in these cases a minimal effect on the completion of the cure reaction. However, the presence of higher amounts of PANI-DBSA in the blends leads to significant reductions in T_g. The glass transition temperature T_g is a parameter which can be used to indicate the differences in the degree of cure. With decreasing crosslinking, the freedom of movement in the polymer network increases. As a result T_g is shifted to lower temperature. The incomplete curing of the blends is further indicated by an exothermal reaction at about 205°C (Figure 5.34). The onset of this exotherm is shifted to higher temperatures and the corresponding ΔH becomes higher as the content of PANI-DBSA in the blends is increased. The sample prepared without the solution process behaves once more in a dissimilar way. Two individual T_g values can be detected, probably corresponding to the PANI-DBSA and EP, respectively. This is another indication of the poor dispersion of this system. Moreover, no other

exotherm is observed for this blend, demonstrating an almost completely cured system.

Figure 5.35 shows the dependence of the complex modulus (*E**) and the mechanical loss tangent (*tan*δ) on temperature, for the neat EP and its blends with various amounts of PANI-DBSA. A slight decrease in the stiffness of the blends is observed by the addition of the conductive salt. For the neat EP only one peak of *tan*δ is detected at about 135°C, which corresponds to the T_g of the crosslinked system. By the addition of PANI-DBSA this α-relaxation peak is shifted towards lower temperature values. This is in agreement with the results obtained by DSC measurements, which also showed a reduction in T_g with addition of the PANI-DBSA. Rodrigues et al. [99] have determined the glass transition temperature of the pure PANI, via DMTA analysis, at 99.3°C. It can therefore be concluded that as the concentration of the conductive salt in the blends increases, T_g tends to reach this value. The maximum of the peak, $tan\delta_{max}$, increases constantly with addition of the conductive salt in the blends, indicating enhancement of the damping properties by the presence of PANI-DBSA in them.

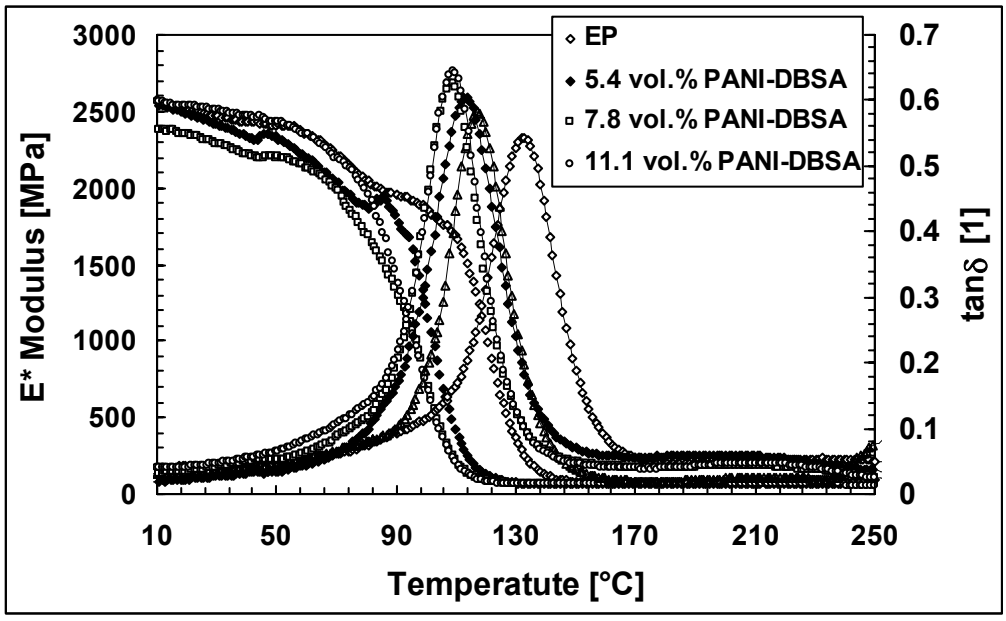

Figure 5.35: DMTA spectra of the EP/PANI-DBSA blends.

TGA thermograms of PANI-DBSA, cured EP, and cured EP/PANI-DBSA blends are presented in Figure 5.36. The PANI-DBSA thermogram shows a small weight loss below 240°C, apparently caused by the loss of water and oligomers. The weight loss

between 240°C and 300°C corresponds to the loss of the excess DBSA, while the slighter weight loss after 300°C may stem from the loss of the bound DBSA. Cured EP exhibits a lower total weight loss (about 74%) compared to PANI-DBSA (almost 91%), and it is more stable for temperatures up to 350°C. The cured EP/PANI-DBSA blends tend to maintain the stability of the EP matrix at higher temperatures, especially for concentrations below 5.6 vol.% of PANI-DBSA. Another interesting observation is that for the EP/PANI-DBSA blends the total weight loss is even smaller than that of EP, ranging between 61-67%.

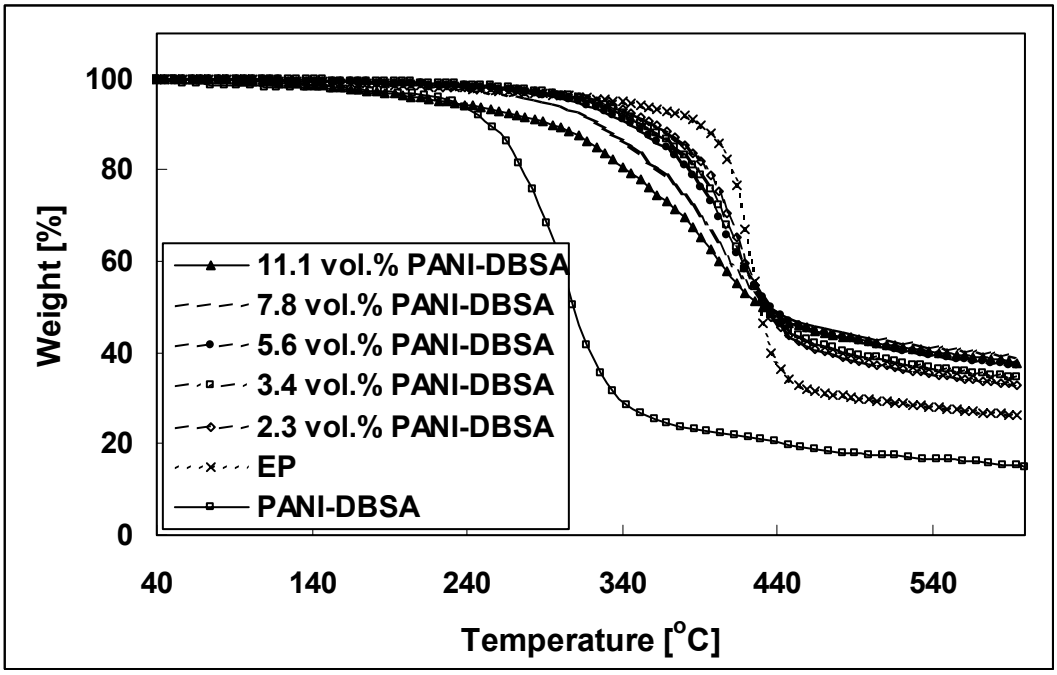

Figure 5.36: TGA thermograms of PANI-DBSA, cured EP, and cured EP/PANI-DBSA blends.

5.2.7 Mechanical Properties

The flexural properties of the neat EP and the EP/PANI-DBSA blends are summarised in Table 5.7. Both flexural strength and modulus are not significantly affected by the addition of up to 7.8 vol.% of PANI-DBSA. However, the presence of 11.1 vol.% PANI-DBSA in the blends leads to an abrupt decrease in the values of the two properties. According to Poussin et al. [108], the Young's modulus of PANI$(DBSA)_{0.7}$ is 300 MPa, and it is decreasing with an excess of DBSA. Therefore, a negative effect on the mechanical properties for higher concentration of the conductive salt is to be expected. Comparing the mechanical properties of the blends

with those from the thermal characterization of the EP/PANI-DBSA blends (c.f. Table 5.6), similarities in the tendencies can be detected. A slight influence of the conductive-salt on both the thermal and mechanical properties of the blends is observed when its concentration is less than 5.6-7.8 vol.%. It can be therefore concluded that up to these concentrations PANI-DBSA affects the curing of the EP-system, and consequently the quality of the crosslinked network, to a minimal degree.

Table 5.7: Flexural properties and microhardness of various EP/PANI-DBSA blends. Note: Blend prepared without solution of PANI-DBSA in toluene is denoted by *.

PANI-DBSA [vol.%]	Flexural Modulus [GPa]	Flexural Strength [MPa]	Elongation at Break [%]	Microhardness *HV* [MPa]
0	3.90	156.4	5.1	232.8
2.3	3.66	161.2	6.4	220.5
2.8	3.63	146.3	6.2	225.8
3.4	3.42	152.9	6.0	219.7
4.5	3.81	153.2	4.7	220.2
5.6	3.53	139.1	4.8	210.9
7.8	3.29	134.4	5.5	200.3
7.8*	3.54	87.1	2.5	225.6
11.1	2.15	71.0	8.3	138.4

Another interesting observation is that the elongation at break reaches a value of 8.3 % for the sample with 11.1 vol.% PANI-DBSA, significantly higher than that of the neat EP (5.1 %). This means that for higher concentrations of the conductive salt, the crosslinking density of the EP matrix is significantly reduced, allowing in this way the possibility for higher deformations. An interesting point is that for the sample without the solution in toluene, a very low flexural strength and elongation at break is determined. Consequently, the preparation process of the blends does not have a significant influence only on their electrical properties (as is was previously shown), but on their final mechanical properties as well. Few studies can be found in the literature regarding the mechanical properties of EP/PANI-salt blends. For instance,

Peltola et al. [41] reported a reduction of 50% in T_g and tensile modulus by addition of 1 wt.% PANI-CSA in EP.

PANI-DBSA has as well a significant effect on the microhardness values of the EP/PANI-DBSA blends. The Vickers hardness is steadily decreasing with the addition of the conductive salt in the blends, as it can be seen from Table 5.7. This behaviour is similar to the one seen for the flexural properties.

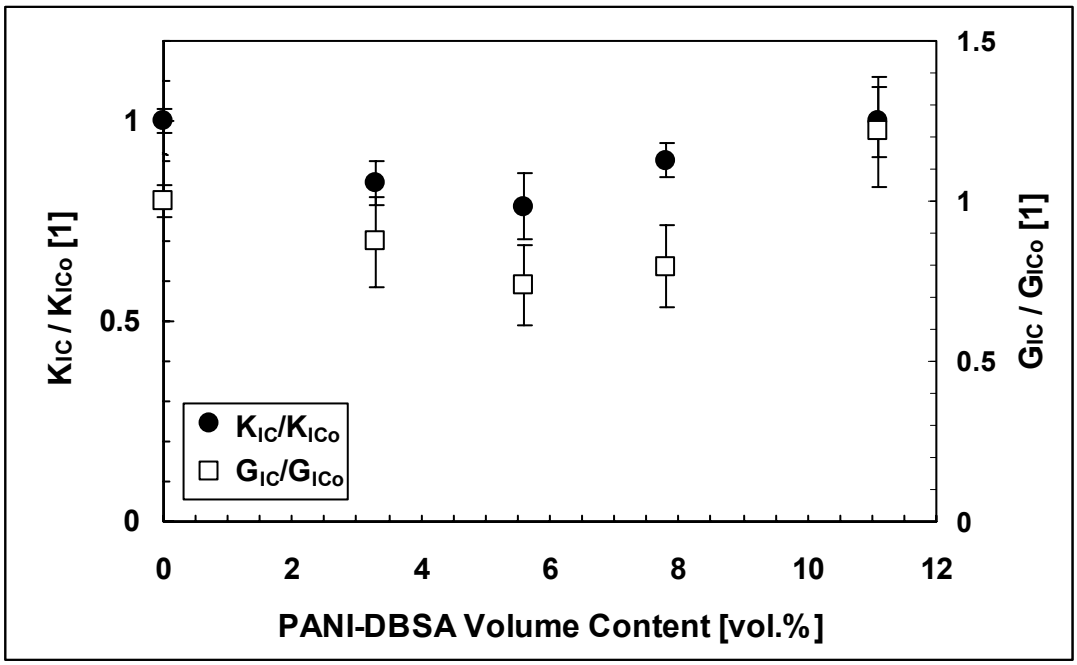

Figure 5.37: Variation of the relative critical stress intensity factor K_{IC} /K_{ICo} and the relative fracture energy G_{IC} /G_{ICo} with the PANI-DBSA content.

The influence of PANI-DBSA content on the relative fracture toughness, K_{IC} /K_{ICo}, and relative fracture energy, G_{IC} /G_{ICo}, is illustrated in Figure 5.37. K_{ICo} and G_{ICo} are the values corresponding to the neat EP and were determined at 1.9 MP.m$^{1/2}$ and 1.5 kJ.m^{-2}, respectively. These values are quite higher than those found in the literature [109-111], especially for G_{IC}. This is probably due to the notch preparation process, which led to insufficiently sharp initial cracks. However, these results will be mainly used to examine the effect of PANI-DBSA on the fracture toughness of the samples, without considering the absolute determined K_{IC} and G_{IC} values. Both fracture mechanical characteristics decrease initially by the addition of the conductive salt in the EP matrix. For higher concentrations (>7.8 vol.% PANI-DBSA) a significant increase of the G_{ICo} is however evident, even in comparison with the values

corresponding to the neat EP, while K_{ICo} rises to the level of EP. Similar behaviour is reported in the literature for various thermoset-thermoplastic blends [109], where an increase of the EP's fracture toughness is observed after a certain concentration of the thermoplastic phase.

One of the major drawbacks of EPs, which results from their highly cross-linked structure, is their poor resistance to impact and to crack propagation [110]. One approach to toughen EPs is the addition of a second phase of polymeric particles such as rubbers [111,112] and thermoplastics [113,114]. It is believed that the additional polymer is able to induce a toughening effect when its single-phase is not dissolved in EP and a phase separation takes place [110]. For this reason, in some cases [109] by low polymer concentrations, no variation or even a decrease in fracture toughness is reported. In a subsequent region, characterised by a dispersion of polymer particles in the EP matrix, a small increase in fracture toughness is observed. Comparing these findings to the behaviour of the studied EP/PANI-DBSA blends, some similarities are apparent. Until a specific concentration the conductive salt appears to be dissolved with the EP. After that, large agglomerates (or rich-in-polymer areas) of PANI-DBSA are created, having a negative influence on the flexural properties as well on T_g. However, the formation of these rich polymer areas results in a slight improvement of the fracture toughness. Moreover, this slight increase of toughness may be attributed to the reduced cross-linking density of the blend with 11.1 vol.%.

A series of scanning electron micrographs of the various fracture surfaces is shown in Figure 5.38. The tearing lines (shear steps) on the fracture surface of the EP sample, randomly flowing from the initial crack front, indicate a high toughness. Although pure epoxies are regarded as brittle materials, inelastic deformation in the form of viscoelastic and/or plastic deformation still occurs during the fracture process. This results in a measured fracture toughness that is much higher than the theoretical estimate for purely brittle material [110]. The sample with 7.8 vol.% PANI-DBSA shows decreased shear deformability compared to EP and this can explain the reduced fracture energy of the system. Similar fracture surfaces were observed for samples with lower concentrations of the conductive salt. For higher PANI-DBSA

content the fracture surface becomes similar to that of EP, as shown in Figure 5.38c, in accordance with the increased fracture toughness of the system.

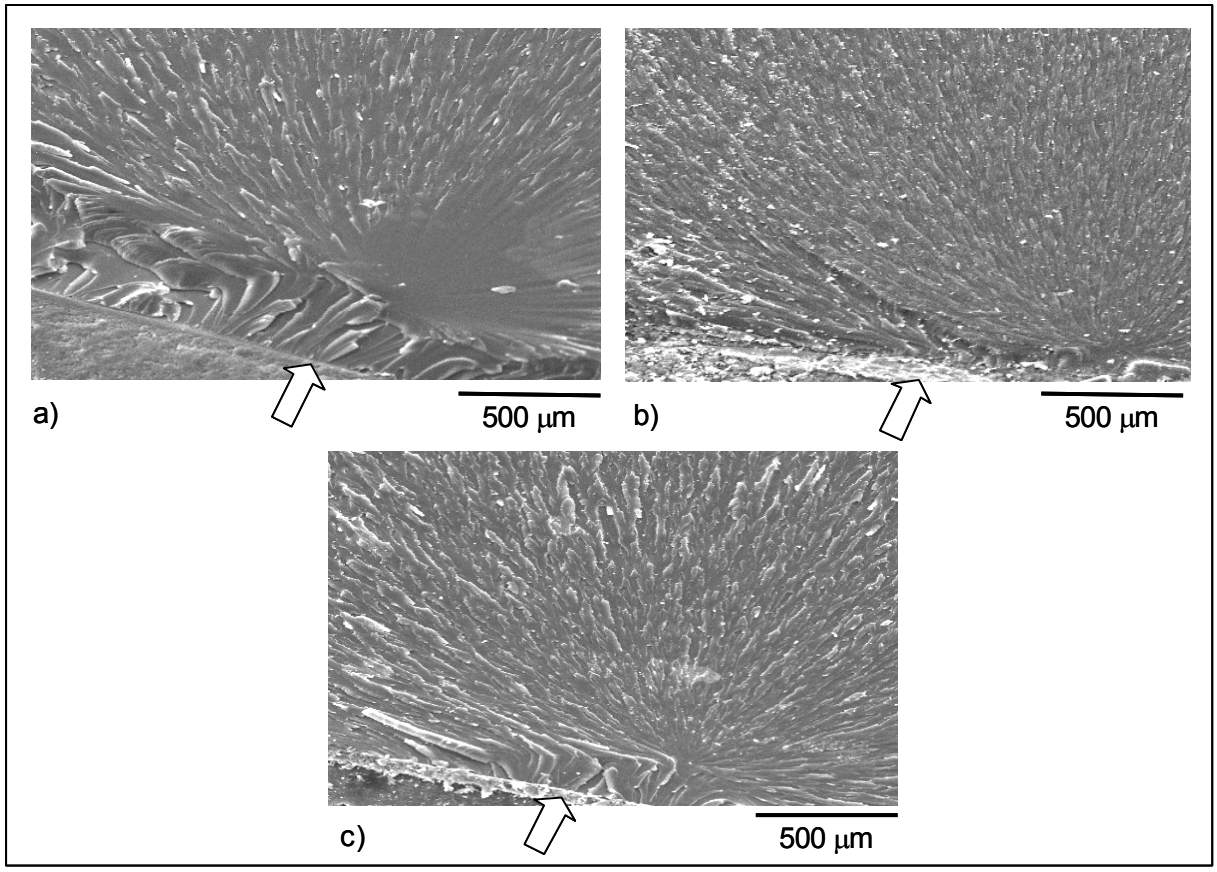

Figure 5.38: SEM pictures taken from the fracture surfaces of a) neat EP, and blends with b) 7.8 vol.%, and c) 11.1 vol.% PANI-DBSA. Note: arrows show the razor blade notch.

5.3 Carbon Fibre Reinforced Epoxy/Polyaniline Blends

PANI-DBSA as a conductive filler was able to form a very fine network within the EP matrix, exhibiting in this way lower percolation value compared to CF. The mechanical properties of the blends remained to the level of the neat matrix and no reinforcing effect was possible via the addition of the conductive salt, in contrast to the performance of CF. An interesting continuation of the above observations and results regarding the incorporation of both types of conductive fillers, i.e. CF and PANI-DBSA, in EP, is presented in the following sections.

5.3.6 Microstructure

The addition of CF in the EP/PANI-DBSA blends led to mixtures with high viscosity, and therefore limited amounts of each conductive filler were able to be acceptably mixed with the liquid matrix. In order to eliminate this problem, only the shorter fibres (SCF) were used in concentrations of up to 7.6 vol.%, combined with various amounts of PANI-DBSA. The addition of the SCF resulted, as expected, in an increased density of the developed isotropic samples.

An attractive aspect of this part of the study was to investigate the formation of the SCF graded profiles by the centrifugation process. During the centrifugation of the EP/PANI-DBSA blends no movement of the PANI-DBSA particles was evident. This was nevertheless anticipated, since the density difference between PANI-DBSA and EP is very small. Due to this fact, for the SCF reinforced samples, the EP/PANI-DBSA blend undertook the role of the polymeric matrix and the movement of the SCF merely was investigated. The application of centrifugal force, controlled by the speed and radius of motion, caused SCF to move towards the applied force direction (*x*-axis) within the EP/PANI-DBSA mixture.

The viscosity of the whole mixture was increasing by the addition of PANI-DBSA and SCF. This fact hindered the migration of SCF in the viscous mixture. It was furthermore observed that for blends with a PANI-DBSA content of 5.6 vol.% or larger, almost isotropic fibre distributions were formed with applied centrifugation speed of 2000 rpm. In order to achieve graded profiles in such viscous mixtures, higher centrifugation speeds, e.g. 5000 rpm, were required. Images of the bottom- and top-side of graded samples with and without PANI-DBSA, centrifuged at 2000

rpm, are shown in Figure 5.39. For the sample containing only SCF a close-packed state is observed at the bottom side, while the addition of PANI-DBSA leads to an almost homogeneous distribution of SCF along the sample thickness.

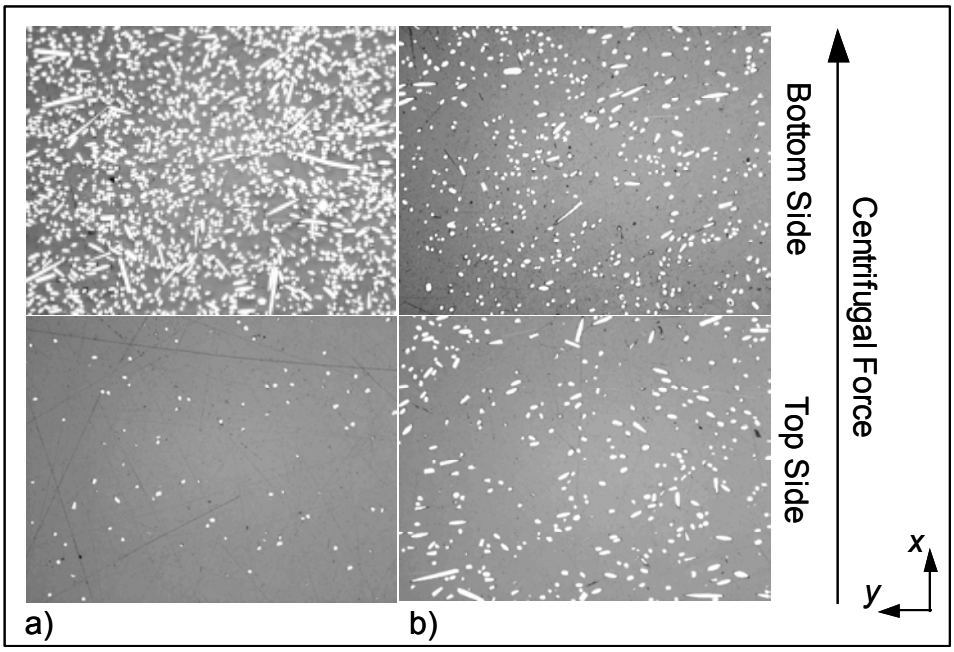

Figure 5.39: Images by light optical microscopy, showing the bottom- and top-side of graded samples centrifuged under 2000 rpm with a total SCF content of 10 vol.%, together with a) 0 and b) 5.6 vol.% PANI-DBSA.

5.3.2 Electrical Properties

By incorporating SCF into the EP/PANI-DBSA blends a significant enhancement of their electrical properties is observed. As it is shown in Figure 5.40, the addition of SCF raises the electrical conductivity of the samples to levels higher than 10^{-6} S/cm. At this point it should be reminded that samples containing only 7.6 vol.% SCF are insulators, as they show values of conductivity similar to that of the neat EP (cf. Figure 5.11). Moreover, the percolation threshold of SCF/EP composites was determined at concentrations higher than 20 vol.% SCF. It is therefore clear that the combination of the two conductive fillers can lead to advanced electrical properties. A kind of synergy effect takes place: the fine conductive PANI-DBSA pathways can act as a connector between the separated SCF.

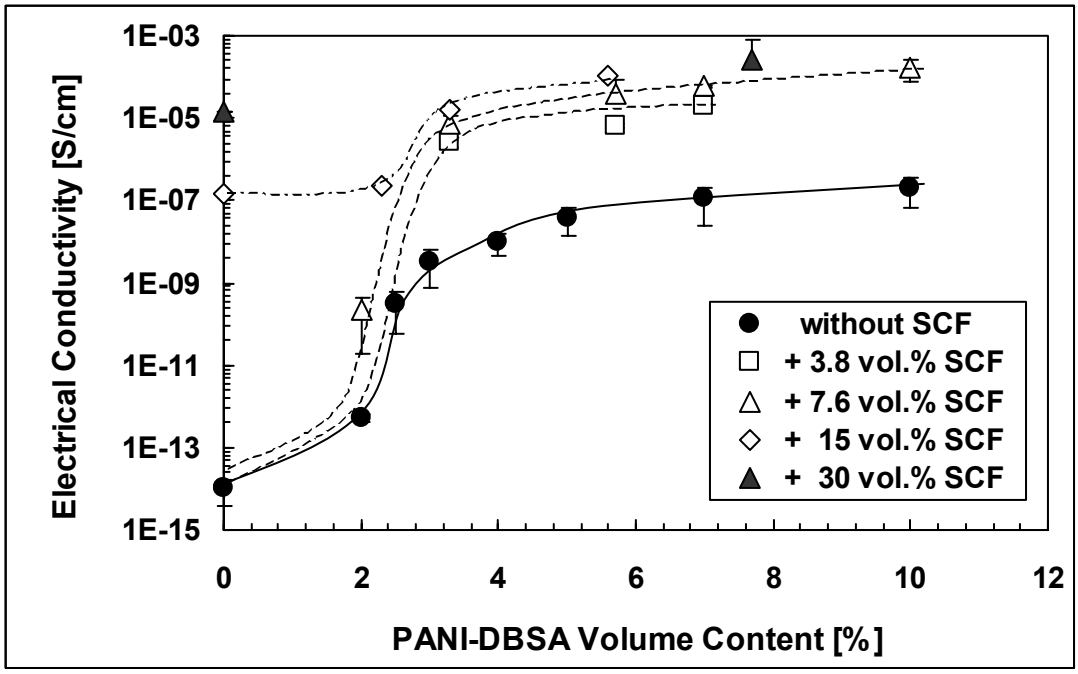

Figure 5.40: Influence of SCF on the electrical conductivity of EP/PANI-DBSA blends

Figure 5.41 illustrates the synergy effect between SCF and PANI-DBSA regarding the electrical conductivity of the samples. The horizontal axes show the proportion of each filler to the total amount of them. The value of 100% represents samples containing only SCF or PANI-DBSA. For these cases, samples with 3.3 vol.% SCF and 7.6 vol.% PANI-DBSA are presented in this diagram. It can be observed that enhanced values of conductivity are obtained when a combination of the two fillers is used. By comparing the two networks as they were observed by TOM (Figure 5.42), significant morphology differences are evident. The micro-scale structure of SCF is surrounded by the translucent pathways of PANI-DBSA. Therefore no contacts are needed between the fibres in order to participate in the conductive network since this is achieved by PANI-DBSA “bypasses”. Another difference between the nature of the two fillers is their inherent conductivity. SCF exhibit a superior inherent conductivity compared to PANI-DBSA, and thus the resulted electrical conductivity of the system becomes much higher. For SCF concentrations above the percolation threshold (e.g. the sample with 30 vol.% SCF), only a slight enhancement of the electrical properties is achieved by the presence of PANI-DBSA in the system. A conductive network of the fibres is already formed at this state, and the conductive salt can participate only

as a joint between the few isolated SCF branches. Analogous results have been observed in CF reinforced PP/PANI blends [115].

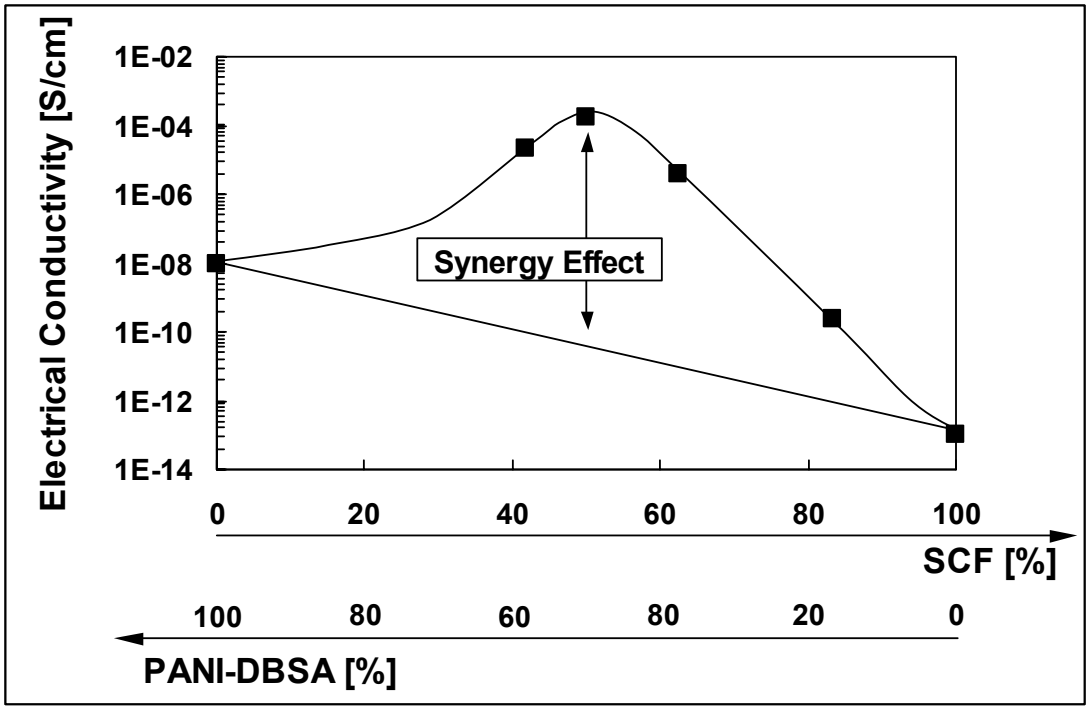

Figure 5.41: The synergy effect between SCF and PANI-DBSA with regard to the electrical conductivity of the samples.

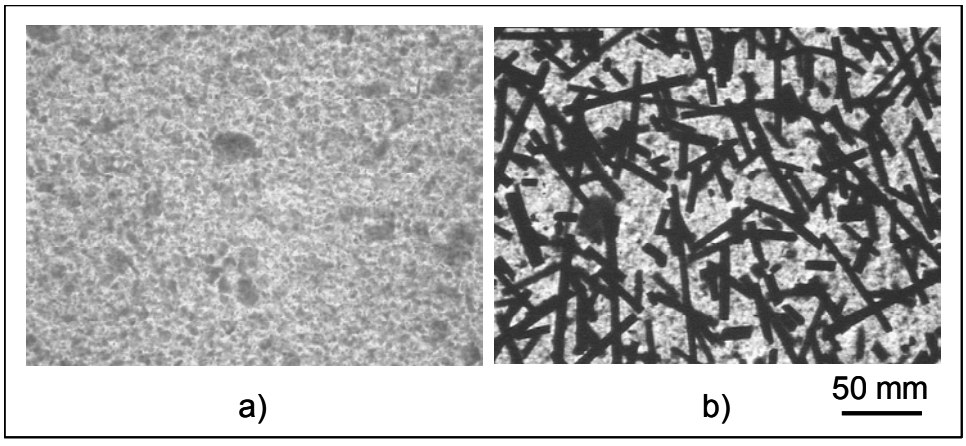

Figure 5.42: TOM micrographs of samples containing 5.6 vol.% PANI-DBSA, a) without SCF, and b) with 7.6 vol.% SCF.

The above results show that fillers with cooperative nature give the opportunity of designing materials with desired electrical properties. By varying the percentage of each fillers in the system, a number of different percolation curves can be achieved, covering the whole range of electrical conductivities.

The application of centrifugal force to the SCF reinforced EP/PANI-DBSA composites had similar effects as the graded electrical properties described previously for the samples without the conductive salt (c.f. paragraph 5.1.3.1). Figure 5.43 depicts the graded profiles of SCF volume content and surface resistance along the thickness of samples with different amounts of PANI-DBSA, centrifuged at 2000 rpm. The total concentration of SCF was in all cases 7.6 vol.%. The sample without PANI-DBSA exhibits the higher SCF content at the bottom side (> 25 vol.%), and a surface resistance of $3 \cdot 10^4$ Ohms at this area. After that, however, the surface resistance increases sharply reaching values higher than 10^{13} Ohms, as the SCF content drops to concentrations lower than 10 vol.%. In this case a harsh conductive-insulating change is taking place across the sample thickness. The addition of 2.3 vol.% PANI-DBSA leads to a smoother change of SCF concentration, and consequently a gradual rise in the surface resistance across the sample thickness.

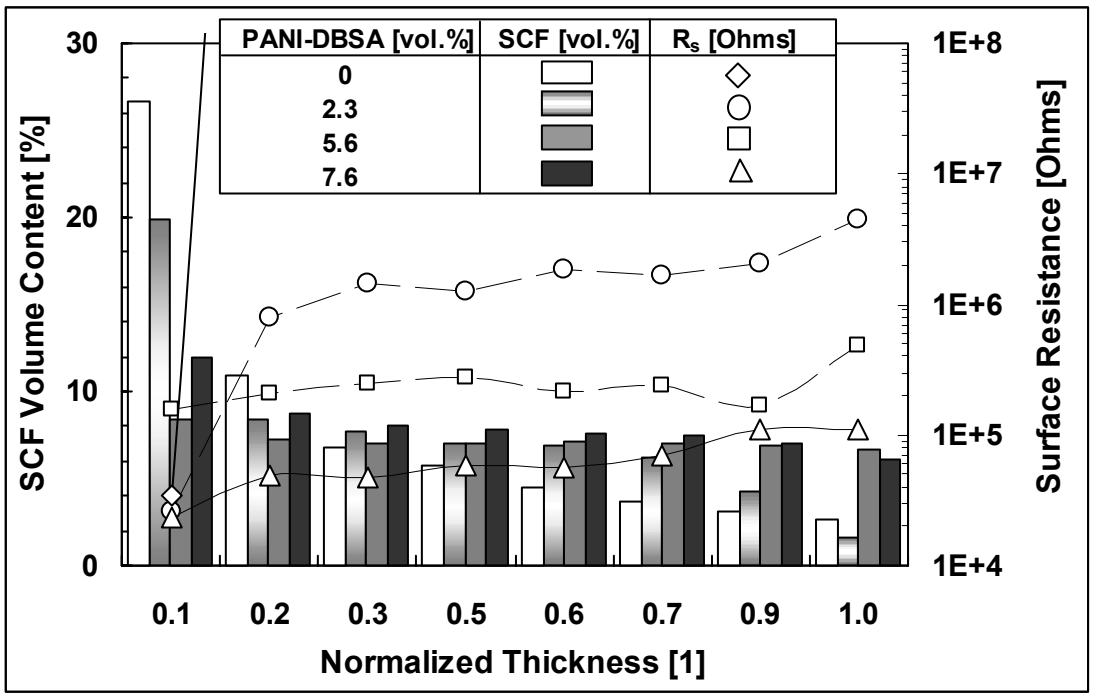

Figure 5.43: Profiles of the SCF content and surface resistance along the thickness of graded samples with different PANI-DBSA contents: centrifugation speed 2000 rpm, total SCF content 7.6 vol.%.

Higher concentration of PANI salt results in reduction of the surface resistance, but no significant gradient in this value is observed. The high viscosity of these mixtures hinders the movement of SCF in the liquid EP/PANI-DBSA and the formation of a

graded structure cannot easily take place. Thus these samples show almost isotropic electrical properties across their thickness. Higher centrifugation speeds are required for producing graded properties. For example, when the sample with 7.7 and 7.6 vol.% of PANI-DBSA and SCF, respectively, was centrifuged at 5000 rpm, a gradient from $2 \cdot 10^3$ Ohms (bottom-side) to $4 \cdot 10^5$ Ohms (top-side) was achieved.

5.3.2 Thermal Analysis

DSC analysis was performed on uncured and cured SCF reinforced EP/PANI-DBSA samples. Some of the obtained results are summarised in Table 5.8. By the addition of SCF in the EP no changes in the position of the peak maximum and the onset of cure are observed. This indicates that SCF do not influence the kinetics of the curing reaction. When PANI-DBSA is incorporated in the mixtures, the cure reaction starts to proceed in much higher temperatures. The heat of cure, ΔH, becomes smaller as the total concentration of the fillers is increasing. Small exothermic peaks were observed for PANI-DBSA concentrations above 5.6 vol.%, indicating incomplete curing of the samples. The T_g values of the SCF reinforced EP is found at the level of the neat matrix, and are gradually reduced by the addition of PANI-DBSA.

Table 5.8: Data from the DSC dynamic scans of uncured SCF reinforced EP/PANI-DBSA samples, and T_g values determined from the DSC thermograms of the cured samples.

SCF [vol.%]	PANI-DBSA [vol.%]	Peak Maximum [°C]	Onset of cure [°C]	ΔH [J/g]	T_g [°C]
0	0	86	70.6	464	112.5
7.6	0	84	68.8	368	114.2
7.6	3.3	91.4	76.8	330	107.2
7.6	7.8	97.8	81.9	283	102.6

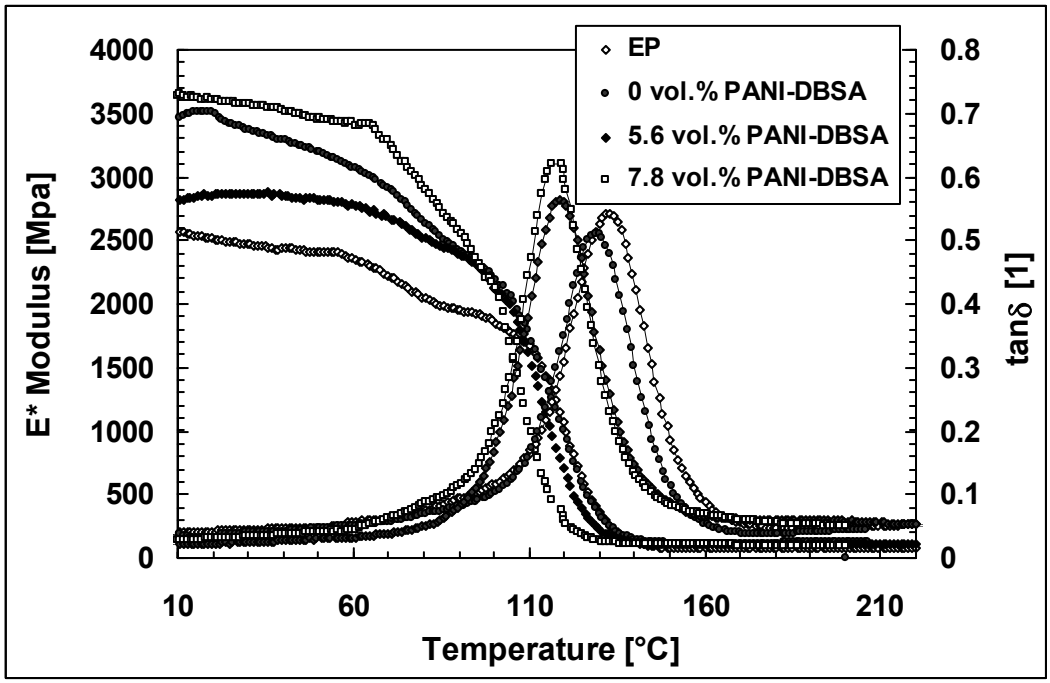

Figure 5.44: DMTA spectra of EP and EP/PANI-DBSA blends with 7.6 vol.% SCF.

In Figure 5.44 the DMTA spectra of EP and different EP/PANI-DBSA with 7.6 vol.% SCF are compared. The complex modulus, E^*, shows higher values for all the SCF reinforced samples compared to neat EP, for the glassy state. By the addition of SCF, the $tan\delta$ peak is reduced. The magnitude of the relaxation process, which relates to the magnitude of the drop, depends upon both the number of mobile entities and their contribution to the compliance. It decreases as the SCF loading increases, indicating a reduction of the mobile units at T_g. This result may be explained by a decrease of the matrix material amount, which exhibits higher damping properties. However, the relative damping is not simply related to the amount of fillers but also to interfacial properties. The addition of PANI-DBSA relocates the $tan\delta$ peak to lower temperatures and increases its maximum. PANI-DBSA exhibited a similar behaviour for the unreinforced systems (c.f. Figure 5.35). In this way the conductive salt can enhance the damping properties of the system, even in the presence of the stiff SCF. On the other hand, this has a negative influence on the final T_g value of the system.

5.3.4 Mechanical Properties

The flexural properties of the SCF reinforced EP/PANI-DBSA samples are presented in Figure 5.45, as a function of PANI-DBSA content. The addition of SCF leads to a considerable increase of flexural modulus of the neat EP (0 vol.% PANI-DBSA). The presence of PANI-DBSA does not disturb the reinforcing effect of the SCF, as the values of the modulus remain almost stable. The comparison of the fracture surfaces showed no significant changes of the SCF related microstructure by the presence of PANI-DBSA (Figure 5.46). As it was expected, the incorporation of SCF in the blends led to a reduction of the elongation at break.

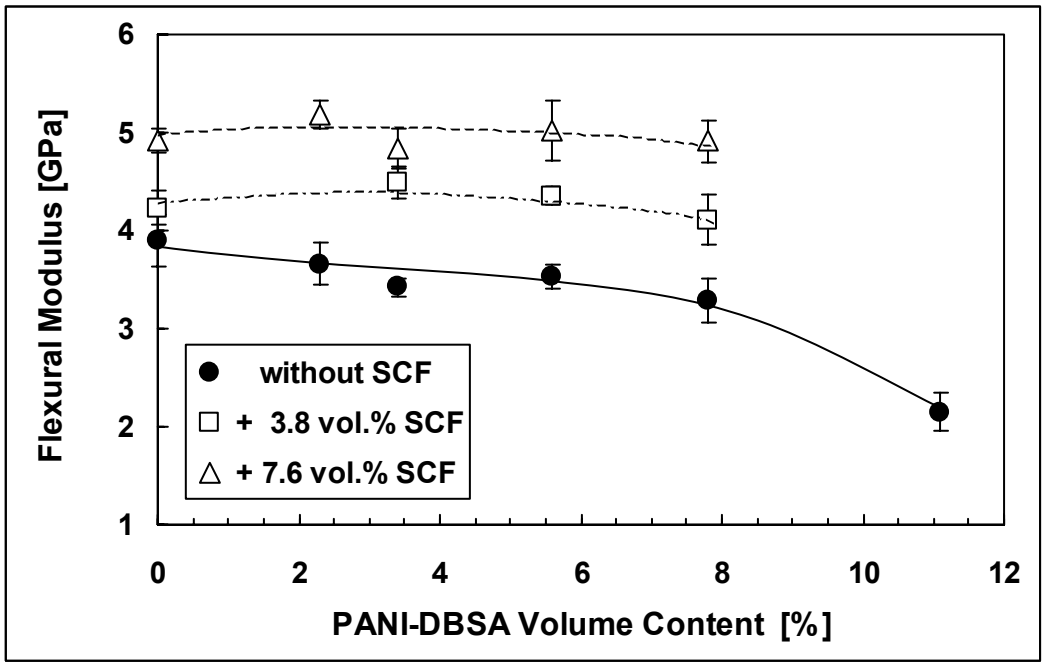

Figure 5.45: Influence of SCF on the flexural modulus of EP/PANI-DBSA blends.

The microhardness of the PANI-DBSA blends was also improved by the incorporation of SCF. HV exhibited a value of 247 MPa for 7.6 vol.% SCF, and it remained to this level for concentrations up to 3.3 vol.% PANI-DBSA. A small reduction of this value was observed for higher contents of PANI-DBSA.

Figure 5.47 depicts the changes of flexural modulus of the same graded samples presented in Figure 5.43. It is obvious that the flexural modulus follows the changes of the SCF content across the samples thickness. The maximum fibre concentrations observed at the bottom side of the samples are connected with high flexural modulus

values. For mixtures with low viscosity (0 or 2.3 vol.% PANI-DBSA), smooth gradients in modulus are observed as the SCF content gradually decreases towards the sample thickness. On the contrary, a higher amount of PANI-DBSA leads to a stable microstructure within the sample. Consequently, the flexural modulus remains unchanged across the sample thickness.

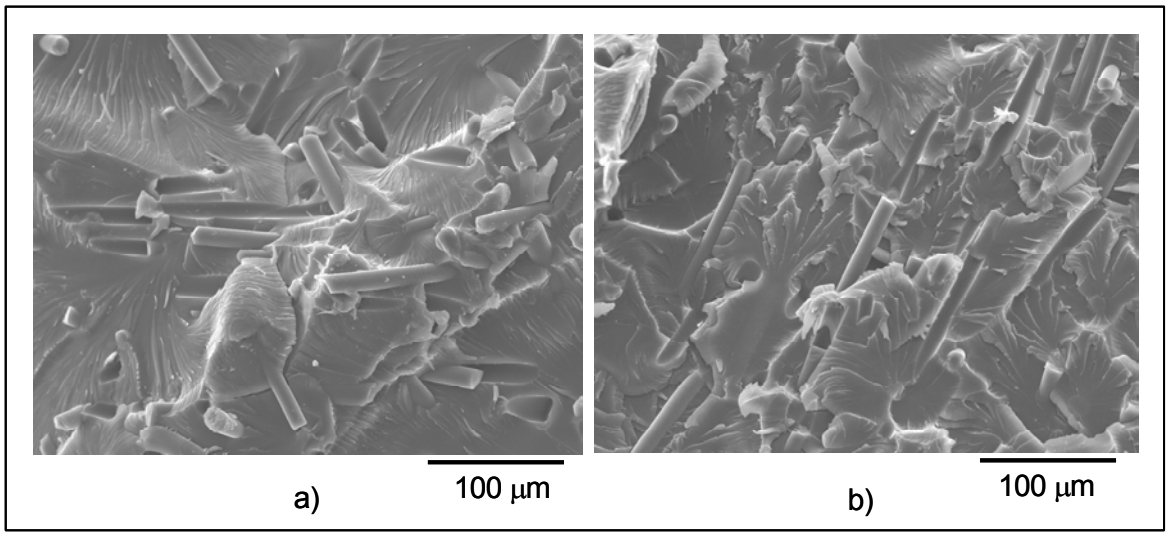

Figure 5.46: SEM pictures from the fracture surfaces of samples containing 7.6 vol.% SCF a) without PANI-DBSA and b) with 7.8 vol.% PANI-DBSA.

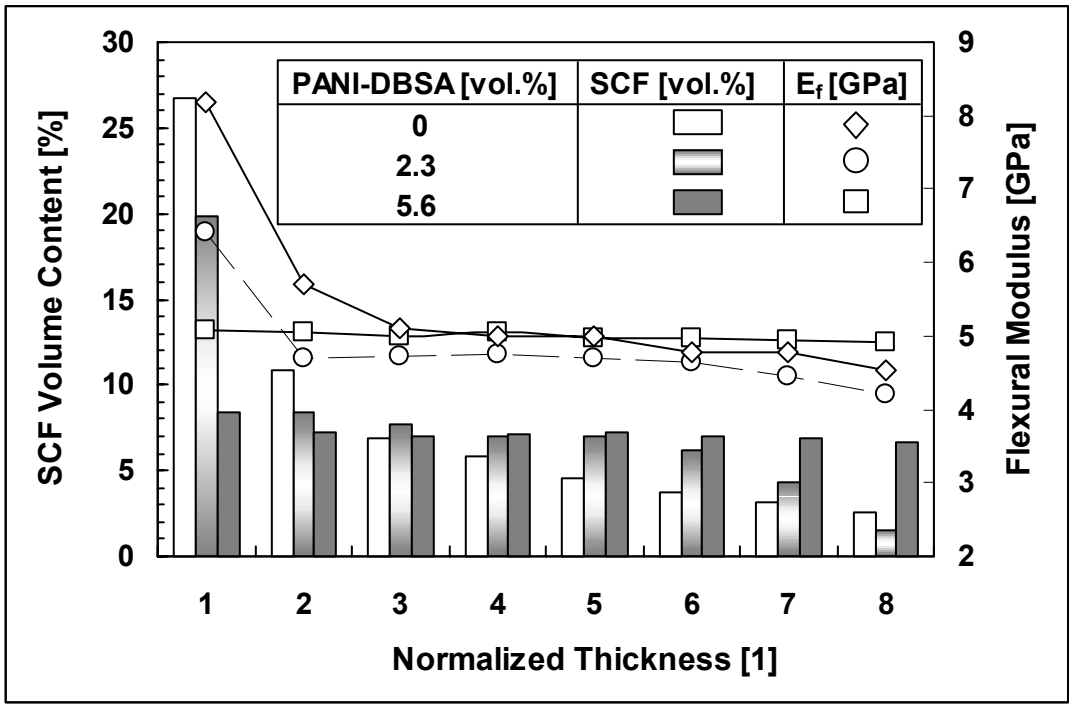

Figure 5.47: Profiles of the SCF content and flexural modulus along the thickness of graded samples: centrifugation speed 2000 rpm, total SCF content 7.6 vol.%.

5.4 Conductivity Modelling Analysis

5.4.1 Carbon Fibre/Epoxy Matrix Composites

As it was mentioned in section 2.2.4.1, the percolation model of Kirkpatrick and Zallen [51,52] suggests that, for concentrations above the percolation threshold, the electrical conductivity of the composite is given by a power law equation (cf. Equation 2.4). The critical volume fraction V_c and the exponent t are used to classify the structure of the percolating system; they are sensitive to various factors, one of the most important being the relative size of conducting and insulting particles.

The critical exponent t can be determined by power law fitting of the experimental data for a defined percolation threshold, V_c. Many researchers have studied the critical fibre content theoretically by using percolation models and Monte-Carlo simulations [116,117]. According to Munson-McGee [117], for a system with aligned fibres V_c=0.22, while V_c is dependent on the fibre aspect ratio α when composites with different fibre orientations are considered. The present CF/EP composites exhibit a random in-plane orientation. Corresponding to the fibre aspect ratio [117], the theoretical V_c values equal to 0.15, 0.10 and 0.07 for the systems with SCF, MCF and LCF, respectively. These values are in agreement with the experimental ones (percolation curves, c.f. Figure 5.11) only for the case of MCF.

For the estimation of the critical exponent t, the experimental values for V_c were used. The fitting of the experimental results resulted in t values of 1.6, 1.9 and 2.0 for the EP system containing SCF, MCF and LCF, respectively. These values are quite smaller than those reported in the literature for other fibre reinforced samples [58]. This is an evidence that the final electrical properties of a composite are strongly dependent not only on the amount and type of filler, but also on the matrix material and the processing method. However, the same trend is observed, indicating an increase in t value for higher aspect ratios.

A second model applied in this study is the fibre-contact model (FCM) of Weber and Kamal [58]. The equation (2.5) can be rewritten in the case of electrical conductivity as:

$$\sigma = \sigma_m + \frac{4}{\pi}\left(\frac{d_c}{d}\cdot\frac{l}{d}\cdot\cos^2\phi\right)\left(V_p\sigma_f\right)X \qquad (5.7)$$

where, σ is the conductivity of the composite, σ_m *the* conductivity of the matrix, σ_f the conductivity of the fibres, d_c the diameter of the circle contact, *d* the diameter of the fibre, *l* the average fibre length, ϕ the fibre orientation angle (V_p and *X* are explained later). A more detailed review of the model in presented in the Appendix. The diameter of the contact circle, d_c, between the fibres is very small, and currently is not feasible to measure this value accurately. It can, however, be estimated by fitting the experimental data to the model calculations when using a certain d_c-value for the composites with different fibre loadings.

The symbol V_p represents the volume fraction of fibres, which participates in the formation of the electrical conductive network. It can be written as:

$$V_p = \beta \cdot V_f \tag{5.8}$$

where is β equal to 0 below the percolation threshold, V_c, and 1 at a "saturated" volume fraction V_t. For concentrations in the range $V_c < V_f < V_t$, β can be calculated by:

$$\beta = \frac{V_f - V_c}{V_t - V_c}. \tag{5.9}$$

The parameter *X* depends on the contact number of fibres, *m*. According to Weber and Kamal, the following mathematical relation can be used for the relation between *X* and *m:*

$$X = 0.59 + 0.15 \cdot m \tag{5.10}$$

where:

$$m = m_{\max} \cdot \left(\frac{V_p}{V_t} \right) \tag{5.11}$$

For all cases, the number of contacts *m* is assumed to vary between 2 and a maximum of 15 [58]. This means that at loadings near the percolation threshold each fibre has a minimum of two contacts, while at the saturated fibre fraction the maximum value of 15 is reached.

In Table 5.9 the microstructural parameters used for modelling the electrical conductivity of the CF/EP composites are summarised. The critical volume fraction V_c was evaluated by the percolation curves of the different types of CF (cf. Figure 5.11). As maximum volume fraction, V_t, those values were used, experimentally defined in paragraph 5.1.1.1. The ratio of the contact diameter to the fibre diameter, d_c/d, was determined by fitting the experimental curves as it is illustrated in Figure 5.48 for the case of SCF/EP composites.

Table 5.9: Values of parameters used in fibre-contact model for the CF/EP composites.

Parameter	Units	SCF	MCF	LCF
Electrical Conductivity, σ	S/cm	67	67	100
Critical Volume Fraction, V_c	%	23.6	10	3.3
Maximum Volume Fraction, V_t	%	37.1	23.0	9.8
Fibre Diameter, d	μm	14.5	18	14
Average Fibre Length, l	μm	107	269	399
Contact/Fibre Diameter, d_c/d	1	$1 \cdot 10^{-8}$	$1 \cdot 10^{-9}$	$1 \cdot 10^{-8}$
Orientation Parameter, $cos^2 \phi$	1	0.61	0.62	0.52

Figure 5.49 compares experimentally measured electrical conductivity values of CF/EP composites with the model predictions. It can be seen that the model closely fits the experimental data for concentrations higher than the percolation threshold. Below V_c the system exhibits the electrical conductivity of the matrix, σ_m.

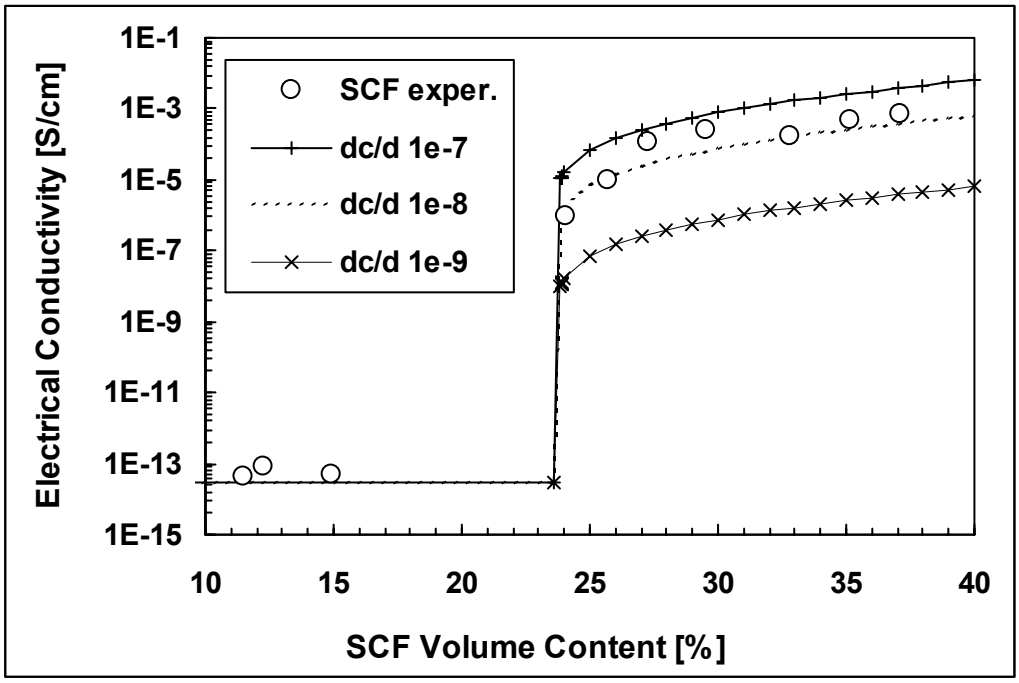

Figure 5.48: Influence of the d_c/d ratio on the simulated percolation curve for the SCF/EP system.

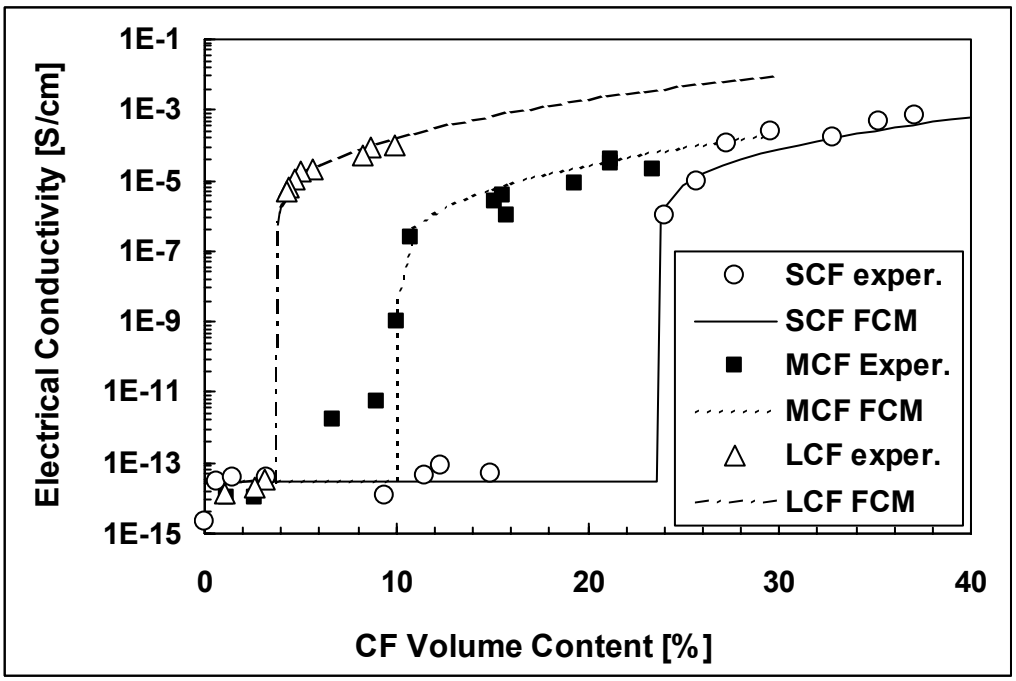

Figure 5.49: Comparison between predicted values by the FCM and experimental results for SCF/, MCF/ and LCF/EP composites.

5.4.2 Epoxy/Polyaniline Blends

The percolation theory was used to model the case of EP/PANI-DBSA blends as well. The fitting of the experimental data for V_c=0.024 resulted in a value of 1.89 for the critical exponent *t*. A variety of *t* values have been reported in the literature for polyaniline blends. Křiva et al. [118] determined values for 1.43 and 1.53 for mixtures of conducting PANI with potassium bromide and ammonium sulphated salt, respectively. For blends of PANI-HCl with different conventional polymers, Banerjee et al. [97] obtained *t* = 1.87-1.96. Other researchers have furthermore reported *t* values below the theoretical limits, but oftentimes also over 2.0 [119,120]. It is clear that in the case of PANI blends, the *t* values are strongly dependent both on the systems modelled and on the blending procedure used to develop them.

Table 5.10: Values of parameters used in fibre-contact model for the EP/PANI-DBSA blends.

Parameter	Units	PANI-DBSA
Electrical Conductivity, σ	S/cm	1
Critical Volume Fraction, V_c	%	2.4
Maximum Volume Fraction, V_t	%	26
Fibre Diameter, *d*	nm	10
Average Fibre Length, *l*	nm	10
Contact/Fibre Diameter, d_c/d	1	$1 \cdot 10^{-7}$
Orientation Parameter, $cos^2 \phi$	1	0.5

In order to apply the FCM model in the case of EP/PANI-DBSA blends, assumptions about their microstructure should be made. The morphological analysis of these systems revealed the formation of a very fine conductive network compared to the one of CF (cf. Figure 5.25). The exact size of the particles participating in the conductive pathways could not be determined, but it was estimated in the range of 5-10 nm. In Table 5.10 the microstructural parameters used for modelling the electrical conductivity of the EP/PANI-DBSA blends are summarised. The critical volume fraction, V_c, was experimentally determined from the percolation curve of the EP/PANI-DBSA blends (cf. Figure 5.28). The maximum volume fraction, V_t, was

assumed to be about 26 vol.%, in accordance with values in the literature [36,115]. The ratio of the contact diameter to the fibre diameter, d_c/d, was determined by fitting the experimental curves.

In Figure 5.50 the experimentally measured electrical conductivity values of EP/PANI-DBSA blends are compared with the predicted ones. An acceptable correlation between these values can be observed. Nevertheless, the experimental percolation curve exhibits a smooth increase above the percolation threshold, while the model predicts a sharper change of conductivity.

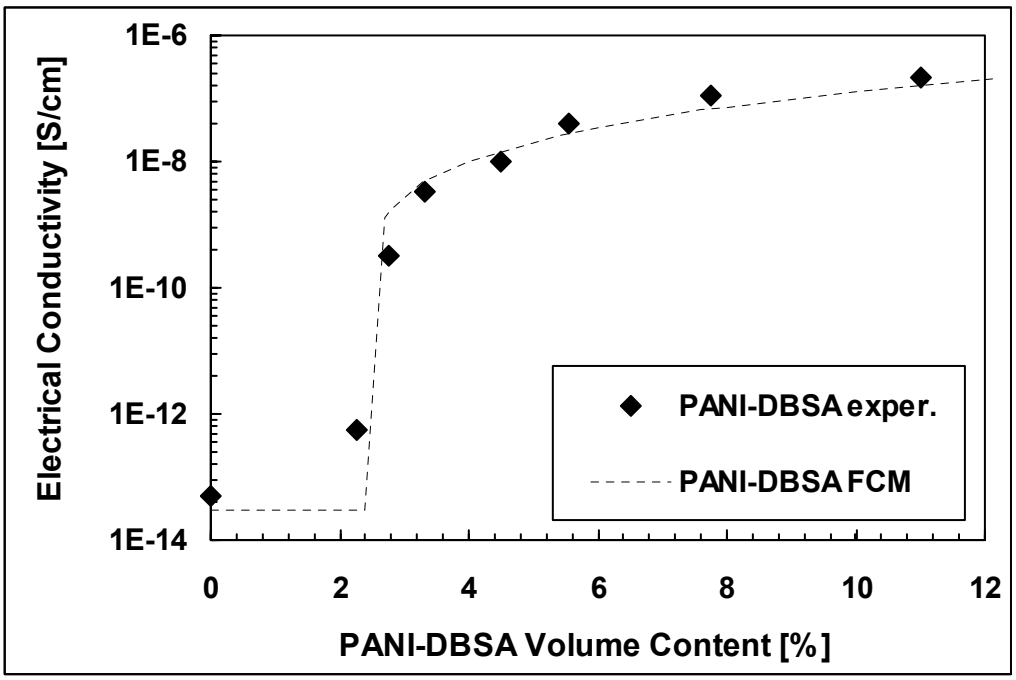

Figure 5.50: Comparison between predicted values by the FCM and experimental results for EP/PANI-DBSA blends.

5.4.3 Carbon Fibre Reinforced Epoxy/Polyaniline Blends

As it was previously demonstrated (c.f. Figure 5.40), enhanced electrical properties can be achieved when a combination of CF and PANI-DBSA is used. In order to model this system, an intersection of two conductive networks, one corresponding to CF and the other to PANI-DBSA, is assumed to take place within the insulating EP matrix. In this way the charge carriers are supposed to have more possibilities to move. Due to the high inherent conductivity of CF, when compared to PANI-DBSA and EP, they are the main mechanism for the increased electrical properties.

Therefore the microstructure characteristics of SCF are used for the theoretical modelling. PANI-DBSA on the other hand plays two different roles in the developed system. Together with EP it composes an electrically conductive matrix and additionally it creates larger contact areas between the CF. Therefore the percolation threshold is repositioned to lower concentrations. The percolation theory would not be applicable for modelling this behaviour, as the electrical conductivity of the matrix, i.e. EP/PANI-DBSA, is not much smaller compared to that of SCF.

The parameters of the FCM should be reconsidered in order to take into account the synergy effect between the two conductive additives. The approach for the whole system will be slightly different than the one presented in Figure 5.40. For the modelling part, as initial material the SCF/EP composite is considered, instead of EP/PANI-DBSA blend, and the chances in conductivity by the varying the PANI-DBSA amount in the matrix are studied (Figure 5.51). It is clear from the experimental results that by the addition of PANI-DBSA the percolation threshold is shifted to much lower values (Table 5.11).

Table 5.11: Values of parameters used in the fibre-contact model for the SCF reinforced EP/PANI-DBSA system.

$V_{PANI\text{-}DBSA}$ [vol.%]	2.1	3.3	5.6	7.8
σ_m [S/cm]	$5.4\cdot10^{-13}$	$3.4\cdot10^{-9}$	$3.9\cdot10^{-8}$	$1.1\cdot10^{-7}$
V_c [vol.%]	8	2.3	2.5	1.5
V_t [vol.%]	36.5	33.7	32.8	29.5
β	0.07	0.228	0.238	0.288
d_c/d	$3\cdot10^{-10}$	$3\cdot10^{-8}$	$8\cdot10^{-8}$	$2\cdot10^{-7}$

Moreover, a small reduction of the maximum volume fraction takes place, as the viscosity of the matrix increases. Calculations suggest that the factor β increases with the PANI-DBSA content and thus V_p, the content of fibres which participate in the conductive network, also increases. The role of PANI-DBSA as conductive matrix is introduced into the model by assuming as σ_m the conductivity of the EP/PANI-DBSA blend with corresponding volume fraction of the conductive salt. Moreover, PANI-DBSA acts as a electrical connector between the SCF. This phenomenon is

introduced to the model by increasing contact diameters, and hence a larger ratio d_c/d for higher amounts of PANI-DBSA. All these results are summarised in Table 5.11.

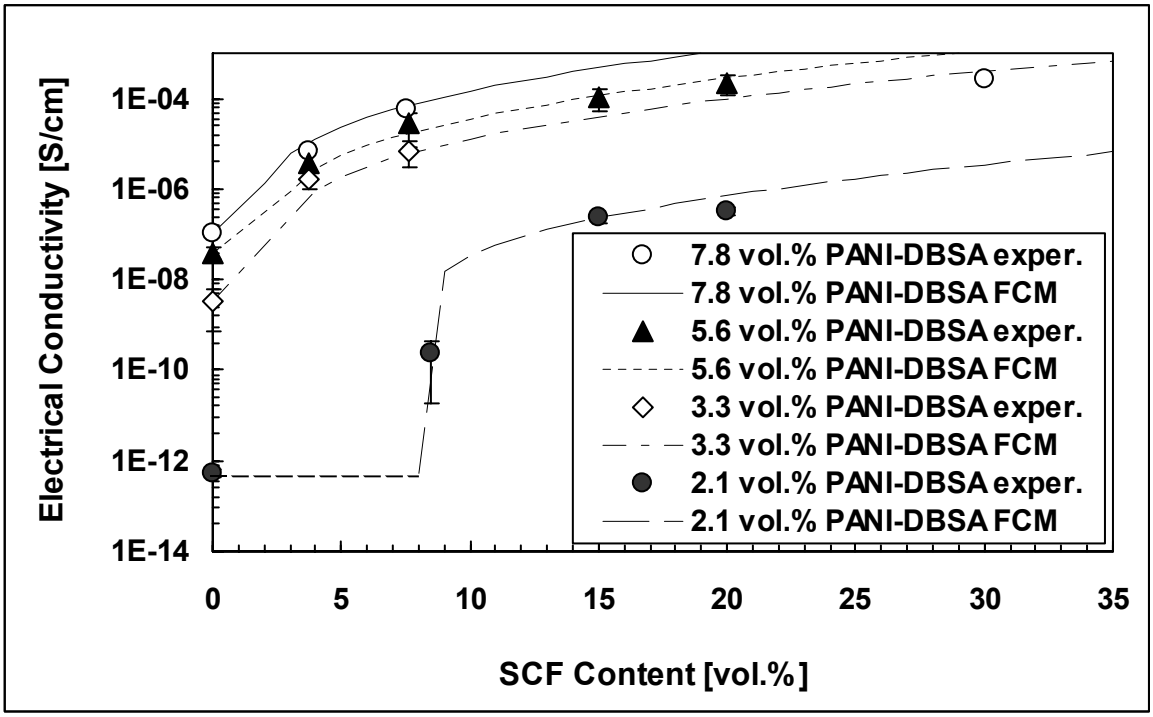

Figure 5.51: Comparison between predicted and experimental results for the SCF reinforced EP/PANI-DBSA composites.

The results of the modelling of the SCF reinforced EP/PANI-DBSA composites are illustrated in Figure 5.51, together with the experimental values. A good correlation between them is evident. By the presence of PANI-DBSA in the matrix, a gradual increase in the electrical conductivity is observed and the percolation threshold cannot be easily detected. Especially for low SCF concentrations, the difference in conductivity between samples without and with PANI-DBSA is remarkable. The FCM predicts however much larger conductivity values for highly reinforced composites. The developed materials were not able to show conductivity above 10^{-4} S/cm. Probably this is a limiting value for the specific system and processing method, which cannot be taken into consideration by the above modelling parameters.

6. Summary and Outlook

The presented study was focused on the development of electrically conductive polymer composites based on an epoxy matrix. For this reason, CF or/and the conductive polymer PANI-DBSA were mixed with the insulating EP in order to achieve various degrees of electrical conductivity. Results and conclusions obtained during this work are summarised and presented in the following paragraphs. Suggestions on possible applications of the developed materials and future studies are as well given within the last paragraphs.

Carbon Fibres

By the use of the centrifugation method graded profiles of the CF distributions were realised along the thickness of the samples. Control of these formations was possible by a variation of the processing parameters, i.e. the centrifugation speed, the viscosity of the matrix, the aspect ratio of the fibres, and the total volume fraction of the fibres.

The electrical properties along the thickness of the sample were closely connected to the local CF concentration. In this way, materials that exhibited low conductivity values at one side, and higher at the other were developed. However, the changes in the surface resistance along the thickness of the samples were abrupt, as a result of the percolation behaviour of the electrical conductivity. For the different CF/EP composites studied, the typical percolation curves were determined. Up to a specific concentration the conductivity remained at the low level of the EP matrix, whereas for higher CF contents a sharp transition to the conductive state was observed. A significant reduction of the percolation value was evident for the fibres with higher aspect ratio, due to an earlier formation of electrically conductive pathways.

The mechanical properties of the graded CF/EP samples, and more specifically flexural modulus and microhardness, exhibited also graded profiles along the thickness of the samples, similar to those of CF distributions. Both of these properties were more sensitive to the changes of the local fibre content, than surface resistance. Especially via the microhardness determination, a good estimation of the graded CF distribution along the thickness of the samples was possible, regarding the small steps at which these measurements can occur.

Polyaniline Salt

The hardener type had a significant influence on the electrical properties of EP/PANI-DBSA blends. Electrical conductivity measurements of the samples showed significant differences when an alkaline or an acidic hardener was used for curing the epoxy system. Samples cured with alkaline hardeners (i.e. amine or imidazole) exhibited very low values of conductivity, close to that of the insulating EP matrix, even at high PANI-DBSA contents. In contrast, when the acidic curing agent (BF_3) was used, PANI-DBSA resulted in drastic increase in the electrical conductivity, which reached the value of $2 \cdot 10^{-7}$ S/cm for 11.1 vol.% PANI-DBSA. The optical observation during the mixing procedure showed that the colour of the blends changed from green to blue by the addition of alkaline hardeners, while in the case of BF_3 no colour change was evident. This fact indicated a PANI-DBSA to PANI-EB conversion when the alkaline hardeners were used, probably due to their basic character. UV-vis analysis confirmed these observations. Additionally, to the hardener type, the dispersion quality of PANI-DBSA proved to be crucial for the resulting electrical properties of the blends. Samples prepared without dissolving PANI-DBSA in toluene showed poor dispersion of the salt in the EP resin, and moreover, low values of electrical conductivity.

The conductive salt had a minimal influence on the thermal and electrical properties of the EP matrix for concentrations up to 5.6 vol.%. After this content, the flexural modulus and the glass transition temperature were significantly reduced. One the other hand, for high PANI-DBSA contents an enhancement of the elongation at break and the fracture toughness of the blends was observed. This was closely connected to the lower degree of cure of these systems, together with the presence of rich in PANI-DBSA regions within their structures.

Combination of Carbon Fibres and Polyaniline Salt

The blending of SCF to the EP/PANI-DBSA resulted in an increase of both electrical and mechanical properties. The percolation threshold could be moved towards a lower PANI-DBSA content, and the conductivity was increased by two orders of magnitude. A synergy effect between SCF and PANI-DBSA was evident, with respect to the electrical conductivity of the composites. Furthermore, the reinforcing effect of SCF was not affected by the existence of PANI.

Functionally graded materials could be effectively manufactured by the centrifugation method in this case as well. PANI-DBSA was not able to move under the centrifugal force due to its low density, and it composed together with EP a conductive matrix for the developed materials. The presence of PANI-DBSA in the graded samples played the role of one more processing parameter. Control of the viscosity and the conductivity of the matrix was possible by the addition of the conductive salt. The surface resistance showed smoother graded profiles for these materials than for those prepared without PANI-DBSA, as a result of the better electrical properties of the matrix. Relevant gradients were also exhibited by the mechanical properties of these graded composites.

The fibre-contact model was used for modelling the electrical conductivity of the developed materials. Initially, the conductivities of CF/EP composites with different fibre aspect ratios were predicted. Their dimensions and orientation were applied in the modelling, and the calculated values were in good agreement with the experimental results. The model was also applied in the case of the EP/PANI-DBSA blends. A sharper increase in conductivity was predicted, compared to the experimental data. Furthermore, the model was extended in order to predict the synergy effect occurred for the SCF reinforced EP/PANI-DBSA composites. Due to the fact that SCF have a higher conductivity compared to PANI-DBSA, their microstructure was used for the modelling. The conductive salt, on the other hand, was assumed to play the role of the conductive matrix, as a mixture with EP. Through reconsideration of key parameters of the model, such as the volume fraction of fibres participating in the conductive network, the enhanced conductivity, resulting from the combination of the two conductive components, could be acceptably predicted.

Each of the conductive fillers used in this study showed advantaged and drawbacks. CF could result in higher electrical conductivities, and additionally, in enhancement of the mechanical properties of the composites. However, these materials are rather unsuitable if ESD applications are considered, regarding the sharp increase in conductivity occurring within the range of 10^{-9}-10^{-6} S/cm. On the other hand, PANI-DBSA showed more controllable electrical properties, but no mechanical reinforcement of the EP matrix. The low inherent conductivity of the salt limits its use

in applications where protection against ESD is needed. The developed blends with PANI-DBSA are therefore categorised as antistatic materials. The fine microstructure of these blends makes them appropriate for sensitive applications where “clean” materials are required. PANI-DBSA formed a fine mixture with the EP matrix, and no removal of particles is possible from the material surface (e.g. in contrast to CB). EP/PANI-DBSA blends can hence be used for packaging applications, in order to protect sensitive electronics from the damaging effects of static electricity.
The combination of CF and PANI-DBSA developed composites with higher and controllable electrical properties, and moreover, enhanced mechanical properties. These materials can be appropriate for a variety of applications, considering that their degree of conductivity can be tailored from antistatic to conductive levels.

FGMs provided even more possibilities for the development of electrically conductive polymer composites. Materials with diverse electrical properties at the opposite surfaces of their thickness could be realised and designed. These structures can be introduced to applications where materials with conductive coatings are traditionally used. An example is the papermaking industry, where static charges are accumulated on the surface of the rollers due to tribological phenomena, and their discharge is often uncontrolled. Such problems can be eliminated via the use of graded rollers, which exhibit an appropriate degree of conductive on their outer surface.

Electrically conductive polymer composites is a quite new category of materials, which is developed rather rapidly in order to follow the advances of technology. Everyday, new fields of applications are born, and the design of advanced materials to cover the requests consists a challenge for the engineers. The tendency is to leave behide traditional conductive fillers, such as CB, and use more sophisticated additives like CNT and ICPs. However, the influence of these additives on the functional properties of the developed conductive compounds is not always clear. Especially for the ICPs, continuous disagreements take place concerning their enviromental stability, solubility, microstructure and processability. It is therefore important to put more effort in understanding better the character and behaviour of these materials.

A further continuation of the present work could be the examination of the thermal properties of the developed materials, considering that a correlation with the electrical properties already specified should exist. Moreover, it would be interesting to study the effect of eviromental parameters, such as temperature and moisture, on the electrical characteristics of the materials, especially in the case of EP/PANI-DBSA blends.

7. Appendix

The model of Weber and Kamal [58] is based on the fact that most of the existing models do not take into consideration the particle-to-particle contacts, and therefore yield no accurate predictions for the conductivity of a composite. The majority of these models assume that the conductivity of the connected fibres is equal to that of the fibre itself. In real composites, however, the contacts between fibres are seldom perfectly end-to-end. They are commonly end-to-body or body-to-body. Hence the area of contact between the fibres is much smaller, and therefore lower conductivity values should be expected.

The FCM is an extension of the Batchelor and O'Brien model [121], which was developed for thermal conductivity of materials consisting of conductive particles in a matrix. The main assumption of FCM is that the conductivity of a composite is determined by the conditions near the contact points of the fibres. The current density in the contact point of particles, which are assumed to be locally spherical is:

$$\left\langle \vec{J} \right\rangle = n\left\langle \sum \vec{r}_i I_i \right\rangle \tag{7.1}$$

where, $\vec{J}$ is the current density, *n* the number of the particles, *i* the location of the contact point *i*, $\vec{r}_i$ the position of the contact point *i*, and I_i the current flowing through the contact point *i*. The symbol $\langle\rangle$ denotes a volume average over a region with a large number of particles.

By the use of Equation 7.1, the case of fibres with a flat circle of contact can be modelled. Consider a fibre with multiple contacts, as the fibre 0 illustrated in Figure 7.1. This fibre is in contact with four others (fibre 1 to 4), and all of them have the same diameter *d* and length *l*. Each fibre has an angle of orientation $\pm\phi$, such as $cos^2\phi$ is equivalent for all fibres. The number of contacts *m* is four in this case, and all the contact points are equally spaced along the length of fibre 0. The origin of coordinate system is at the centre of this fibre length.

For particles with a flat area of contact, the current may be written:

$$I = \sigma_f d_c \Delta U \tag{7.2}$$

where is σ_f the conductivity of the fibres, d_c the diameter of the circle contact and ΔU the potential difference between the centres of two particles.

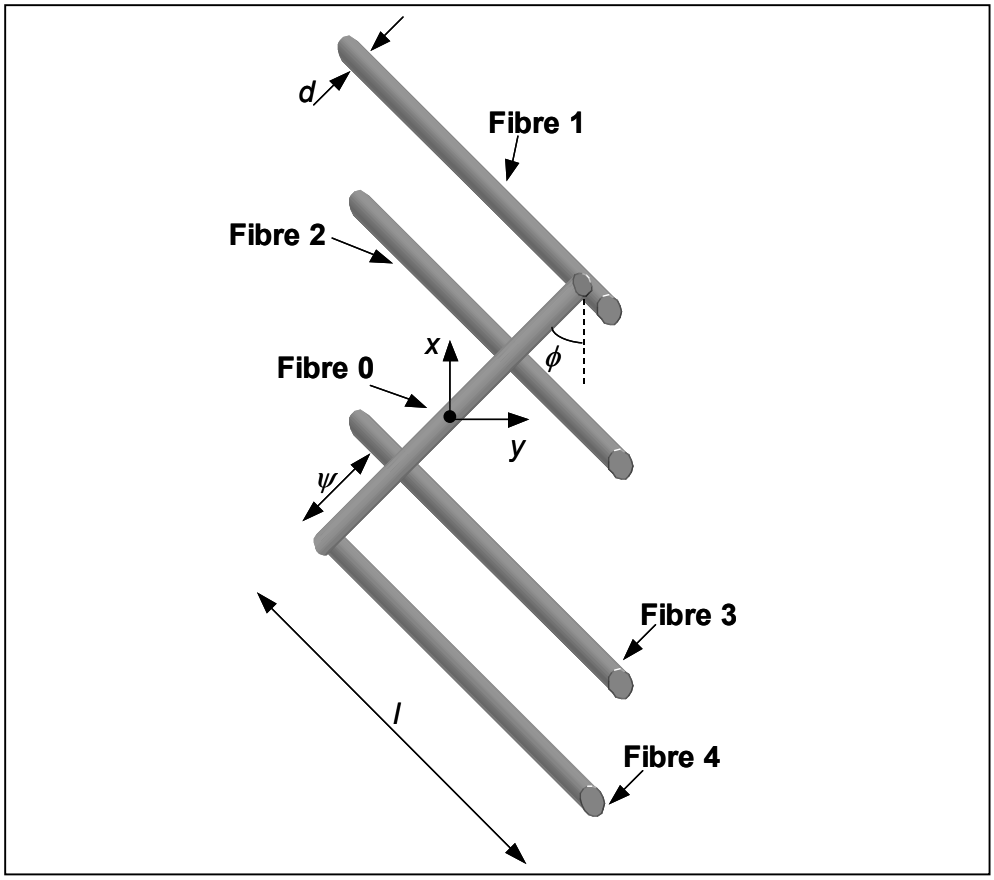

Figure 7.1: Arrangement of fibres with multiple contacts [58].

The potential difference can be substituted by:

$$\Delta U = -2\vec{r}_i \langle \Delta U \rangle \tag{7.3}$$

Replacing Equations 7.2 and 7.3 into Equation 7.1 and relating the number density of fibres to the fibre volume fraction V_f, we obtain:

$$\left\langle \vec{J} \right\rangle = -\frac{8V_f}{\pi d l} \cdot d_c \sigma_f \langle \Delta U \rangle \sum_{i=1}^{m} \vec{r}_i^{\,2} \tag{7.4}$$

The longitudinal position of the contact point can be expressed as:

$$\vec{r}_i = x_i \cos\phi \tag{7.5}$$

In the direction *i* the relation between current density and potential can be defined by the Ohm's law:

$$\left\langle \vec{J} \right\rangle = -\sigma \langle \Delta U \rangle \tag{7.6}$$

where σ is the conductivity of the composite.

Using Equation 7.5 and 7.6, Equation 7.4 can be rewritten as:

$$\sigma = \frac{8V_f d_c \sigma_f \cos^2 \phi \sum_{i=1}^{m} x_i^{\,2}}{\pi d^2 l} \tag{7.7}$$

Since fibres 1 and 3 are lying in the same distance from the centre of fibre 0, as are fibres 2 and 4, the following equation can be formed:

$$\sum_{i=1}^{m} x_i^{\,2} = 2\sum_{i=1}^{\frac{m}{2}} x_i^{\,2} \tag{7.8}$$

The distance between two contact points is defined as:

$$\psi = \frac{l}{m-1} \tag{7.9}$$

The component x_i can be written in terms of the distance between the contact points:

$$x_i = \left(\frac{l}{m-1}\right) \cdot \left(i - \frac{1}{2}\right) \tag{7.10}$$

Then, the sum term becomes:

$$\sum_{i=1}^{\frac{m}{2}} x_i^{\,2} = \frac{l^2}{4(m-1)^2} \sum_{i=1}^{\frac{m}{2}} (2i-1) \tag{7.11}$$

The combination of Equations 7.7 and 7.10 gives:

$$\sigma = \frac{4V_f d_c \sigma_f \cos^2 \phi}{\pi d^2} \cdot X \tag{7.12}$$

where:

$$X = \frac{\sum_{i=1}^{\frac{m}{2}} (2i-1)^2}{(m-1)^2} \tag{7.13}$$

The above derivation has be applied by Weber and Kamal for various cases contacts *m*, and a general relation between X and m was obtained (cf. Equation 5.10).

In the relation for the conductivity of the composite applied in this study (Equation 5.7), the term of matrix conductivity, σ_m, is also introduced. In this way the influence of matrix is also taken into consideration. Moreover, the model can be also used for modelling of composites where the conductivity difference between matrix and fibre is not so large. This modification of Equation 7.11 has been firstly applied to CF

reinforced polypropylene systems with and without polyaniline [59], showing good agreement between the predicted and the experimental values.

8. Literature

[1] English, L.K.: The ABC's of EMI/RFI/ESD shielding. ME (1989) pp.37-40.

[2] Blythe, A.R.: Conduction in polymers/ Static charges. In "Electrical Properties of Polymers". Cahn, R.W., Thompson, M.W., Ward, I.M. (ed.). London: Cambridge University Press 1980, pp.90-139 and 156-180.

[3] Bhattacharya, S.K., Chaklader, A.C.D.: Review on metal-filled plastics. Part 1. Electrical conductivity. Polymer-Plastics Technology and Engineering 19 (1982) Nr.1, pp.21-51.

[4] RTP Co.: Imagineering Plastics, EMI shielding. Dramatic cost reduction for electronic protection 2000.

[5] Angelopoulos, M.: Conducting polymers in microelectronics, IMB Journal of Research and Development 45 (2001) pp.57-76.

[6] Kimmel, W.D., Gerke, D.D.: Conductive coating and applications. Conformity 2003: The Annual Guide (2003) pp.126-134.

[7] Applied Coating Technologies Ltd: Advantages in conductive coating for EM/RFI shielding- a response to increased demand for recyclability. www.applicoat.com

[8] Bigg, D.M.: Properties and processing of short metal fibre filled polymer composites. In "Short fibre-polymer composites" De, S.K., White, J.R. (ed.). Cambridge: Woodhead 1996, pp.144-166.

[9] Klason, C., McQueen, D.H., Kubat, J.: Electrical properties of filled polymers and some examples of their applications. Macromolecular Symposia 108 (1996) pp.247-260.

[10] Zhang, M.Q., Zeng, H.M.: Conducting thermoplatics composites. In: "Handbook of thermoplastics". Olabisi, O. (ed.). New York, USA: Marcel Dekker, Inc. 1997, pp.873-891.

[11] Funt, J.M., William, L.S., Tomme, M.: Carbon in Plastics. In "Carbon Black". Donner J.-B. (ed.) New York, USA: Marcel Dekker, Inc. 1993, pp.389-408.

[12] Tchoudakov, R., Breuer, O., Narkis, M.: Conductive polymer blends with low carbon black loading: Polypropylene/Polyamide. Polymer Engineering and Science 36 (1996) 10, pp.1336-1346.

[13] Clingerman, M.L., Weber, E.H., King, J.A., Schulz, K.H.: Development of an additive equation for predicting the electrical conductivity of carbon-filled composites. Journal of Applied Polymer Science 88 (2003) pp.2280-2299.

[14] Schueler, R., Peterman, J., Schulte, K., Wetzel, H.-P.: Percolation in carbon black filled epoxy resin. Macromolecular Symposia 104 (1996) pp.261-268.

[15] Dani, A., Ogale, A.A.: Electrical percolation of short-fiber composites: experimental characterisation and modelling. Composites Science and Technology 56 (1996) pp.911-920.

[16] Dani, A., Ogale, A.A.: Electrical resistivity of short fibre composites. Antec '93 (1993) pp.609-613.

[17] Agari, Y., Ueda, A., Nagai, S.: Electrical and thermal conductivities of polyethylene composites with biaxial oriented short-cut carbon fibers. Journal of Applied Polymer Science 52 (1994) pp.1223-1231.

[18] Taipalus, R., Harmia, T., Friedrich, K.: Short fibre reinforced PP/PANI-complex blends and their mechanical and electrical properties. Applied Composite Materials 6 (1999) pp.167-184.

[19] Tanaka, K., Yamaguchi, M., Takahashi, T., Miyagawa, H., Yoshimatsu, H.: Electrical conductivity of poly(vinyl chloride) filled with PAN-based and pitched-based carbon short-fibers. Advanced Composite Materials 4 (1994) 1, pp.1-15.

[20] Wang, J., Varadan, V.V., Varadan, V.K.: EMI shielding with lightweight metal fiber composites. SAMPE Journal 32 (1996) 6, pp.18-22.

[21] Rosenow, M.W.K., Bell, J.A.E.: EMI shielding effectiveness of nickel coated carbon fiber as long fiber thermoplastic concentrate. 43rd International SAMPE Symposium, 1998, pp.854-864.

[22] Galli, E.: Update: Conductive and magnetic fillers. Plastic Compounds (1992) pp.51-56.

[23] Sandler, J., Shaffer, M.S.P., Prasse, T., Bauhofer, W., Schulte, K., Windle, A.H.: Development of a dispersion process for carbon nanotubes in an epoxy matrix and the resulting electrical properties. Polymer 40 (1999), pp. 5967-5971.

[24] Chiang, C.K., Fincher, C.R., Park, Y.W., Heeger, A.J., Shirakawa, H., Kouis, E.J., Gau, S.C., MacDiarmid, A.G.: Electrical conductivity in doped polyacetylene. Physical Review Letters 39 (1977) 17, pp.1098-1101.

[25] MacDiarmid, A.G., Epstein, A.J.: Conducting polymers: past, present and future... Materials Res Symposium Proceedings 328 (1994) pp.133-144.

[26] Friend R.H.: Conductive polymers II. From science to applications. Rapra Review Reports 63 (1993) 6, pp.1-28.

[27] Kohlman, R.S., Joo, J., Epstein, A.J.: Conducting polymers: Electrical conductivity. In “Physical Properties of Polymers Handbook”. Mark, J.E. (ed.). New York, USA: AIP Press 1996, pp.453-478.

[28] Epstein, A.J.: Electrical conductivity in conjugated polymers. In “Conductive polymers and plastics in industrial applications”. Rupprecht, L. (ed.). Plastics Design Library 1999, pp.1-9.

[29] Stejskal, J., Kratochvil, P., Jenkis, A.D.: The formation of polyaniline and the nature of its structure. Polymer 37 (1996) 2, pp.367-369.

[30] Chiang, J.-C., MacDiarmid, A.G.: Polyaniline: Protonic acid doping of the emeraldine form to metallic regime. Synthetic Metals 13 (1986) pp.193-205.

[31] Wan, M., Yang, J.: Mechanism of proton doping in polyaniline. Journal of Applied Science 55 (1995) pp.399-405.

[32] Cao, Y., Qiu, J., Smith, P.: Effect of solvents and co-solvents on the processibility of polyaniline: I. Solubility and conductivity studies. Synthetic Metals 69 (1995) pp.187-190.

[33] Cao, Y., Smith, P., Qiu, J.: Counter-ion induced processibility of conducting polyaniline and of conducting polyblends of polyaniline in bulk polymers. Synthetic Metals 48 (1992) pp.91-97.

[34] Heeger A.J.: Self-assembled networks of conducting polyaniline: A new class of conducting polymer blends. Trends in Polymer Science 3 (1995) Nr.2, pp.39-47.

[35] Shacklette L.W., Han, C.C. Luly, M.H.: Polyaniline blends in thermoplastics. Synthetic Metals 55 (1993) pp.3532-3537.

[36] Zilberman, M., Titelman G.I., Siegmann, A., Haba, Y., Narkis, M., Alperstein, D.: Conductive blends of thermally dodecylbenzene sulfonic acid-doped polyaniline with thermoplastics. Journal of Applied Polymer Science 66 (1997) pp. 243-253.

[37] Taipalus, R. Harmia, T., Friedrich, K.: Influence of PANI-complex on the mechanical and electrical properties of carbon fiber reinforced polypropylene composites. Polymer Composites 21 (2000) 3, pp.396-416.

[38] http://www.epnconductivepolymers.com/

[39] RTP Company: Storage system finds new material. Compounding Lines 17 (2001) Nr.3, pp.1.

[40] RTP Company: Carriers cleans up wafer transport. Compounding Lines 16 (2001) Nr.2, pp.1.

[41] Peltola, J., Cao, Y., Smith, P.: Epoxy adhesives made with inherently conducting polymers. Adhesives Ages 38 (1995) pp.18-20.

[42] Laasko, J., Österholm, J.-E., Järvinen, H.: Electrically conducting thermoset polymer compositions with hydroxy containing protonic acid dopant. United States Patent 5,662,833, 1997.

[43] Kathirgamanathan, P.: Curable electrically conductive resins with polyaniline fillers. Polymer 34 (1993) 13, pp.2907-2908.

[44] Jeevananda, T., Palaniappan, S., Siddaramaiah: Electrical, mechanical and thermal properties of polyaniline-epoxy novolac composite materials. Journal of Polymer Materials 17 (2000) pp.313-318.

[45] Jia, W., Tchoudakov, Segal, E., Joseph, R., Narkis, M., Siegmann., A.: Electrically conductive composites based on epoxy resin with polyaniline-DBSA fillers. Synthetic Metals 132 (2003) pp.269-278.

[46] Wang, Y., Wang, X., Zhao, X., Li, J., Mo, Z., Jing, X., Wang, F.: Conducting polyaniline confined in semi-interpenetrating networks. Macromolecules Rapid Communications 23 (2002) 2, pp.118-121.

[47] Amaral, T.P., Barra, G.M.O., Barcia, F.L., Soares, B.G.: Polyaniline/epoxy resin conducting blend. Polimeros: Ciencia e Tecnologia 11 (2001) 3, pp.149-157.

[48] Chandrasekhar, P., Zay, B.J., Bazhutin, Y., McQueeney, T., Volodarsky, L.: Conducting polymer based conductive composites for structural and EMI shielding applications. Proceedings of ACUN-4, Sydney, 2002.

[49] Lux, F.: Review. Models proposed to explain the electrical conductivity of mixtures made of conductive and insulating materials. Journal of Materials Science 28 (1993) pp.285-301.

[50] Clingerman, M.L., Weber, E.H., Schulz, K.H., Meyers, J.D.: Evaluation of electrical models for conductive polymer composites. Journal of Applied Polymer Science 83 (2002) pp.1341-1356.

[51] Kirkpatrick, S.: Percolation and conduction. Review of Modern Physics 45 (1973) 4, pp.574-588.

[52] Zallen, R.: The percolation model. In “The physics of amorphous solids” New York: Jonh Wiley & Sons, Inc. 1983, Chapter 4.

[53] Sumita, M., Sakata, K.: Double percolation effect on the electrical conductivity of conductive particles filled polymer blends. Colloid & Polymer Science 270 (1992) pp.134-139.

[54] Wessling, B.: Dispersion hypothesis and non-equilibrium thermodynamics: key elements for a materials science of conductive polymers. A key to understand polymer blends or other multiphase polymer systems. Synthetic Metals 45 (1991) pp.119-149.

[55] Mamunya, E.P., Lebedev, E.V.: Influence of filling method on conductivity and structure of carbon black-filled polymer blends. In “Eurofillers 97”. Manchester, UK: 1997, pp.449-452.

[56] Malliaris, A., Turner, D.T.: Influence of particle size on the electrical resistivity of compacted mixtures of polymeric and metallic powders. Journal of Applied Physics 42 (1971) 2, pp.614-618.

[57] Bhattacharya, S.K., Chaklader, A.C.D.: Review on metal-filled plastics. Part1: Electrical conductivity. Polymer Plastics Technology and Engineering 19 (1982) pp.21-51.

[58] Weber, M., Kamal, M.R.: Estimation of the volume resistivity of electrically conductive composites. Polymer Composites 18 (1997) 6, pp.711-725.

[59] Taipalus, R., Harmia, T., Friedrich, K.: The electrical conductivity of carbon-fibre-reinforced polypropylene/polyaniline complex-blends: experimental characterisation and modelling. Composites Science and Technology 21 (2001) pp.801-814.

[60] Hirai, T.: Functional gradient materials. In “Materials science and technology: a comprehensive treatment” Cahn, R.W. (ed.). Weinheim: VCH Verlagsgesellschaft GmbH 1996, pp.295-337.

[61] Watanabe, Y., Fukui, Y.: Fabrication of functionally-graded aluminium materials by the centrifugal method. Aluminium Transactions 2 (2000) pp.195-208.

[62] Gasik, M.: Principles of functional gradient materials and their processing by powder metallurgy. Acta Polytechnica Scandinavica, Chemical Technology Series No.226 (1995) pp.2-73.

[63] Hirai, T., Chen, L.: Recent and prospective development of functionally graded materials in Japan. Materials Science Forum 308-311 (1999) pp.509-514.

[64] Kaysser, W.A., Ileschner, B.: FGM research activities in Europe. MRS Bulletin (1995) pp.22-26.

[65] Nishida, T., Pezzoti, G., Spiono, T.: Preparation and characterization of substrates with functionally graded dielectric constant. Materials Science Forum 308-311 (1999) pp.539-543.

[66] Choe, C.-R., Park, M., Lee, N.-J.: Fabrication of functionally gradient polymer composites using a centrifugal method. Proceedings of the International Conference on Composites Materials and Energy, Montreal, Canada (1995) pp.293-300.

[67] Funabashi, M.: Gradient composites of nickel coated carbon fibre filled epoxy resin moulded under centrifugal force. Composites Part A 28A (1997) pp.731-737.

[68] Lee, N.J., Jang, J., Park, M., Choe, C.R.: Characterization of functionally gradient epoxy/carbon fibre composite prepared under centrifugal force. Journal of Materials Science 32 (1997) pp.2013-2020.

[69] Watanabe, Y., Yakanama, N., Fukui, Y.: Control of composition gradient in a metal-ceramic functionally graded material manufactured by the centrifugal method. Composites Part A 29A (1998) pp.595-601.

[70] Watanabe, Y., Kawamoto, A., Matsuda, K.: Particle size distributions in functionally graded materials fabricated by the centrifugal solid-particle method. Composites Science and Technology. 62 (2002) pp.881-888.

[71] Brinkman, H.C.: The viscosity of concentrated suspension and solutions. Journal of Chemical Physics 20 (1952) 4, pp.571.

[72] Choe, C.R., Klingshirn, C, Friedrich, K.: Functionally graded polymer composites: Simulation of fiber distrubution. Macromolecular Research 10 (2002) pp.236-239.

[73] Hull, D: Geometrical aspects. In “Introduction to composite materials” Cambridge, UK: University Press 1981, pp.59-80.

[74] Williams, J.G.: K_C and G_C at low speeds for polymers. In “Fracture mechanics testing methods for polymers adhesives and composites”. Moore, D.R., Pavan, A., Williams, J.G. (eds.). Oxford: Elsevier 2001, pp.11-26.

[75] Vilcakova, J., Saha, P., Kresalek, V., Quadrat, O.: Re-exponential factor and activation energy of electrical conductivity in polyester resin/carbon fibre composites. Synthetic Metals 113 (2000) pp. 83-87.

[76] Feller, J.F., Linossier, I., Grohens, Y.: Conductive polymer composites: comparative study of poly(ester)-short carbon fibres and poly(epoxy)-short carbon fibres mechanical and electrical properties. Materials Letters 57 (2002) pp. 64-71.

[77] Mamunya, Ye.P., Davydenko, V.V., Pissis, P., Lebedev, E.V.: Electrical and thermal conductivity of polymers filled with metal powders. European Polymer Journal 38 (2002) 1887-1897.

[78] Mamunya, E.P., Davydenko, V.V., Lebedev, E.V.: A relationship between the percolation threshold and geometric parameter of the filler particles in the electroconductive polymer composites. Physical Chemistry 5 (1991) pp.127-130.

[79] Watanabe, Y., Eryu, H., Matsuura, K.: Evaluation of three-dimensional orientation of Al_3Ti platelet in Al-based functionally graded materials fabricated by a centrifugal casting technique. Acta Materialia 49 (2001) pp.775-783.

[80] Jana, P.B., Mallick , A.K., De, S.K.: Electrical conductive rubber and plastic composites with carbon particles or conductive fibres. In “Short fibre-polymer composites”. De, S.K., White, J.R. (eds.). Cambridge: Woodhead 1996, pp.170-172.

[81] Carmona, F., Barreau, F., Delhaes, P., Canet, R.: An experimental model for studying the effect of anisotropy on percolative conduction. Journal de Physique- Lettres 41 (1980) pp.534-534.

[82] Bigg, D.M.: Electrical properties of metal-filled polymer composites. In “Metal-filled polymers”. Bhattacharya, S.K. (ed.). New York: Marcel Dekker, Inc. 1986, pp.165-191.

[83] Krumova, M., Klingshirn, C., Haupert, F., Friedrich, K.: Microhardness studies on functionally graded polymer composites. Composites Science and Technology 61 (2001) pp.557-563.

[84] Baltá Calleja, F.J., Fakirov, S.: Microhardness of polymer blends, copolymers and composites. In: “Microhardness of polymers” Cambridge, UK: University Press 2000, pp.125-175.

[85] Skinner, J., Gane, N.: The deformation and twinning of graphite crystals under a point load. Philosophical Magazine 28 (1973) pp. 827-837.

[86] Oliver, W.C., Pharr, G.M.: An improvement technique for determing hardness and elastic modulus using load and displacement sensing indentation experiments. Journal of Materials Research 7 (1992) Nr.6, pp.1564-1580.

[87] Gong, J., Miao, H., Peng, Z.: Simple method for determing the initial unloading slope for ceramics nanoidentation tests. Journal of Materials Science Letters 22 (2003) pp.267-268.

[88] Hull, D: Fibres and matrices. In “Introduction to composite materials” Cambridge, UK: University Press 1981, pp.29.

[89] Pud, A., Ogurtsov, N., Korzhenko, A., Shapoval, G.: Some aspects of preparation methods and properties of polyaniline blends and composites with organic polymers. Progress in Polymer Science 28 (2003) pp.1701-1753.

[90] Wessling, B.: Dispersion as the link between basic research and commercial applications of conductive polymers (polyaniline). Synthetic Metals 93 (1998) pp.143-154.

[91] Sertova, N., Geffroy, B., Nunzi, J.-M., Petkov, I.: PVC as photodonor of HCl for protonation of polyaniline. Journal of Photochemistry and J. Photobiology. A: Chemistry 113 (1998) pp.99-101.

[92] Gospodinova, N., Terlemezyan, L., Mokreva, P., Kossev, K.: On the mechanism of oxidative polymerization of aniline. Polymer 34 (1993) pp.2434-2437.

[93] Huang, W.S., MacDiarmid, A.G.: Optical properties of polyaniline. Polymer 34 (1993) pp.1833-1845.

[94] Xia, Y., Wiesinger, J.M., MacDiarmid, A.G.: Camphorsulphonic acid fully doped polyaniline emeraldine salt: Conformations in different solvents studied by ultraviolet/visible/near-infrared spectroscopic method. Chemistry of Materials 7 (1995) pp.443-445.

[95] Wessling, B.: Electrical conductivity in heterogeneous polymer systems. V(1): Further experimental evidence for a phase transition at the critical volume concentration. Polymer Engineering and Science 31 (1991) pp.1200-1206.

[96] Planes, J., Samson, Y., Chequettine, Y. Atomic force microscopy phase imaging of conductive polymer blends with ultralow percolation threshold. Applied Physics Letters 75 (1999) pp.1395-1397.

[97] Banarjee, P. Mandal, B.: Conducting polyaniline nanoparticle blends with extremely low percolation thresholds. Macromolecules 28 (1995) pp.3940-3943.

[98] Karger-Kocsis, J., Gryshchuk, O., Schmitt, S.: Vinylester/epoxy-based thermosets of interpenetrating network structure: an atomic force microscopy study. Journals of Materials Science 38 (2003) pp.413-420.

[99] Berger, M.A., McCullough, R.L.: Characterization and analysis of the electrical properties of metal-filled polymer. Composites Science and Technology 22 (1985) pp.81-106.

[100] Truong, V.T., Codd, A.R., Forsyth, M.: Dielectric properties of conducting polymer composites at microwave frequencies. Journal of Materials Science 29 (1994) pp.4331-4338.

[101] McCullough, R.L.: Generalized combining rules for predicting transport properties of composite materials. Composites Science and Technology 22 (1985) pp.3-21.

[102] Ku, C.C., Liepins, R.: Dielectric constant of polymers. In “Electrical properties of polymers” Munich; Vienna; New York: Hanser Publishers 1987, pp.20-56.

[103] Blythe, A.R.: Dielectric Relaxation. In: “Electrical properties of polymers” New York, USA: Cambridge University Press 1979, pp.38-67.

[104] Hedvig, P.: Dielectric spectroscopy of polymers. Bristol: Adam Hilger Ltd. 1977, pp.282-307.

[105] Efros, A.L., Shklovskil, B.I.: Critical behaviour of conductivity and dielectric constant near the metal-non-metal transition threshold. Physical Status Solidi B 76 (1976) pp.475-485.

[106] Psarras, G.C., Manolakaki, E., Tsangaris, G.M.: Electrical relaxations in polymeric particulate composites of epoxy resin and metal particles. Composites: Part A 33 (2002) pp.375-384.

[107] Kupke, M.: Entwicklung elektrisch leitfähiger Glasfaserverbundwerkstoffe mittels Kohlestoff-Nanopartikel. PhD Thesis, Technische Universität Hamburg-Harburg, Cuvillier Verlag Göttingen, 2001, pp.45-47.

[108] Poussin, D., Morgan, H., Foot, P.JS.: Thermal doping of polyaniline by sulfonic acids. Polymer International 52 (2003) pp.433-438.

[109] Kinloch, A.J., Yuen, M.L., Jenkins, S.D.: Thermoplastic-toughened epoxy polymers. Journal of Materials Science 29 (1994) pp.3781-3790.

[110] Yee, A.F., Du, J., Thouless, M.D.: Toughening of epoxies. In “Polymer blends. Volume 2: Performance“ Paul, D.R., Bucknall, C.B. (eds.). New York: Wiley-Interscience Publication 2000, pp.225-199.

[111] Karger-Kocsis, J., Friedrich, K.: Microstructure-related fracture toughness and fatigue crack growth behavior in toughened, anhydride-cured epoxy resins. Composites Science and Technology 48 (1993) pp.263-272.

[112] Gryshchuk, O., Jost, N., Karger-Kocsis, J.: Toughening of vinylester-urethane hybrid resins by functional liquid nitrile rubbers and hyperbranched polymers, Polymer 43 (2002) pp.4763-4768.

[113] Varley, R.J., Hodgkin, J.H., Simon, G.P.: Toughening of trifunctional epoxy system Part VI. Structure property relationships of the thermoplastic toughened system. Polymer 42 (2001) pp.3847-3858

[114] Girard-Reydet, E., Vicard, V., Pascualt, J.P. Sautereu, H.: Polyetherimide-modified epoxy networks: Influence of cure conditions on morphology and mechanical properties. Journal of Applied Polymer Science 65 (1997) pp.2433-2445.

[115] Taipalus, R.: Elektrische und mechanische Eigenschaften von unverstärkten, glas- und kohlestofffaserverstärkten elektrisch leitfähigen Thermoplasten. PhD Thesis, Institut für Verbundwerkstoffe - Schriftreihe, Band 7 (2000) pp.125-143.

[116] Wang, S.F., Ogale, A.A.: Simulation of percolation behavior of anisotropic short-fiber composites with a continuum model and noncubic control geometry. Composites Science and Technology 46 (1993) pp.389-398.

[117] Munson-McGee, S.H.: Estimation of the critical concentration in an anisotropic percolation network. Physical Review B 43 (1991) pp.3331-3336.

[118] Křiva, I., Prokeš, J., Tobolková, E., Stejskal, J.: Application of percolation concepts to electrical conductivity of polyaniline-inorganic salt composites. Journal of Materials Chemistry 9 (1999) pp.2425-2428.

[119] Cruz-Estrada, R.H., Folkes, M.J.: Structure formation and modelling of the electrical conductivity in SBS-polyaniline blends. Part I Percolation theory approach. Journal of Materials Science Letters 21 (2002) pp.1427-1429.

[120] Shacklette, L.W., Han, C.C., Luly, M.H.: Polyaniline blends in thermoplastics. Synthetic Metals 55 (1993) pp.3532-3537.

[121] Batchelor, G.K., O'Brien, R.W.: Thermal or electrical conduction through a granular material. Proc. R. London. A 355 (1977) pp. 313-333.

9. List of Publications

1. Tsotra, P., Friedrich, K.: Composites with a graded electrical conductivity. 2th National Conference HELLAS-COMP. Patras, Greece (2001) pp. 304-313.
2. Tsotra, P., Friedrich, K.: Influence of PANI-DBSA on the electrical and mechanical properties of epoxy/carbon fiber composites fabricated by centrifugal method, ACUN-4, UNSW. Sydney, Australia (2002) pp. 20-25.
3. Tsotra, P., Friedrich, K.: Electrical and mechanical properties characterization of epoxy resin/polyaniline-dodecylbenzenesulphonic acid salt composite materials. Journal of Polymer Science 19 (2002), pp.389-394.
4. Tsotra, P., Friedrich, K.: Electrical and mechanical properties of functionally graded epoxy-resin/carbon fibre composites. Composites Part A 34 (2003), pp. 75-82.
5. Tsotra, P., Friedrich, K.: Composite materials with a graded electrical conductivity. IVW Kolloquium, IVW-Schriftreihe, Band 33 (2002), pp.211-215 .
6. Tsotra, P, Friedrich, K.: Conductive epoxy resin/polyaniline blends. 11. Problemseminar “Polymermischungen”. Merseburg, Germany (2003) pp. 29.
7. Tsotra, P., Friedrich, K.: Electrically conductive epoxy resin/polyaniline blends, 1st International Workshop on Polymers and Composites at IVW. Kaiserslautern, Germany (2003), pp. 55-54.
8. Tsotra, P., Friedrich, K.: Elektrisch leitfähige Epoxidharz/Polyanilin-Blends mit Gradientenverteilungen von kurzen Kohlestofffasern. „Verbundwerkstoffe und Werkstoffverbunde“. Vienna, Austria (2003) pp. 500-504.
9. Tsotra, P. Friedrich, K.: Thermal, Mechanical, and Electrical Properties of Epoxy Resin/Polyaniline-Dodecylbenzenesulfonic Acid Blend. Synthetic Metals 143 (2004) pp. 237-242.
10. Tsotra, P. Friedrich, K.: Short Carbon Fibers Reinforced Epoxy Resin/Polyaniline Blends: Their Electrical and Mechanical Properties. Composites Science and Technology 64 (2004) pp.2385-2391.
11. Tsotra, P. Gatos, K.G., Gryshchuk, O., Friedrich, K.: Hardener type as critical parameter for the electrical properties of epoxy resin/polyaniline blends (to be submitted).

12. Tsotra, P. Friedrich, K.: Polyaniline as conductive filler for epoxy resin. ECCM 11 Rhodes, Greece (2004).

10. List of Student Support Works

1. Theodorou, L.: Untersuchung der elektrischen Leitfähigkeit, mechanische und Dämpfungseigenschaften von Verbundwerkstoffen. Studienarbeit, Technische Universität Kaiserslautern (2004).